Laser-Micromachined Under-Water Micro Gripper Using Ionic Conducting Polymer Film (ICPF)

KWOK, Yiu-fai

A Thesis Submitted in Partial Fulfillment
of the Requirements for the Degree of
Master of Philosophy
in
Mechanical and Automation Engineering

July 2000

ABSTRACT

The manipulation of biological elements is a key technology for many new demanding applications in bio-MEMS. Many micromachined actuators now exist which operate with electrostatic, thermal, magnetic, or pneumatic control principles. However, almost none of these micro actuators can be used in any biological applications due to one hindrance: they must operate in a dry-environment. Ionic conducting polymer films (ICPF) is a newly invented material. It is a sandwich of perfluorosulfonic acid polymer that is between two thin film layers of metallic electrodes such as gold. Strips of ICPF can give large and fast bending displacement in the presence of a low applied voltage in wet condition. However, specially coated ICPF actuators can also be made to operate in dry conditions. The ability to produce a large deflection with a small input voltage (~±4.5V) means that this type of material has high potential not only for biological applications, but also for under-water MEMS and artificial muscles for space robots. A special laser-micromachining process is introduced to cut out arrays of gripping devices, which ICPF structures with dimensions of 200μm x 200μm x 3000μm were realized, and which is at least 5 times reduction in width dimension than all previously reported ICPF actuators. We will report on design, fabrication procedures and operating performance of the polymer actuators. The successful development of these actuators will enable effective and fast control of under-water micro objects and lead to new applications in cellular manipulation. We have also successfully actuated star-patterned (500μm wide, 4mm long) appendages. To the best of our knowledge, these are the smallest ICPF actuators in the world at the time when this manuscript is written.

Submitted by: KWOK, Yiu-fai
For the degree of Master of Philiosophy
at The Chinese University of Hong Kong in July,2000

摘要

對於操控生物細胞活動的微電子機械系統，一向都有強烈的需求。現存的微加工的執行器大多數基於電動，熱動，磁動，或氣動的原理。由於這些微型執行器必需在乾燥的環境下操作，一般都不能應用於生物技術中，所以在生物科技的領域上還未能得到認同和肯定。

ICPF 是一種新興的智能材料，這種材料是由一層聚合物及兩層超薄金屬（用金作爲電極層）所組成。一條細長的 ICPF，可以在低電壓及濕度高的環境下作出快速及大幅度的彎曲。如果經過特殊的表面處理來保持一定的濕度，它在沒水的環境下仍可以作出同樣的彎曲反應。因此，我們深信 ICPF 能在要求大幅度移動的感應器或執行器技術上有很大的發展空間。

本文論述運用 ICPF 所研制的微型細胞鉗。透過突殊的激光切割技術，我們成功地製造出寬度小於 200 微米，長度少於 3000 微米的微型細胞鉗，而這細胞鉗比起現存的 ICPF 致動器至少小於 5 倍以上。而這種微型細胞鉗將會配合於晶片科技。如能成功地發展出這種致動器將可以實現高效能的水中細胞操控裝置及帶出新的細胞操作應用。經過一系列的研究工作，我們成功地以少於 15 伏電壓去操作一寬 500 微米，長 4 毫米的星形微細胞鉗 （近據我們的研究顯示，那是當時世界上最微細而能操作的 ICPF 致動器）。

總括而言，我們應用研究得來的生產技術，加上激光技術，我們成功地研製出寬度少於 200 微米的水中微細胞鉗。將來，我們將重點研究其操控系統及改進生產技術，希望能達成研製出少於 100 微米寬的生物微細胞鉗。

ACKNOWLEDGMENTS

This dissertation can never be made successful without the great help from many nice people. First, I would like to thank my supervisor, Professor Wen J. Li. During these two years, he gave a lot of patience and guidance in teaching me how to make decisions, how to solve problem and provided a very good research condition and atmosphere in the Advanced Microsystems Laboratory (AML). As a student and friend, he deserves my true heart acknowledgment. Besides, I would like to thank Dr. W. Y. Cheung from the Electrical Engineering department. He has given very kind and valuable guidance and support in teaching me how to operate equipments in cleanroom. Without him, fabrication of ICPF can never be made possible. Winston Sun, who is a PhD student in AML, must be thanked for sharing ideas and experience in many aspects during the research period. Terry Ho, Antony To, F. F. Hui, Gordon Chan, Neil Ching and Julia Qin, are all my dear colleagues in AML, have to be named for sharing great moments and bringing high morale in these two years of campus life. In addition, our technicians, Allan Mok, Tong Hang, Philip Lee, should be thanked for giving full support in building professional experimental setups and components efficiently. I would also like to grant our computer staffs, Mr. Alex Lee and Miss Y. K. Chan in software and network supports. Furthermore, I am grateful to Miss Y. L. Kan, Joyce Wong, and Maggie Chan for their help in handling documentation work.

TABLE OF CONTENT

LIST OF FIGURES

1 INTRODUCTION

1.1 Background

Ionic conducting polymer film (ICPF) is a newly invented material. Strip of ICPF can give large and fast bending displacement in the presence of a low applied voltage in wet condition. However, as mentioned in the abstract, a special coating can also be added so that it can be operated in dry conditions. Research groups in NASA, New Mexico and Japan have put lots of effort in developing metal polymer composites and ionic polymer. Applications of wiper, gripper and biomechanics devices have been presented. However, to the best of our knowledge, all reported ICPF actuators have dimensions of greater than 1cm in length, greater than 2mm in width and a standard thickness of 200μm. At best, these actuators can be classified as meso-scale actuators.

1.2 Motivation of this project

Many micromachined actuators now exist which operate with different principles as mentioned. However, almost none of these micro actuators can be used in any biological applications because they must operate in a dry-environment. Although pneumatic micro grippers were ingeniously used under water to capture biological cells recently [1], slow frequency response and the inability to control individual appendages of the grippers impede these micro grippers from gaining general acceptance from the biological community. Therefore, in order to fulfill the great demand for new breed of under-water actuators and contribute to bio-MEMS and under-water MEMS, we would like to use ICPF to realize the concept of under-water micro gripper.

1.3 Organization

In this dissertation, background of perfluorosulfonic acid polymer and electroactive polymer is given in introduction. Applications of polymer materials in the past including biomechanics, biomimetics and space devices will be discussed in Chapter 2. Since the development of micro gripper has been a demanding issues in bio-MEMS in decade, which bring us to this research. Although other research groups have been developing micro grippers, however, in terms of materials and mechanisms, there is still plenty of room to make improvements. We have studied different polymer composites in order to invent a new breed of actuating material. Related studies on the choice of materials are reported in Chapter 3. After that, we will present a novel fabrication process in the next chapter that uses laser-micromachining to produce Nafion actuators with widths and lengths dimensions less than 500μm. Hence, a new breed of micro scale actuators is introduced to the MEMS community: actuators that can be actuated in an aqueous environment with large deflection, while using low actuation voltage. The design of the micro gripper is explained in Chapter 5, followed by the fabrication process. In addition, laser-micromachining technique (Chapter 6) can offer a relatively fast and inexpensive fabrication method, and will potentially give cheap and batch-fabricable Nafion micro actuators for biological applications. Our goal is to eventually create an array of micro actuators capable of operating in biological fluids. Details of the initial experimental results from our micro under-water actuators are presented in Chapter 7, after analyzed the relation between ICPF's material properties and bending performance, conclusion is drawn and future research path will be discussed.

2 LITERATURE SURVEY

2.1 Ionic Conducting Polymer Film (ICPF)

Ionic conducing polymer film is a kind of materials that can give large deflection in the presence of low applied voltage. The mechanism of ICPF is discussed later in this thesis. Generally, ICPF actuators give the best performance in a humid environment or wet condition, but they can be made as self-contained encapsulated actuators to operate in dry environments. They have been modeled as artificial muscles for biomechanics and biomimetics applications [2]. Melcher and Grodzinsky were the first to present a plausible continuum model for the electrochemistry of deformation of charged polyelectrolyte membranes and were the first to perform the same type of experiment on animal collagen fibers essentially made of charged natural ionic polymers and were able to describe the results through an electro-osmosis phenomenon. Kuhn and Katchalsky, however, were the first investigators to report the ionic chemomechanical deformation of polyelectrolytes such as polyarylic acid (PAA) and polyvinyl chloride (PVA) system. Kent et al. were also the first to report the electrochemical transduction of the PVA-PAAA polyelectrolyte system. More recently, De Rossi, et al., [2] have been experimenting with various chemically active as well as electrically active ionic polymers and their metal composites as artificial muscle actuators. Shahinpoor and his co-workers have recently presented a number of plausible models for micro electro-mechanics of ionic polymeric gels as electrically controllable artificial muscles in different dynamic environments.

2.2 *Electroactive Polymer (EAP)*

In recent years, electroactive polymers (EAP) materials have been recognized as potential actuators with unique capabilities of implementing biological muscles. Ion-exchange membrane metallic composites (IPMC) are one of the EAP materials with such a potential. The strong bending performance by IPMC offers attractive actuation for developing new mechanisms. Consider the practical applications for EAP has begun only in this decade because of the emergence of new materials that induce large displacements [Hunter and Lafontaine, 1992; Kornbluh, et al., 1995; and Bar-Cohen, 1999]. These materials are highly attractive for their low-density and large strain capability, which can be as high as two orders of magnitude greater than the striction-limited, rigid and fragile electroactive ceramics (EAC) [Bar-Cohen, et al., 1997; Osada & Gong, 1993]. In addition, these materials are superior to shape memory alloys (SMA) in their spectral response, lower density, and resilience. However, EAP materials reach their elastic limit at low stress levels, with actuation stress that falls far shorter than EAC and SMA actuators. The most attractive feature of EAP materials is their ability to emulate biological muscles with high toughness, large actuation strain and inherent vibration damping. EAP are referred as "Artificial Muscles" because of the similarity to biological muscles and potentially can be used to develop biologically inspired robots [3]. Such biomimetic robots can be made highly maneuverable, noiseless and agile, with various shapes including insect-like. Effective EAP offers the potential of making science fiction ideas a faster reality than feasible with any other conventional actuation mechanism. Unfortunately, the force actuation and mechanical energy density of EAP materials are relatively low and therefore limit the practical applications that can be considered. Further, there are no commercially available effective and robust EAP materials. To overcome these limitations there is a need for development in numerous multidisciplinary areas from computational chemistry, comprehensive material science, electromechanical

analysis as well as actuation characterization and improved material processing techniques. Efforts are needed to gain a better understanding of the parameters that control the electromechanical interaction. The processes of synthesizing, fabricating, shaping and handling will need to be refined to maximize their actuation capability and robustness.

2.3 Micro Active Guide Wire Catheter System

A new prototype model of micro catheter with active guide wire that has two bending degrees of freedom using Ionic Conducting Polymer Film (ICPF) has been presented by S. Guo [4]. Experimental results have shown that the model of the ICPF active catheter is reasonable for practical applications. The active catheter is one having the micro devices, which is installed with sensing and actuating elements. It can smoothly navigate through body cavities and even around soft tissue (aneurysms), and teleoperated by the surgeon. In order to implement intracavity intervention, micro active catheter (MAC) with multi-degrees of freedom has been demanding for long. Recently, several types of MAC have been reported, but compact structure is a difficult problem. Previously, active catheter with multi-degrees of freedom using SMA wire actuator has been presented. However there are some problems, such as cooling, response delay, leaking electric current, safety and so on. The MAC with multi-degrees of freedom and safety has never been developed so far. Researchers have put it a target to develop the MAC that has the characteristics of flexibility, driven by a low voltage, good response and safety in body. A new prototype model of micro catheter with active guide wire by using ICPF actuator on its front end as the servo actuator is presented. Active guide wires consist of micro hollow cable, ICPF actuator put into copper sheet electrode at the tip part is fixed by bonding. The lead wires for supplying electrical energy to ICPF as set through the lumina of

catheter. Since the displacement of the ICPF is proportional to the electrical voltage input on it as the swelling of polymer gels. It is because that electrical condenser is generated on the polymer membrane. The bending angle of active guide wire can be controlled by teleoperation. As a result, the catheter can select the moving direction at divergence's by inserting along the active guide wire, the photo of the catheter is shown in Figure 1.

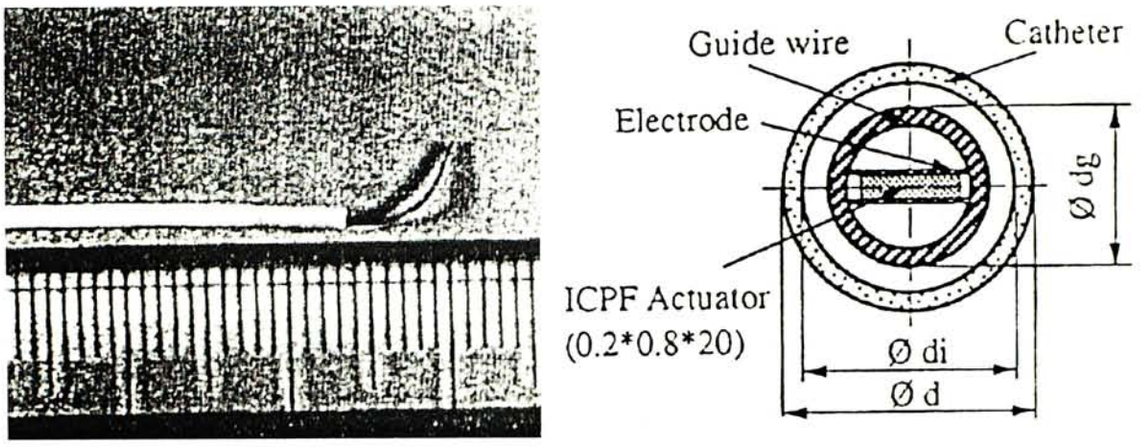

Figure 1 (Left) Photo of developed catheter (Right) Cross section of micro catheter [4].

2.4 Space Application – Dust Wiper

Other than ICPF, another kind of composite has recently been introduced by Y. Bar-Cohen [3]: ion-exchange polymer membrane metallic composites (IPMC), which are a perfluorocarboxylate-gold composite with tetra-n-butylammonium and lithium cations, and is claimed to have one of the most significant improvement of the material's electroactivity. Under less than 3V, a more then 90 degrees bending movement is achieved. The bending characteristic of IPMC offered an attractive actuation capability for a dust wiper in planetary applications and it was explored for the Nanorover's infrared camera window of the MUSES-CN mission. Like ICPF, since IPMC can also be used as actuators that are light, compact and driven by low power, the authors sought to take advantage of their resilience and fracture toughness to develop space applications. The harsh environment associated with space poses great challenges to the application of IPMC. These challenges have been the subject

of the NASA task called Low Mass Muscle Actuators (LoMMAs). Various issues that can affect the application of IPMC were examined including operation in vacuum, low temperatures, and the effect of the electromechanical and ionic characteristics of IPMC on its actuation capability. It has been proven that IPMC can be activated at low temperatures and vacuum, paved the way for the serious consideration of this class of materials for space applications [Bar-Cohen, et al, 1997]. Its bending characteristics offered the potential to address the critical issue of planetary dust that affects solar cells and imaging instruments on such planets as Mars. NASA Viking and Mars Pathfinder missions indicate that operation on Mars involves an environment that causes accumulation of dust on hardware surfaces. The dust accumulation is a serious concern that hampers long-term operation of optical instruments due to loss of visibility and degrades the efficiency of solar cells to produce power. To remove dust from surfaces one can use a similar mechanism as automobile windshield wipers. Contrary to conventional actuators, bending IPMC has the ideal characteristics that are necessary to produce a simple, lightweight, low power wiper mechanism. Specifically, the IPMC responds to activation signals at a frequency of less that 1 Hz with a bending angle that can exceed 90 degrees spans each way depending on the polarity. Since and IPMC wiper was demonstrated to remove dust effectively, the MUSES-CN mission selected it as a baseline technology for the Nanorover's infrared camera window. This mission is a joint effort of NASA and the NASDA (National Space Development Agency of Japan), which is scheduled to launch from Kagoshima, Japan, in January 2002, to explore the surface of a small near-Earth asteroid. An IPMC actuator drove the dust wiper, which was used for the technology demonstration. A blade with a fiberglass brush was attached to the actuator and it was used to mechanically remove dust particles that were sprinkled onto a glass plate [3].

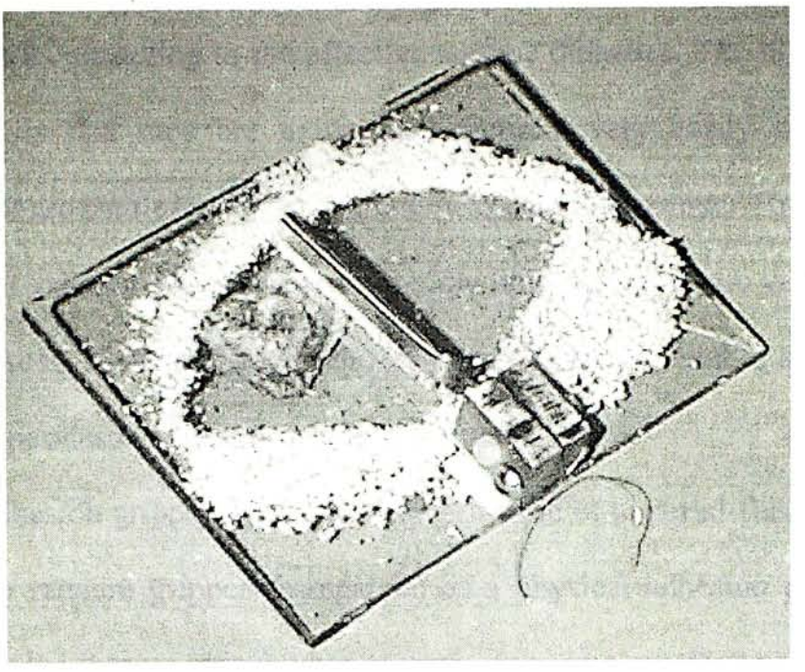

Figure 2 IPMC dust wiper removing sawdust from a glass window [3].

2.5 Micro gripper

As Microelectromechanical systems (MEMS) has become one of the leading research areas in the world. There is a high demand in the development of micro actuators and sensors, especially in the field of micro gripper. The goal of gripper development was the step-wise adjustment of conventional gripping techniques coming from macro-assembly to micro assembly. Hence, several gripper prototypes have been built which predominantly operate with conventional principles for holding force generation. With these prototypes, the required holding force is applied either by vacuum, by adhesion or mechanically by jaws using a DC-motor or piezoactoric drive. In this section, few types of grippers will be introduced, they are vacuum grippers, adhesion gripper, mechanical tong grippers with DC-motor drive, tong gripper with combined DC-motor and piezoactoric drive (Piezo-grippers).

In case of the vacuum grippers, it deals with miniaturized suctioning grippers with effective surface diameters between 0.1mm and 0.8mm. Thus, it is possible to already grip components with an admissible gripping surface of slightly more than

$0.01mm^2$. The holding forces to be produceable with these grippers range between 0.6mN and 38mN according to the effective surface diameter. The big advantage of these grippers is that they are to be manufactured very easily in miniaturized dimensions and are thus useable for extremely small components. The disadvantage however is that vacuum grippers-due to the low holding forces-are very sensitive to interference forces. This may lead both to an early loosening and to adhering of the part to the gripper despite switching off the vacuum.

The adhesion gripper is based on the principle of material-flush gripping and can-just as the vacuum gripper-be regarded as a physical adhesion process. As an adhesive, a small adhesive strip is used in case of the implemented prototype, which after each gripping process is further-cycled by a DC-motor. Loosening of the components is implemented by one or several needles penetrating the adhesive strip from above and thus pushing the components off the adhesive.

The developed mechanical tong grippers are driven by a DC-motor. The rotation of the motor is being converted via a gear-box and a threaded spindle into a linear motion of the gripper jaws. Apart from a two-jaw gripper in the case of which both gripping jaws are being driven by a left-right threaded spindle, a single-jaw gripper has been implemented too. In case of this, only one gripping jaw will be moved whilst the other is stationary. The latter variant has the advantage that the object to be assembled is principally centered to the stationary gripping jaw. Thus, the inaccuracies of the drive and the kinematics have no influence on the positioning and thus the repetitive accuracy of the gripper.

Base on the kinematics of the single-jaw gripper, another gripper with combined electro-motoric and piezoactroic drive has been implemented, the so-called piezo-gripper. In case of this gripper, the gripper finger of the mobile jaw is replaced by a piezo-bending-converter (see Figure 3). The electro-motoric drive thus enables to

pre-position the gripper jaws whilst with the help of the piezo-actor the requested gripping force can be applied in a very sensitive way [5].

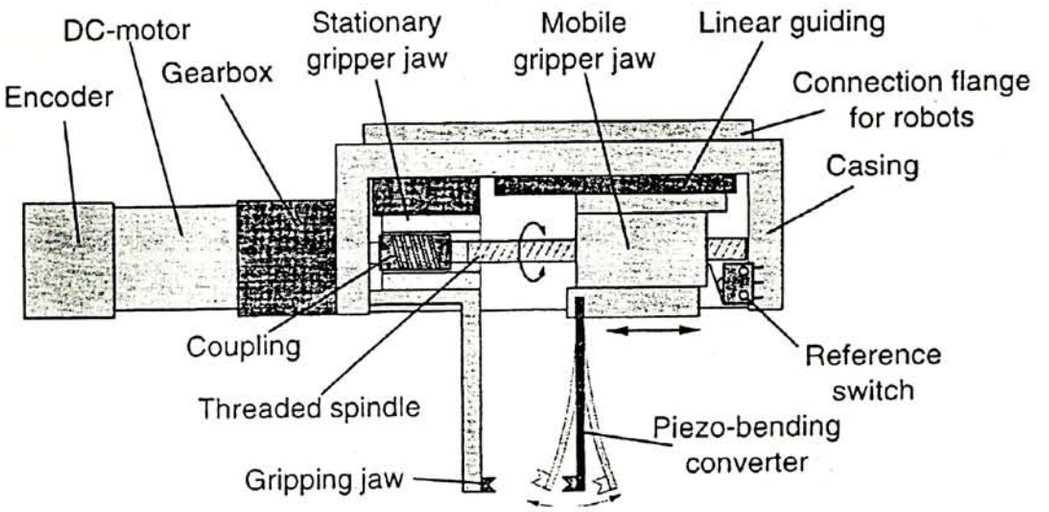

Figure 3 Basic built-up of piezo-gripper based on the single jaw gripper [5].

From the above grippers, it is noticeable that the ability to achieve a high repetitive accuracy is the most important focus point in building micro gripper. In this section, few types of micro grippers by other research groups are presented. A brief description of individual mechanism principle and theory of micro grippers will be discussed as introductory references of micro gripping concept. First of all, two kinds of micro grippers using SMA as a actuators are introduced, which are developed by Y. Bellouard [6] in Switzerland and S. Buttgenbach [7] in Braunschweig respectively. Then a laser powered micro gripper by W. Nogimori [8] in Japan is shown.

In the field of robotics, grippers using SMA technologies have been developed, but, so far, SMA is only used as the actuating part of the mechanical device. Y. Bellouard from Institut de Microtechnique, which use a high-resolution camera calibration, passive auto focus algorithms and 2D object recognition, can position the micro gripper in the 3D workspace so that it can be guided in future micro assembly tasks. The concept is to integrate all the functionality of the gripper within the same part: the jaws, the actuators, the reference surfaces and the interface

with the environment are cut out from the same sheet of material. Therefore, the only assembly operation is the fixing of the gripper on a support. The gripper is a shape like "crab-like tweezer" one and to achieve a good accuracy, the grasped object is referenced to two surfaces in the form of V groove shape (see Figure 4). Reversible motion is obtained by a training process, which leads to the so-called "Two-Way-Shape-Memory- Effect". The SMA material used in this gripper was a 200μm thick NiTiCu strip. The material was annealed for 10mins at 480°C (Ms=48°C, Mf=32°C, As=63°C, Af=82°C).

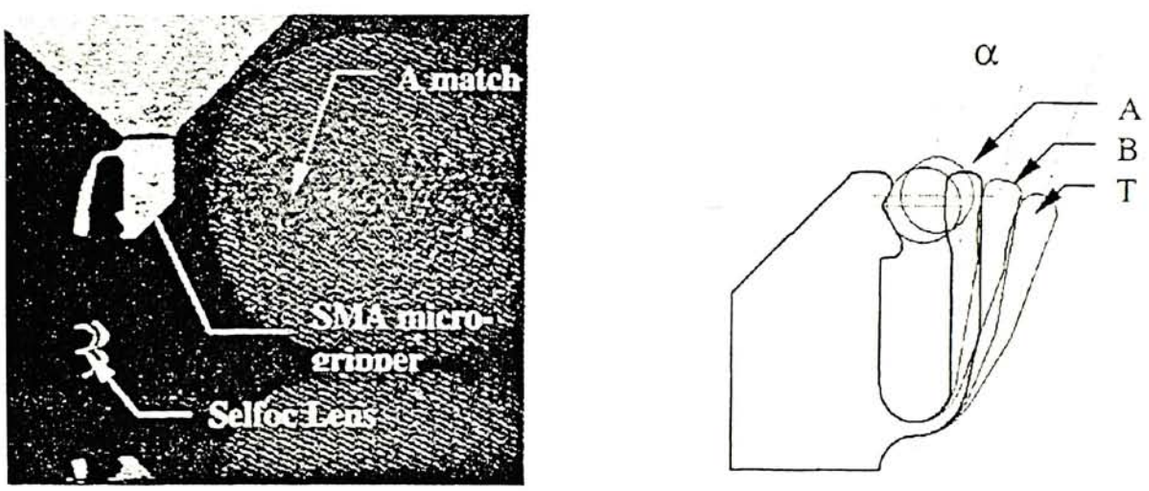

Figure 4 (Left) The micro gripper (Right) Design (A: austenitic shape, B: martensitic shape, T: "training shape") [6].

Another kind of SMA gripper is done by S. Buttgenbach. Based on the principle that tong-type grippers (grippers that are driven by a DC motor) are able to center the grasped objects and allow the measurement and control of the gripping force. However, the bearings and actuators generally used in conventional grippers are not suitable for application in cleanrooms because they release particles and lubricant while operating. Furthermore, friction and stick-slip effects in the bearings decrease the achievable accuracy and it is difficult to reduce the size of grippers equipped with such bearings and actuators. These problems can be overcome by

replacing conventional bearings and actuators by flexure hinges and new actuators such as shape memory actuators. Figure 5 (Left) shows the schemes of a gripper with flexure hinges that is based on a toggle mechanism. The gripper uses a single shape memory actuator in the form of a NiTi-wire with a diameter of 200μm. This gripper achieves the following characteristics: maximum gripping force = 0.5N, closing time = 0.5s, opening time =1.5s. The dynamical behavior can be improved significantly by using the differential-type configuration. Figure 5 (Right) shows the schemes of such a device. The first actuator closes the gripper, while the second actuator opens it. When the gripper is open, the actuators are balanced. To grasp and hold an object, the first actuator is heated quickly. If the second actuator is heated in the same way as the first one, the gripper will open and release the object as fast as it has closed before. The release time is reduced to the period that is necessary to heat the second actuator. After a complete closing-opening cycle, both actuators have to cool down. The shape memory elements consist of helical springs made of NiTi-wire with a diameter of 200μm. The gripper achieves closing and opening times of about 0.5s. The use of thinner wire or flat rolled wire would result in faster response. Since flexure hinges allow only angular motion a special four-bar linkage is used to center the grasped objects.

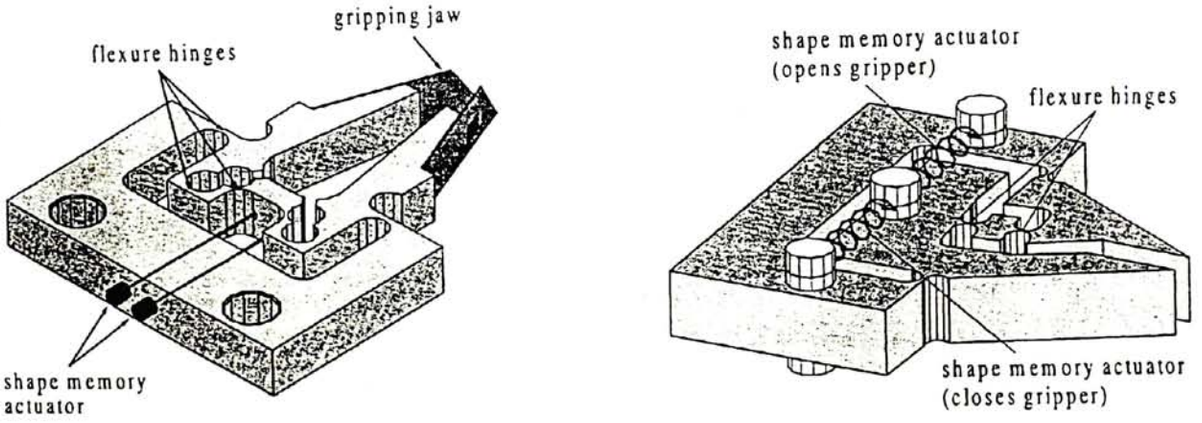

Figure 5 (Left) Toggle-type gripper with single actuator (Right) Differential-type gripper [7].

Apart from SMA actuated micro gripper, a micro gripper actuated by laser power was developed by W. Nogimori [8] in Japan. It is designed for handling micro objects in very narrow space or very crowded places, consists of a laser powered linear actuator and a photoformed micro gripper. This linear actuator's maximum output power was 2.3mN and the stroke length was 900μm, and the total dimension of the linear actuator is about 25mm in length and 2mm in diameter. The advantages associated with the laser powered actuation are that high energy density concentration in a tiny spot and high-energy transfer efficiency can be achieved. The energy of laser light is first absorbed and converted into heat, and then the low-boiling point power fluid is used to transform the heat into working force. The micro devices using this method can have a quick response and a micro pump (dimension 15mm x 4mm x 1.4mm) has been fabricated with this method. The gripper is shown in Figure 6. The laser power (wave length 830nm) is transmitted to the system through an optical fiber. The energy is transformed and output in form of mechanical actuation, and the actuator's end effectors is a micro gripper fabricated with photoforming technique. Further, micro gripper comprises a cylinder, a rod, operating fluid and power fluid.

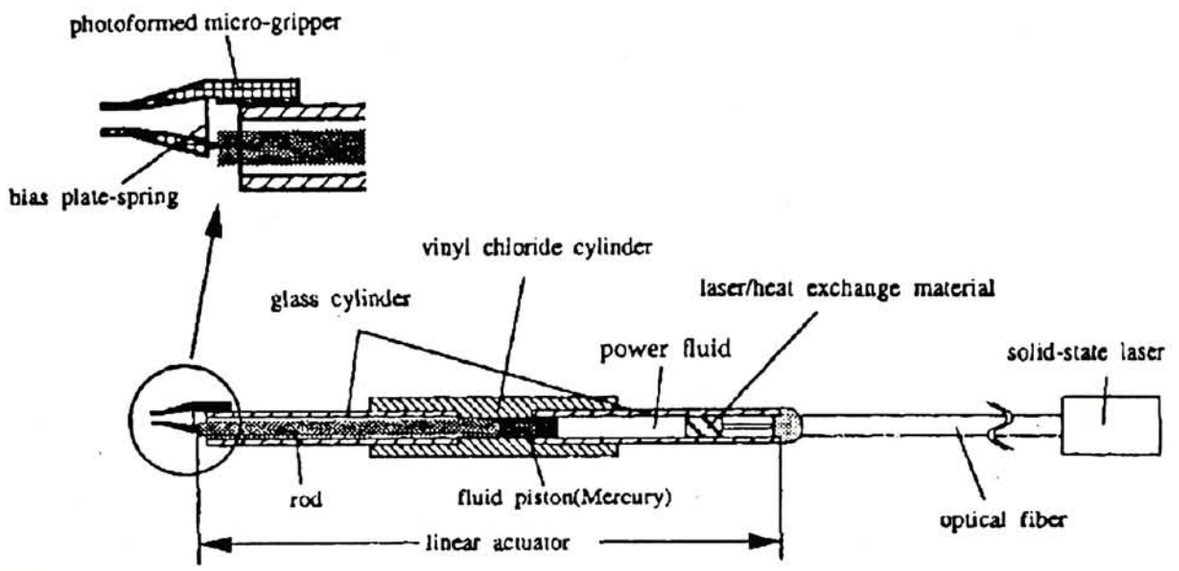

Figure 6 A laser powered micro gripper [8].

2.6 Summary of literature survey

As there has been a great demand for new actuating mechanism for micro devices especially in the development of micro grippers, it has been proved that a practical approach to realize micro gripping using SMA. Besides, few micro grippers is using other principles and designs have also been presented. However, material property limit is always a hindrance that prohibit further realization of gripping application for those micro gripping devices. To sum up, different from macro-gripping devices, the invention of micro grippers require high repetitive accuracy, low weight mechanism, actuation in small space, and possible for sensor integration and visual assembly monitoring. New materials that are able to give large deflection with low voltage such as EAP or ICPF are taking an important role as actuating mechanisms for micro grippers. With the special characteristics of polymer composites, it has become one of the key trends in developing charged polyelectrolyte membranes or ionic polymers and their metal composites as micro grippers, artificial muscles and micro sensors and actuators. Recently, research on ionic polymer composite has become more mature not only on macro devices, but also to MEMS and space application.

3 METAL-POLYMER COMPOSITIONS

3.1 Introduction

There is always an interest in developing new materials which can be served as micro actuators or sensors as well as to discover new applications for MEMS. Based on the ion absorption characteristic of acid polymer, it has become possible by the swelling of ion exchange membranes to act as micro actuators. In this Chapter, we will discuss the theory of ionic conducting polymer film. After that, comparison and analysis on using different kind of metals to serve as seed layer and electrodes are discussed. The goal of these findings is to develop a workable and reliable composition, which can gives the largest deflection without any defect on the metal thin film. One key factor to the choice of metal is the adhesion performance. To ensure a large deflecting actuation, a good metal to polymer attachment is needed. Furthermore, based on mechanical property like the elasticity, a new breed of metal-polymer composites can be chosen.

3.2 Perfluorosulfonic acid polymer (Nafion)

Nafion 117 (Figure 7), produced by Dupont, with a thickness of 0.18mm is chosen to serve as the polymer part for the composition. Nafion 117 membranes are non-reinforced films based on Nafion 117 resin, a perfluorosulfonic acid copolymer in the acid (H^+) form, the chemical formula is shown as below:

$$[-(CF_2\text{-}CF_2)_n\text{-}CF\text{-}CF2\text{-}]_m$$
$$|$$
$$O\text{-}CF\text{-}CF_2\text{-}O\text{-}CF_2\text{-}(SO_3^-)M^+$$
$$|$$
$$CF_3$$

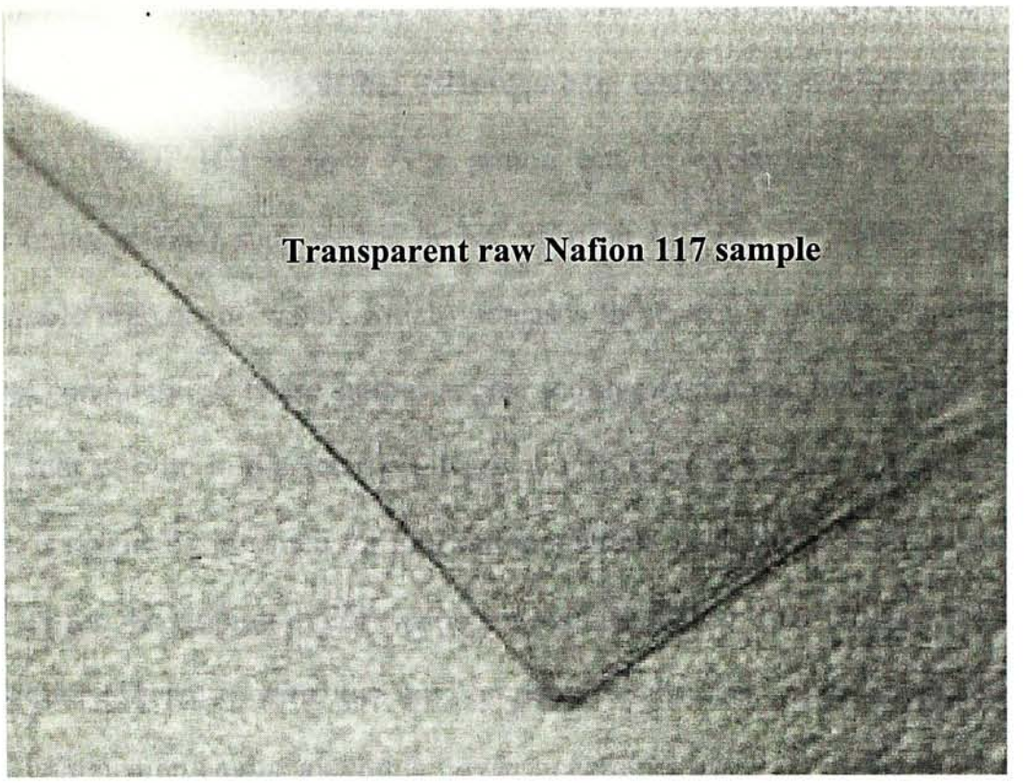

Figure 7 Nafion 117 sample piece.

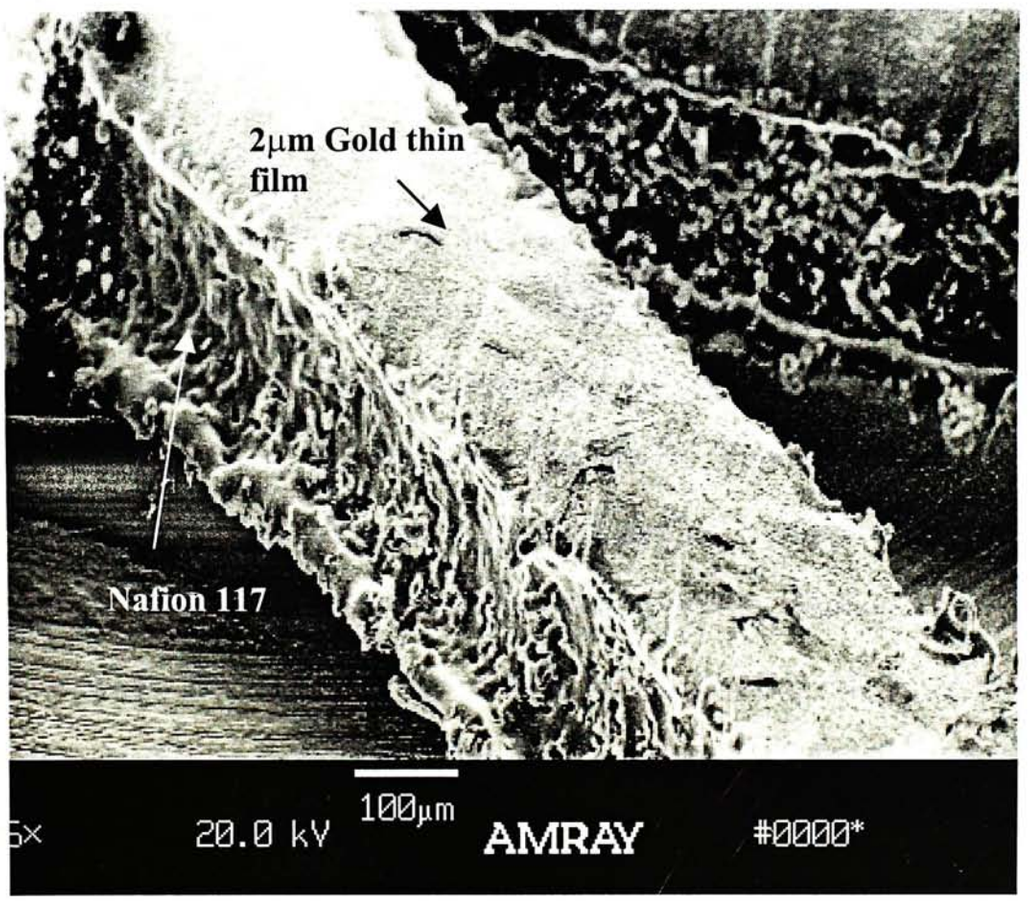

Figure 8 SEM image showing the composition of gold thin film and Nafion.

where n ~6.5, 100<m<10000, and M^+ is the counter ion (H^+, Li^+ or Na^+). These polymers consist of hydrophobic (fluorocarbon backbone, semi-crystalline) and Hydrophilic ($-SO_3^- H^+$) regions. The proton can be exchanged for other mobile cations (counter-ions) such as Li^+ or Na^+. Nafion 117 has the ability to absorb a considerable amount of water, which increases the cation's mobility and therefore electrical conductivity. These cations appear to migrate through hydrophilic channels on the order of 5nm in diameter [9]. Nafion, according to product information from Dupont, is originally invented for fuel cell membrane application. Fuel cells utilizing H_2 and O_2 are developing rapidly as power sources due to their unique combination of high fuel efficiency with low environmental emissions, when compared to the internal combustion engine and other power generators based on the burning of fossil fuels.

A Nafion membrane separates the H_2 (anode) side of the cell from the O_2 (cathode) side of the cell. A catalyst, coated onto each side of the Nafion membrane, promotes the dissociation of H_2 at the anode and the formation of water at the cathode. Successful movement of the fuel cell relies on the fact that the membrane transports the H^+ formed at the anode, yet will not allow significant O_2 or H_2 to cross. Electrons, released from the H_2 are drawn out of the cell through a load device and returned to the cathode, thereby producing power. Highly conductive Nafion membranes allow the fuel cell to run at high currents and voltages. A fuel cell stack contains many layers of individual cells in order to provide additional power. Fuel cells have run for thousands of hours without failure, possibly due to the excellent stability of the Nafion membrane. Table 1 shows the properties of Dupont Nafion perfluorinated membrane.

Properties of Nafion® Perfluorinated Membrane

A. Thickness and Weight Caliper Properties[2]

Membrane Type	Typical Thickness (mm)	Weight Caliper (g/dm^2)
NF-112	0.051	1.0
NF-1135	0.089	1.9
NF-115	0.127	2.5
N-117	0.183	3.6

B. Physical and Electrical Properties

Property[3]	Typical Value	Test Method
Physical Properties		
Tensile Modulus, MPa (kpsi)		
50% RH, 23 °C	249 (36)	ASTM D 882
water soaked, 23 °C	114 (16)	ASTM D 882
water soaked, 100 °C	64 (9.4)	ASTM D 882
Tensile Strength, maximum , MPa (kpsi)		
50% RH, 23 °C	43 (6.2) in MD, 32 (4.6) in TD	ASTM D 882
water soaked, 23 °C	34 (4.9) in MD, 26 (3.8) in TD	ASTM D 882
water soaked, 100 °C	25 (3.6) in MD, 24 (3.5) in TD	ASTM D 882
Elongation at Break, %		
50% RH, 23 °C	225 in MD, 310 in TD	ASTM D 882
water soaked, 23 °C	200 in MD, 275 in TD	ASTM D 882
water soaked, 100 °C	180 in MD, 240 in TD	ASTM D 882
Tear Resistance - Initial, g/mm		
50% RH, 23 °C	6000 in MD, TD	ASTM D 1004
water soaked, 23 °C	3500 in MD, TD	ASTM D 1004
water soaked, 100 °C	3000 in MD, TD	ASTM D 1004
Tear Resistance[4] - Propagating, g/mm		
50% RH, 23 °C	>100 in MD, >150 in TD	ASTM D 1922
water soaked, 23 °C	92 in MD, 104 in TD	ASTM D 1922
water soaked, 100 °C	74 in MD, 85 in TD	ASTM D 1922
Density, g/cm^3	2.0	-
Electrical Properties		
Conductivity, S/cm	0.083	see footnote [5]

[2] Measurements taken with membrane conditioned to 23 °C, 50% relative humidity (RH).

[3] Where specified, MD - machine direction, TD - transverse direction. Conditioning state of membrane given. Measurements taken at 23 °C, 50% RH.

[4] Tear resistance (g/mm) of dry membrane increases with thickness. Values given are typical for 0.05 mm membrane.

[5] Conductivity measurement as described by Zawodzinski, et.al, *J.Phys. Chem.*, 95 (15), 6040 (1991). Membrane conditioned in 100 °C water for 1 hour. Measurement cell submersed in 25 °C D.I. water during experiment. Membrane impedance (real) taken at zero imaginary impedance.

Table 1 Properties of Nafion Perfluorinated Membrane (provided by Dupont's product information).

3.3 Working principle of ICPF

Ionic Conducting Polymer Film (ICPF) is a newly invented material. A sandwiched film of perfluorosulfonic acid polymer (Nafion) is placed between two thin film layers of metal such as platinum and gold, which serve as metallic electrodes. We have chosen gold as the electrodes. Details will be discussed later. As shown in Figure 8, ICPF is the composition of a thin film layer of gold (2μm thick) on both sides of Nafion 117 (180μm thick) as the electrodes. In other words, ICPF is a gold and polymer composite. Strips of these composites can undergo large bending and flapping displacement in the presence of a low applied voltage in wet condition.

The mechanism of the bending motion is roughly due to uni-directional electroosmosis by cations, with their water solvent sheath, toward the cathode. Water enrichment at the cathode and depletion at the anode cause bending due to differential swelling and shrinkage [9]. As in Figure 9, when a voltage is applied to a normal electrolyte, cations and anions migrate in opposite directions because no net momentum is transferred to the solvent due to electroosmotic pressure. No solvent is transported other than those contained in the solvation shells. However, in ion exchange membranes the solvent can be carried by both ion-dipole interaction and momentum transfer. In Nafion 117, the $-SO_3^-$ group is fixed to the matrix while the counter-ion (cation) is free to move. When voltage is applied to the hydrated sample, the counter-ion will migrate to the cathode and simultaneously push water to this side. Thus, swelling and expansion at the cathode results (see Figure 10).

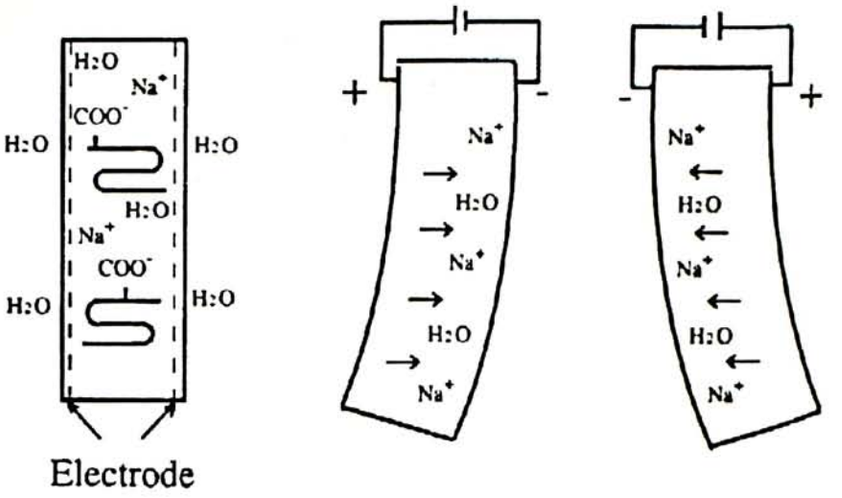

Figure 9 Schematic of the bending motion [10].

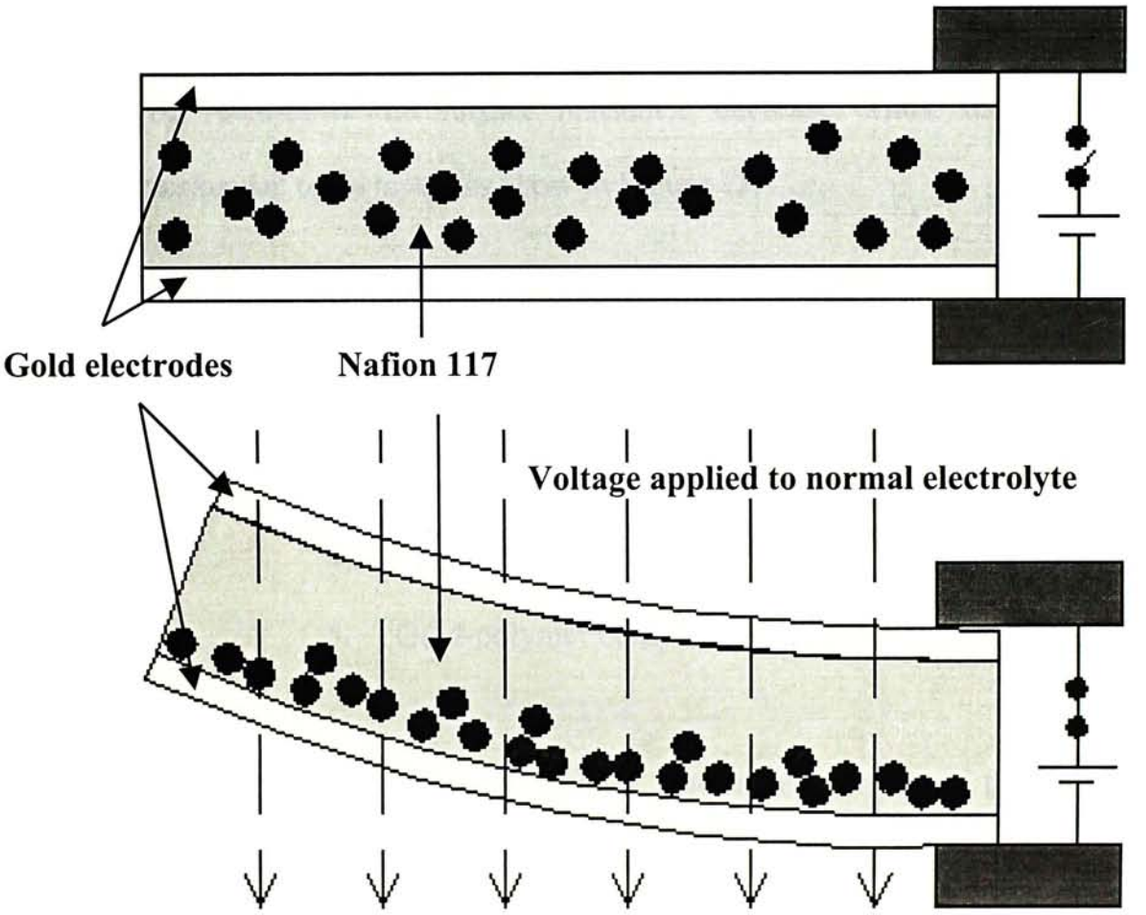

Figure 10 Series of bending principle drawings.

3.4 Different types of composition

In the previous Chapter, the working principle of ICPF is discussed. Based on this special mechanism, we are able to develop and fabricate a high bending performance metal-polymer composite. Before fabricating the composites, we have found a suitable match up between metal and polymer in order to achieve good adhesion and high deflection. We will demonstrate different metal-polymer composites and report their behaviour. There are three criterias that help us find the most suitable composite for fabrication. The first factor is the adhesion between the composite; if the metal film does not stick well on the polymer surface, it will peel off during actuation, hence give no bending motion. The second factor is that we have to compare the elasticity of the metal-polymer composites because they affect the magnitude of deflection. Power consumption can be reduced if the surface resistance decrease. Thus, the following five composites are to be tested as show in Figure 11.

1. Chromium-gold-polymer
2. Platium-gold-polymer composite
3. Silver-polymer composite
4. Silver/Copper-polymer composite
5. Gold-polymer composite

Since Nafion 117 films have a fluorinated structure, the poor surface adhesion of any coating restricts the controllability & stability of actuators. Metal deposited on the polymer surface peels off easily without any appropriate surface pre-treatment. Bar-Cohen et al. [9] reported workable solutions using a chemical etchant (Tetra-etch®) to etch the surface or to introduce a seed layer between the metal and the polymer. In this project, we develop a thin film of seed layer in

between Nafion 117 and metal to overcome the peeling problem. Gold is chosen to be the electrodes in order to make sure a good adhesion. Chromium, platinum and silver coating compounds were tested as a seed layer. All the fabricated composites were cut into identical strips before running any test and making any comparisons, as shown in Figure 12.

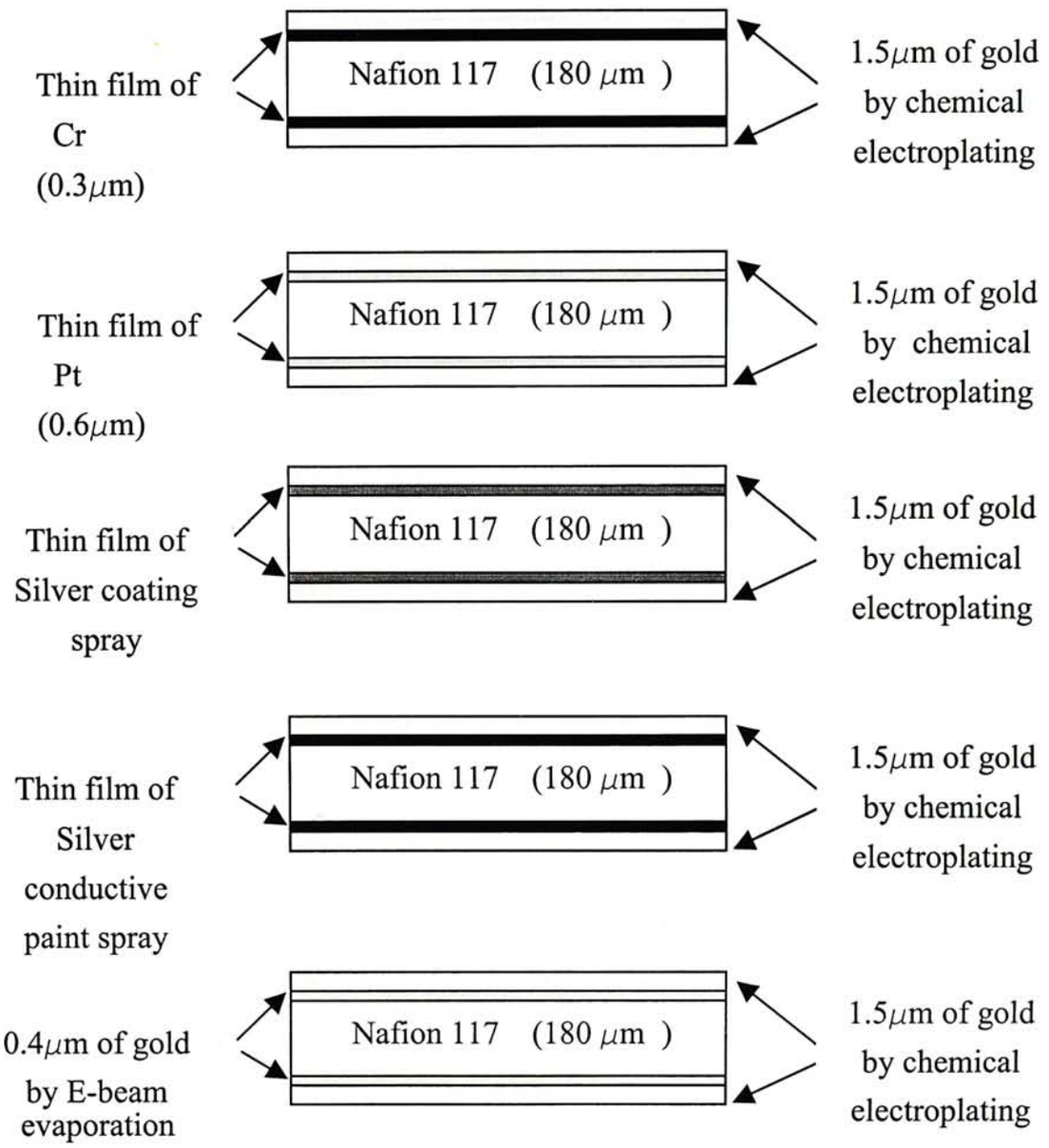

Figure 11 Different metal and polymer composition.

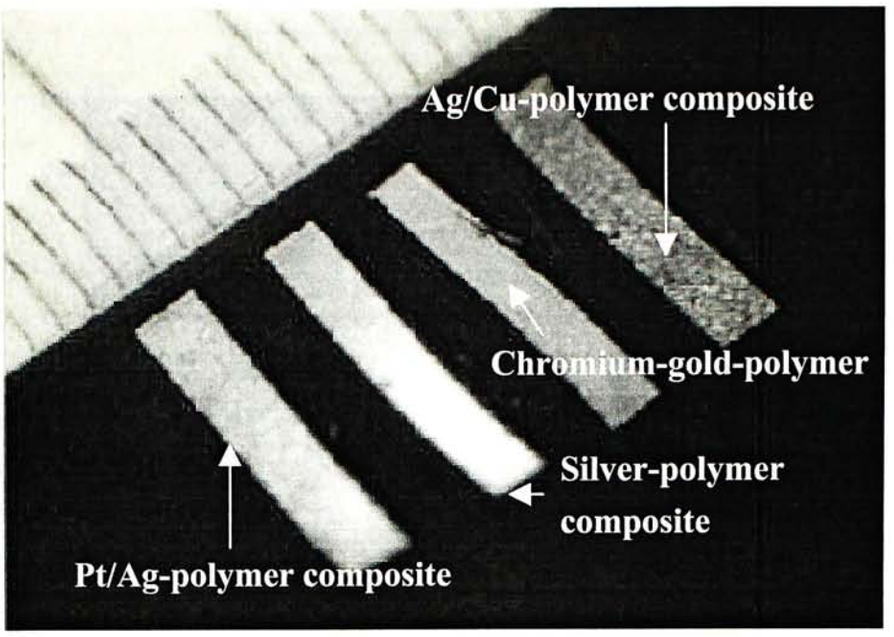

Figure 12 Four different kinds of metal-polymer composites with dimensions of 6mm x 1.5mm.

3.4.1 Chromium-Gold-polymer composite

We first apply a surface treatment on the raw Nafion 117 to remove impurities and dusts. Details of fabrication technique will be discussed in Chapter 4. After pretreatments, a thin film layer of 0.3μm chromium is evaporated on both sides of Nafion 117 film, followed by a deposition of 1.5μm of gold. Since chromium has good adhesion with many materials, especially metals, we decide to use it as a seed layer on the composition. However, residual stress is induced due to the high temperature process in evaporation (~1000 °C) and different thermal expansion rate between chromium and gold, as a result, the surface or the composite is cracked as shown in Figure 13. Existence of cracks greatly reduced the adhesion between the metal and the polymer surface; the consequence is that the metal will peel off easily. In addition, as shown in Table 2, chromium has a high modulus of elasticity which becomes a limiting factor for the chromium-gold-polymer composite to produce large deflection. In short, cracking of metal layer surface due to residual stress between gold and chromium, leads to peeling problem after voltage is applied on the samples. Hence, this kind of composite is not a good choice in making ICPF actuators.

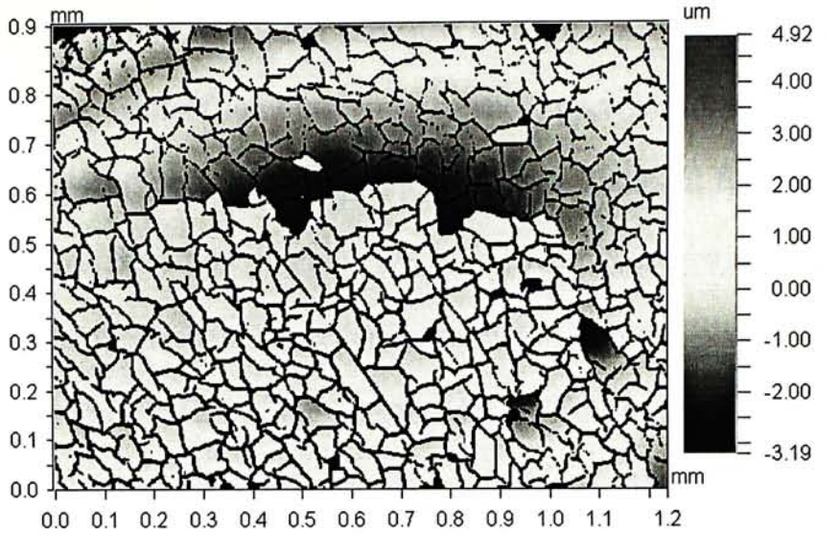

Figure 13 An interferometric image showing a cracked surface of chromium-gold-polymer composite.

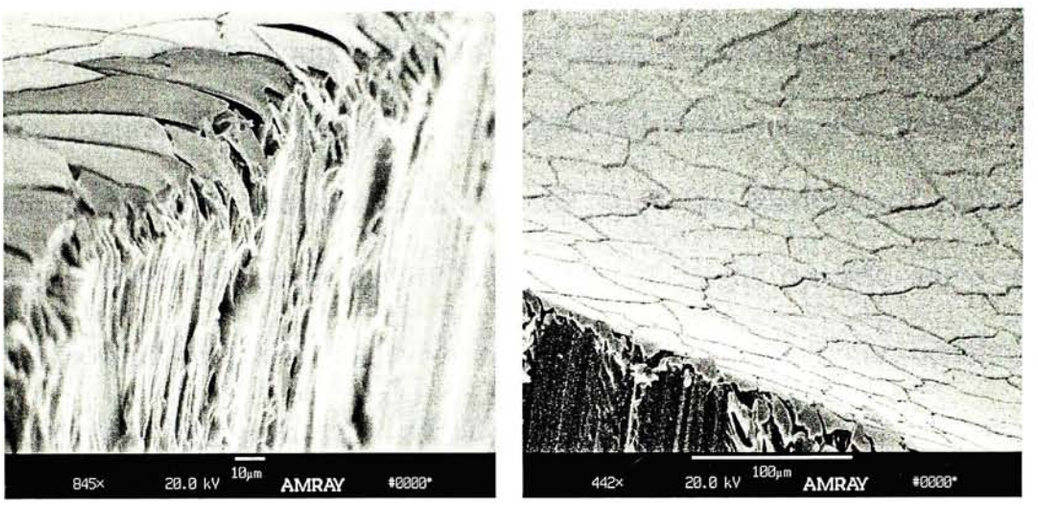

Figure 14 SEM image showing (Left) close up of cracks (Right) cracked Cr/Ag on Nafion .

	Standard Mechanical Property Modulus of elasticity (GPa)	**Thin film used in semiconductor Modulus of elasticity (GPa)**
Gold (Au)	77.2	80
Chromium (Cr)	248	185-215
Platinum (Pt)	171	170
Silver (Ag)	76	-

Table 2 Mechanical property, the Modulus of elasticity of sample testing metals [11].

3.4.2 Platinum-Gold-polymer composite

Besides chromium, platinum was also tested as seed layer of the composite. In the early development of ionic polymer science, platinum has been chosen to be the electrodes of metal polymer composite by Osaka National Research Institute in Japan for few years. Based on this fact, we have tried to use platinum as a seed layer and also part of the electrodes. However, as shown in Table 1, platinum is still a hard metal compared to gold. This is the reason why we do not prefer to deposit 2μm of platinum as the electrode. Instead, 0.4μm to 0.6μm of platinum are first added on both sides of cleaned Nafion 117 as a seed layer for adhesion and then followed by 1.5μm of gold as the electrodes. By doing this, we wish to develop a new composite that has good metal-polymer adhesion with adequate elasticity to produce large deflecting motion. Compared to chromium-gold-polymer composite, the hardness of platinum-gold-polymer composite is reduced since the Modulus of elasticity of platinum is much less than that of chromium. A larger bending angle without cracking the surface can be achieved, in other words, the maximum bending angle that the composite can withstand without cracking the metal thin film is increased as shown in Figure 15. In spite of this advantage, the residual stress problem due to high temperature process during evaporation still exists, but definitely better then chromium since the thermal expansion of gold and platinum is much closer to each other (Table 3). However, when voltage of over 7V is applied on a testing strip, the metal layer still peel off. When this happens, the deflecting motion of the testing composite stops consequently.

	Coefficient of linear expansion at 25°C (1E x –6 K^{-1})
Chromium (Cr)	4.9
Gold (Au)	14.2
Platinum (Pt)	8.8
Silver (Ag)	18.9

Table 3 The thermal property of different metal [11].

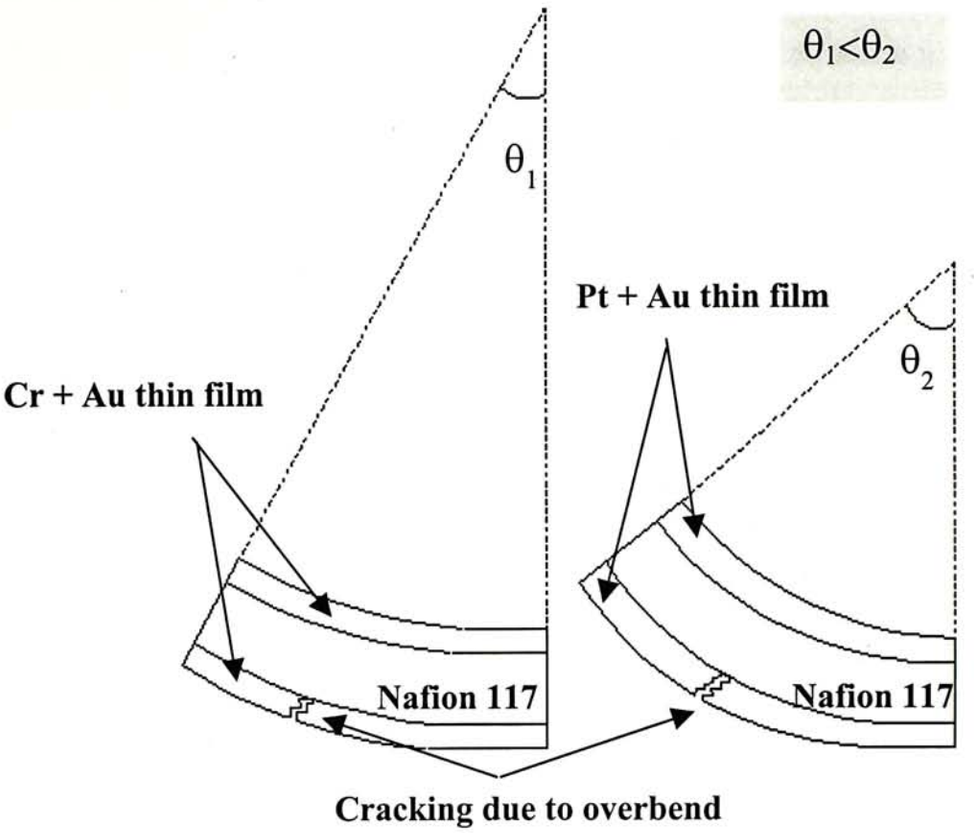

Figure 15 Different bending limit for different metal-polymer composite.

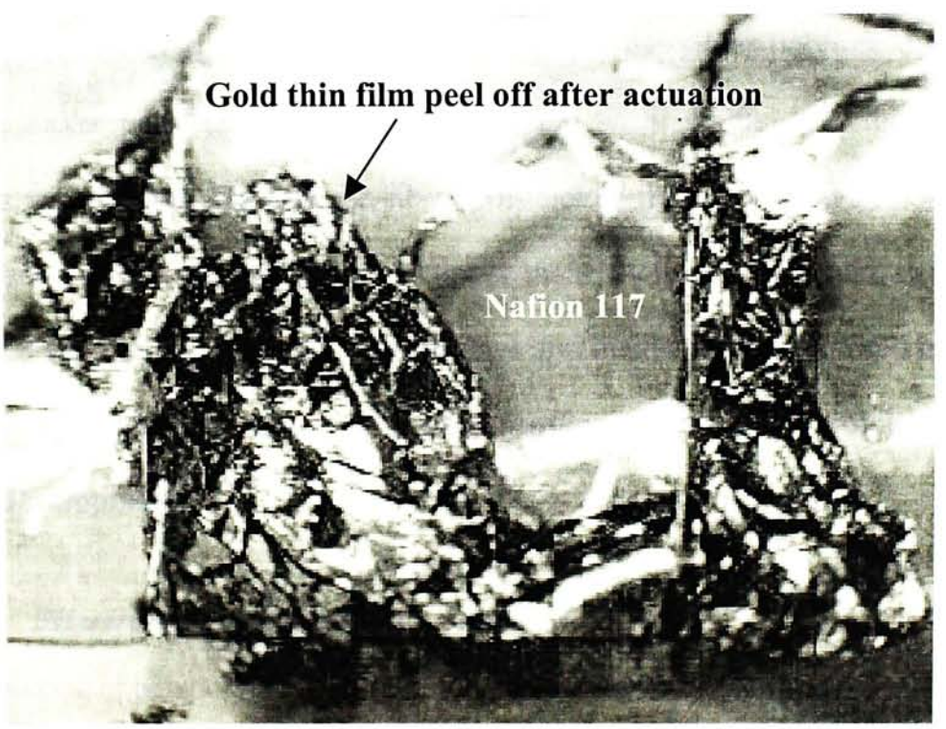

Figure 16 Peeling off problem.

3.4.3 Silver-polymer composite

Due to the limitation of the evaporation process, we cannot lower the deposition temperature to alleviate the unbalanced thermal expansion effect of different layers of thin film. In order to solve this problem, we have to find another way of doing the thin film deposition. In this case, we use direct metal printing technique instead of thermal evaporation; we painted the metal thin film onto Nafion 117 for deposition. Silver conductive paint (product of Electrolube®) is used. Silver conductive paint is normally used to create a thin, smooth, flexible and adherent film that has a high electrical conductivity (electrical conductivity: 0.1 to 1.0W/cm^2, sheet resistance: 0.01 to 0.03Ω/sq). We tried to use silver-polymer composite because silver has a close flexibility to gold (Table 2). Since silver has similar modulus of elasticity as gold, it can be used as the electrodes on Nafion 117 without introducing any seed layer in between but can still have high flexibility. Thus, we do not use silver as a seed layer, but use it as a electrode layer for actuation. This is the reason why no further layer of gold thin film is added on the silver-polymer composites. Basically, silver paint has a very good adhesion with Nafion 117, the composite made was not too hard. Though, the silver-polymer composite testing strip gives very little deflection 5V actuation, if voltage larger then 10v is applied on the strip instead, such a high voltage will burn the silver surface and makes the layer turned into black, performance significantly decay. The poor bending performance prohibited further actuator development.

3.4.4 Silver/Copper-gold polymer composite

Silver/Copper-polymer composite actually is a combination of a silver coated copper screening compound film and Nafion. Silver coated copper screening compound (product of RS Components Limited) is designed to give low resistance even in thin layers on plastic electronic housings and will adhere to a wide variety of

substrates. It is commonly used on the inside of computer cabinets, which has surface resistivity of 0.3-0.7Ω/sq. Thin film of silver coated copper screening compound is sprayed on the surface of Nafion, it will touch dry after 5 minutes and give maximum conductivity after 24 hours. However, in practical situation, we have to spray several times in order to achieve a good conductive surface, a significant drawback is the uncertainty of the thickness. It is extremely hard to measure the thickness of the sprayed metal because after spraying, the silver/copper compound will form a rough surface, which is unable to be measured by optical instruments or unreliable to be measured by means of mechanical methods. Furthermore, after several times of spraying, the dried spray film gives a low flexibility, it is not like silver-polymer composite which can give large deflection angle without any cracks. In summary, although the use of silver coated copper screening compound has solved the adhesion problem, but surface roughness as well as the calibration of the thickness, and also the poor elasticity of the composite that limited the magnitude of deflection led us to relinquish this potential alternative.

3.4.5 Gold-polymer composite

Based on the experiences, we have much clearer idea on choosing a suitable metal-polymer composite. It turns out that we have two approaches to go; the first one is to avoid high temperature process, which is to look for a direct printing or spraying method with a reliable and workable calibrating technique and with good flexibility. The other way is to retain evaporation practice, but in a sense that to work out an alternative in order to minimize cracking effect brought from residual stress. It is not easy to fulfill the former approach because of the limitation from both the material's availability and equipment constraints. Silver painting or silver-copper mixing spray is the most practical material used in semi-conductor. However, most of them are applied on silicon or metal substrates, but not on polymer areas. In

addition, in daily IC manufacturing, all the spraying and printing procedures are automatically run in semi-conductor fabrication process with high-resolution sensors to calibrate the deposition conditions. In addition, the flexibility of the above material is not a major concern. Base on these criteria, we have to move to the second direction, which is evaporation. As mentioned before, the major concern of doing thermal evaporation is the different thermal expansion rate among different metals. The most vital thing is to avoid cracking. Finally, we have decided not to involve any seed layer between the electrodes and Nafion 117 in order to eliminate the residual stress effect. This can ensure the metal layer will not crack and in a sense that the composite can finally be possible to became ICPF actuators. We actually use 0.2μm of gold as the electrodes and served as the seed layer at the same time, which is gold-polymer composite. In next Chapter, we will further discuss the details of how to fabricate the gold–polymer composite.

4 ICPF FABRICATION

4.1 Introduction

The development of ionic polymer-metal composites actuators requires an interdisciplinary study in chemistry, materials science, controls and robotics. Mechanisms such as micro end-effectors, grippers and micro robotic arms involve great deflection and have unique design and fabrication challenges. After testing different metal-polymer composites, gold-polymer is found to be the most suitable combination in term of adhesion and flexibility. However, a reliable and repeatable fabrication is highly desired. Concentrations of the working solution, temperature of evaporation and deposition rate are some of the major parameters. Besides, a thin film calibration and measurement should be done. The ICPF fabrication process can be classified into three parts; surface pre-treatment, gold thin film deposition and laser micromachining. The first two processes will be discussed in this chapter, and laser micromachining will be discussed in Chapter 6. Our main target is to develop a novel and reliable fabrication process to deposit 2μm of gold on Nafion 117 and then laser micromachined by laser. In order to ease the peeling problem and residual stress mentioned in Chapter 3, two levels of gold depositions are specially designed, evaporation and chemical electroplating. Filament evaporation and Electronic-beam (E-beam) evaporation are used. Details will be discussed in the following sections. The second level deposition is chemical electroplating, which is a more effective and economical way of doing gold thick film deposition. After added gold electrodes on Nafion 117, the final stage is to laser micromachine the gold-polymer composite, which will become an ICPF actuators. Two kind of lasers have been applied to do the cuts; CO_2 laser and Nd:YAG laser. Cutting performances and results will be covered in Chapter 6. A summary of fabrication process and outline flow chart (Figure 17) are shown as follow:

4.2 ICPF fabrication process

The fabrication process can be summarized as the following 10 steps, and details of individual procedures will be discussed in the following sub-Chapters.

1. Raw Nafion 117, a kind of perfluorosulfonic acid polymer film from DuPont® (thickness = 0.18mm in A4 size).
2. Use cutter to separate the Nafion 117 film into sample pieces, 25 cm^2/sample.
3. Rough the sample surface using Silicon carbide with class 1500CW.
4. Rinse the roughed sample piece by DI water to remove residual.
5. Fully immerse the roughed sample piece into 10% Hydrochloric acid, and clean the surface using N_2 blow dry.
6. Use deionized water to rinse the sample again to make sure that there are no impurities left on the polymer.
7. Repeat steps 5 and 6 several times.
8. By using E-beam evaporation, deposit a thin film (0.4μm) of pure gold on both side of the treated sample under pressure of 10^{-7}torr, with E-beam current of 1.1A, power of 3700V x 110mA and with deposition rate of around 7 Angstroms/sec.
9. Deposit another 1.5μm of gold using chemical electroplating solution (Elconac138, chemical product from Chartermate International Ltd.) with 0.02A, 2.3V for 5 minutes at room temperature.
10. Laser micromachine ICPF sample pieces to cut out the designed actuators.

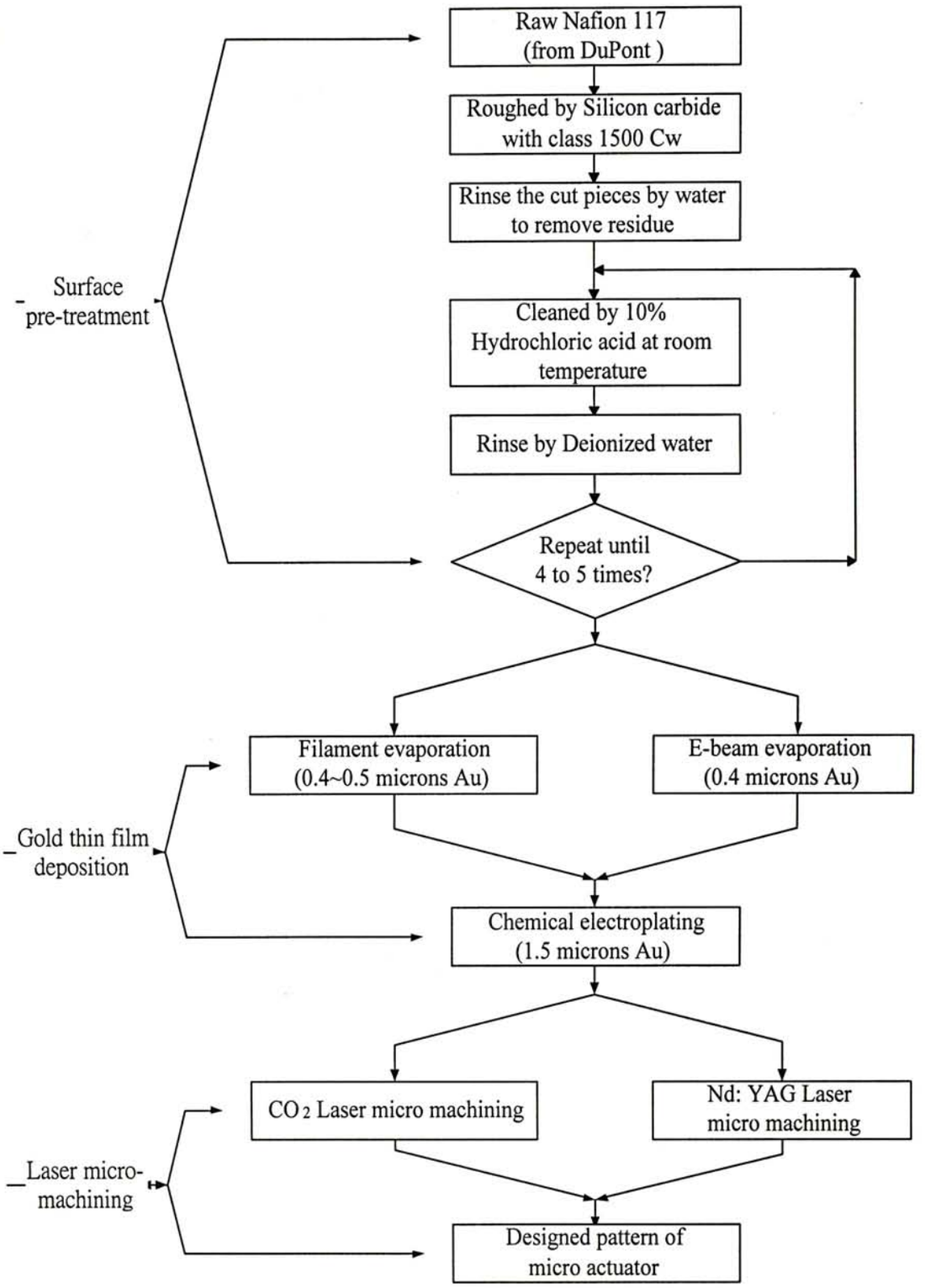

Figure 17 Flow chart showing the process flow of ICPF actuator.

4.3 Surface pre-treatment

In Chapter 3, different metal-polymer composites were discussed. Basically, electrode-coating was an obstacle due to poor adhesion of the fluorinated polymer structure. Peeling-off problem always appears in the deposited metal layer if no appropriate treatment were done beforehand. In our fabrication method, before any metal deposition, an inevitable surface pre-treatment is needed in order to make sure the surface of the Nafion 117 is ready for deposition. The polymer membrane surface is roughed by fine sand paper (Silicon carbide with class 1500CW) in order to increase the surface area. Tiny grids were roughed on the Nafion surface, (see Figure 18), and the existence of the grids present a good adhesion medium for deposition of gold thin film, which allowed a reliable attachment between the two different materials.

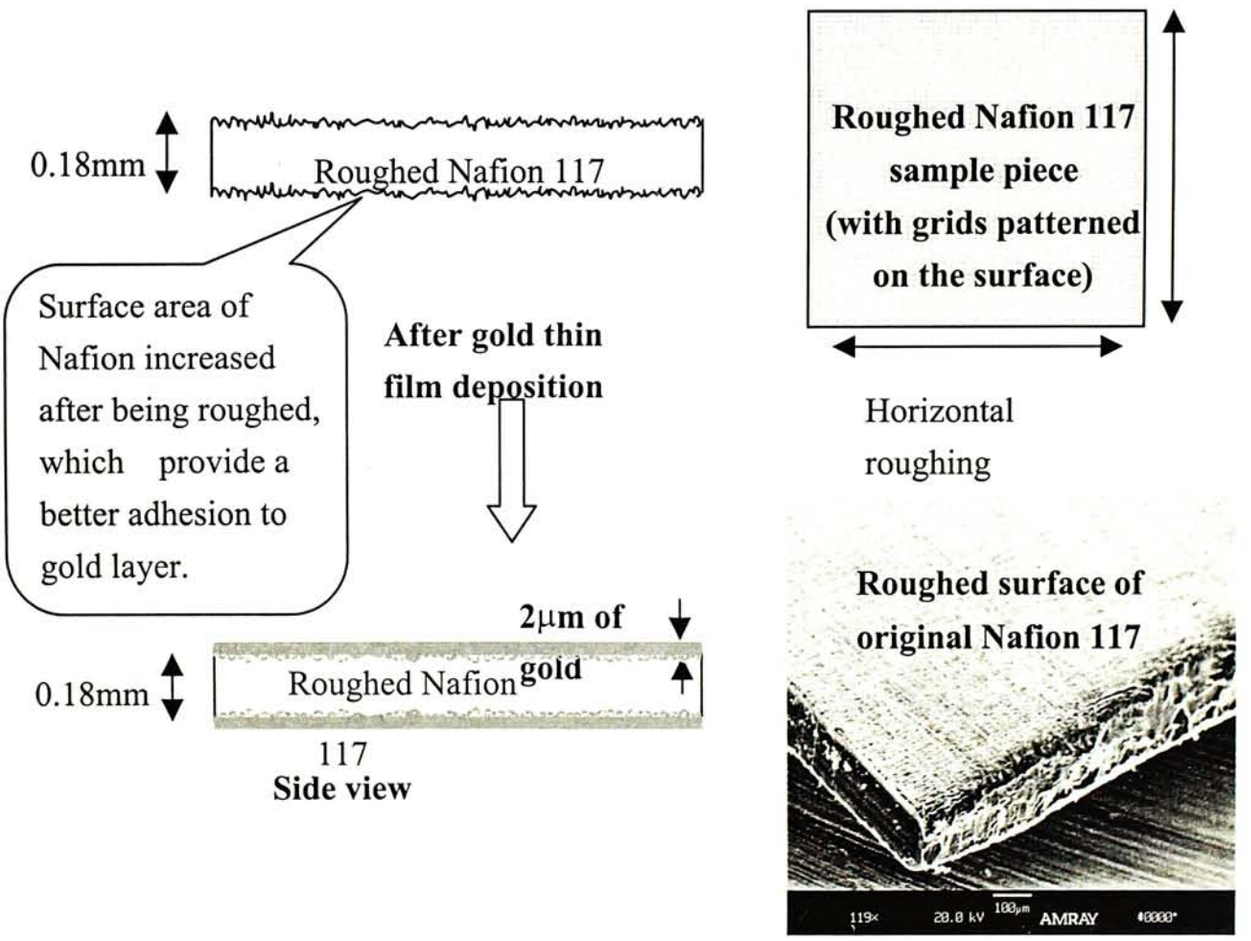

Figure 18 Drawings explaining how pre-treatment (roughing) is done and SEM image of roughed surface.

4.4 Gold thin film deposition (Evaporation)

In section 3.4.5 (Gold-polymer composite), we have demonstrated that selection of seed layers for polymer composites is important to ICPF actuators in terms of material elasticity and thermal residual stress. Two approaches of making the composite have been suggested previously but due to reliability and repeatability, we have shifted to use evaporation for deposition in order to thrust aside the residual stress problem. No seed layer from different metal is added in between the gold layer and the surface of the polymer. Since gold layer is the only material placed on Nafion 117, residual stress due to different thermal expansion rates of metals does not exist; this can greatly reduce the chance of having cracks on the thin film thus improve the peeling off problem. Since there is no seed layer involved in the process, a new concern is developed: how to make 2μm of gold stick well on polymer? A special process was designed to eliminate this complication. A thin film (about 0.4μm) of gold is first deposited on both sides of the roughed polymer film using E-beam evaporation (the difference between using filament evaporation and E-beam evaporation will be discussed later). Then, a thick film (about 1.5μm) of gold is coated on the polymer surface by chemical electroplating. A satisfactory adhesion is achieved based on the above fabrication procedures. The purpose of doing 0.4μm of gold deposition is similar to the function of seed layer. After thin film of gold is evaporated on both sides of Nafion by E-beam evaporator, then an additional 1.5μm of gold can be placed on the existing gold layer by chemical electroplating. The pre-deposited layer of gold can serve as the conductive medium with good adhesion for chemical electroplating. Since this process only involves one kind of metal, which is gold, therefore the peeling problem mentioned in Chapter 3 is eliminated. We will point out in the section below why we use E-beam evaporation rather then filament evaporation for the 0.4μm deposition.

4.4.1. Filament evaporation

Evaporation is a widely used physical deposition process. Gold deposited starts out as a solid and is transported to Nafion surface where a thin film of gold is slowly built up. The transport takes place by thermally converting gold into vapor. The system consists of a large bell jar evacuated to a low base pressure, generally less than 10^{-7}torr (a low the base pressure gives a purer growing film). Inside the evaporation system there is a vacuum chamber and gold is evaporated and transported to Nafion in the vapor phase. The vapor condenses on the Nafion film, and builds up to become the film composite. Because inside the bell jar is a vacuum, the mean free path of the evaporated gold atoms is long. This means that collisions between gold atoms and background gas molecules are rare; thus, there is little scattering of the vapor as it travels form the crucible to the Nafion surface. The result is that evaporated films are not particularly conformal [12]. To prevent this, Nafion films are mounted on a rotating system, which rotates about their own axis. In addition, since the source emits vapor over a well-defined solid angle, the substrates (Nafion in our case) must be placed at a considerable distance from the source to obtain reasonable substrate-to-substrate uniformity. Filament evaporator (Figure 20) consists of a vacuum system containing a filament which can be heated to melting point of source metal. In Figure 21, small loops of a target metal are hung from a filament formed of a refractory (high-temperature) metal such as tungsten. Evaporation is accomplished by gradually increasing the temperature of the filament until the metal melts and wets the filament. Filament temperature (Figure 22) is then raised to evaporate the metal from the filament. In our case, gold evaporation is done at base pressure of 10^{-6}torr, filament has to be heated up to around 1000°C. Although filament evaporation systems are easy to set up, contamination levels can be high.

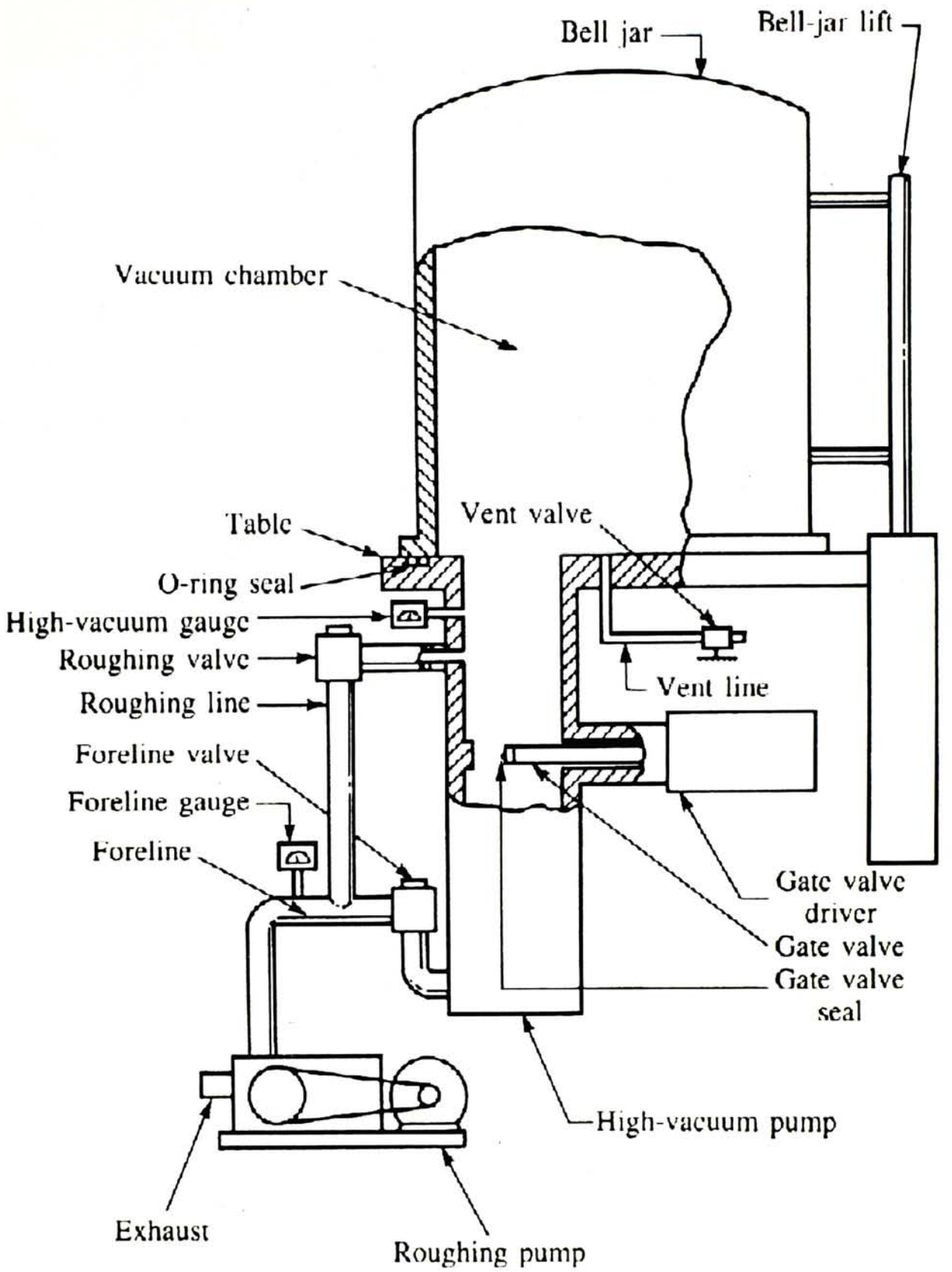

Figure 19 Typical vacuum system used for evaporation including vacuum chamber, roughing pump, high-vacuum pump, and various valves and vacuum gauge [13].

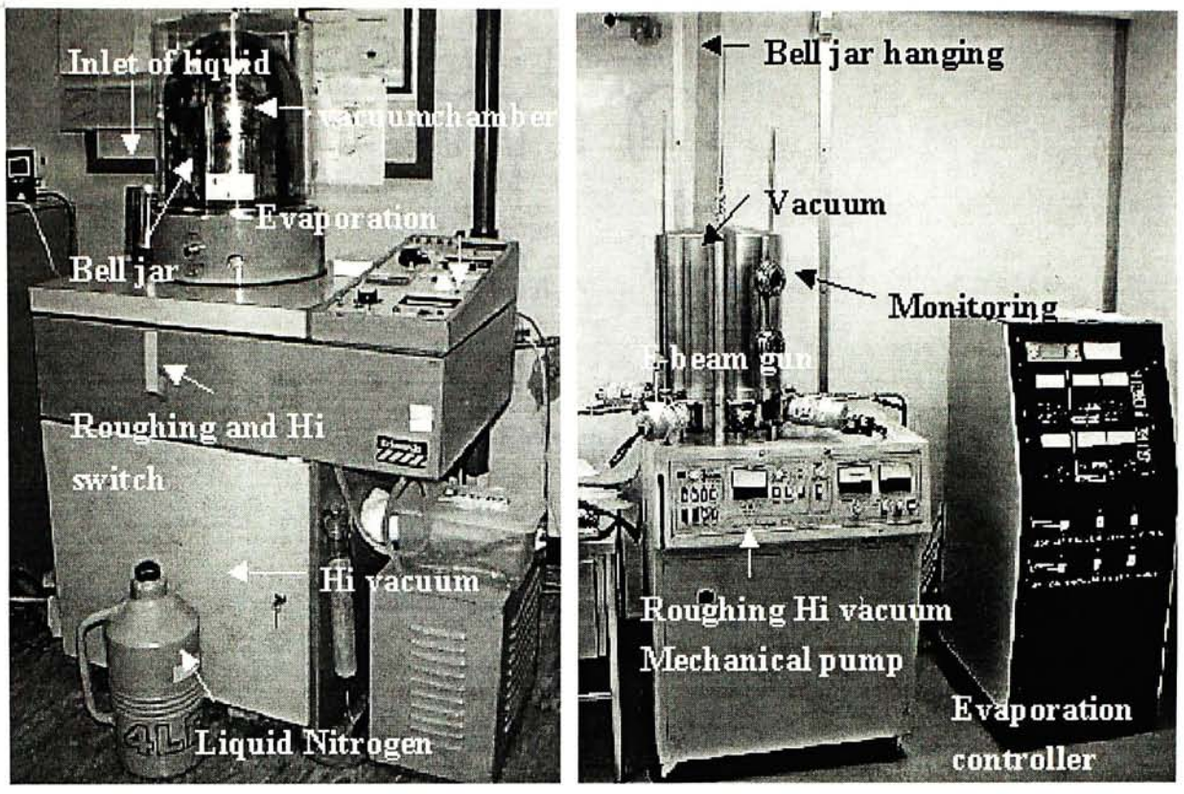

Figure 20 (Left) Filament evaporator (Right) E-beam evaporator.

Figure 19 shows a basic vacuum deposition system consists of a vacuum chamber, a mechanical roughing pump, a diffusion pump, valves, vacuum gauges, and other instrumentation. In operation, the roughing valve is opened first, and the mechanical pump lowers the vacuum chamber pressure to an intermediate vacuum level of approximately one Pascal (0.0075torr). If a higher vacuum level is needed, the roughing valve is closed, and the foreline and high-vacuum valves are opened. The roughing pump now maintains a vacuum on the output of the diffusion pump. A liquid-nitrogen (77K) cold trap is used with the diffusion pump to reduce the pressure in the vacuum chamber to approximately 10^{-4} Pa. Ion and thermocouple gauges are used to monitor the pressure at a number of points in the vacuum system, and several other valves are used as vents to return the system to atmospheric pressure [13].

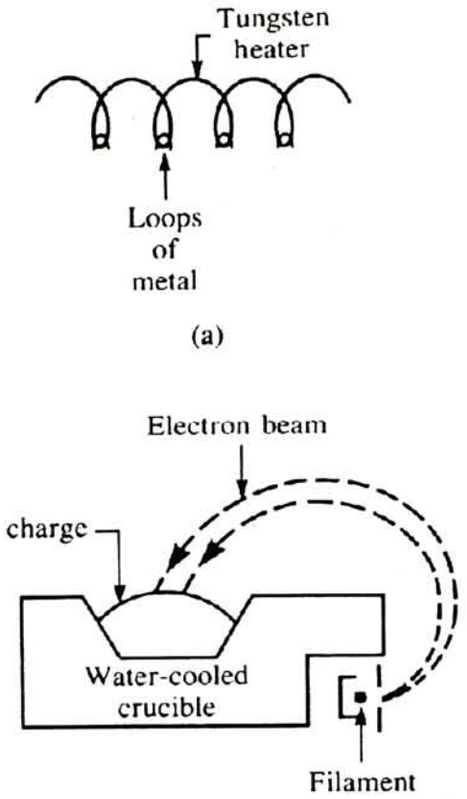

Figure 21 Two forms of evaporation sources. (Top) Filament evaporation, in which loops of wire hang from a heated filament; (Bottom) Electron-beam source in which a beam of electrons is focused on a metal charge. The beam is bent in a magnetic field [13].

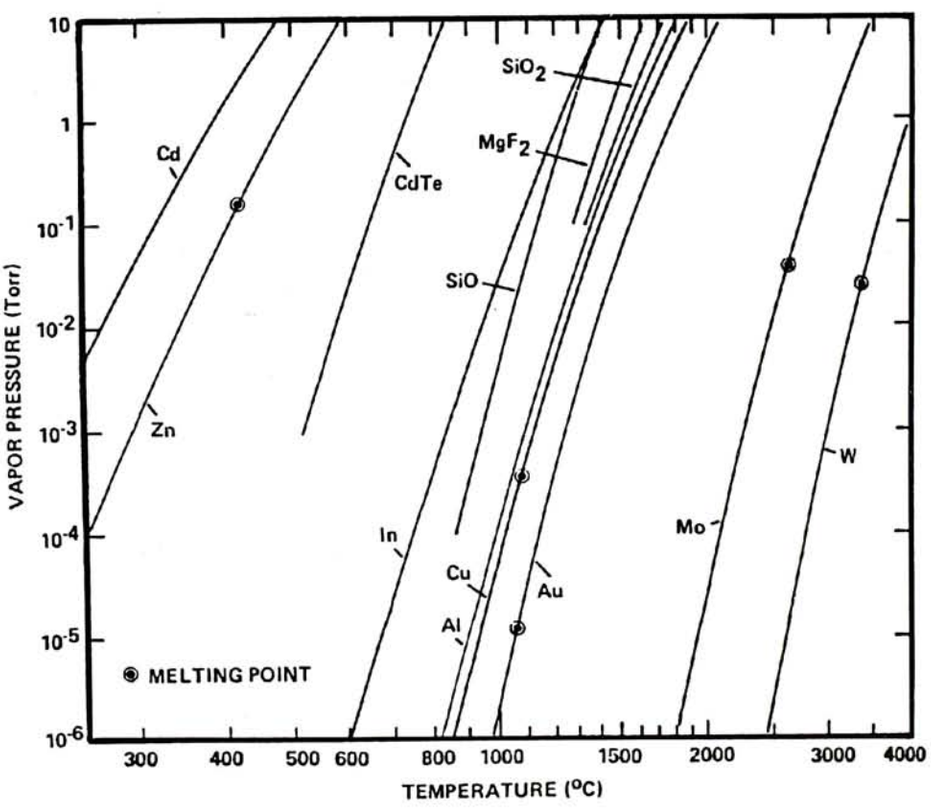

Figure 22 Temperature of filament needed for evaporation under different vapor pressure [14].

4.4.2 Electronic-beam evaporation

Electronic-beam (E-beam) systems (Figure 20) are also a common method to deposit metal thin film to a substrate, as they are capable of high deposition rates and can provide extremely pure films since only the source metal is heated. Thermal system has the advantage of not illuminating the sample with soft x-rays which are produced when the electrons from an E-beam system strike the source. This is generally not a problem except where electronic defects arising from radiation damage in SiO_2 layers is of concern [12]. However, we believe that damage did not happen in our fabrication process since our substrate is a film of polymer. In E-beam evaporation systems, (Figure 21), the high-temperature filament is replaced with an electron beam. A high-intensity beam of electrons is focused on a gold source, which has been placed in the crucible. During evaporation, beam current of 1.1A, power of 3700V x 110mA is used with deposition rate of 7-8 Angstroms/sec, which are by a control panel. The energy from the electron beam melts a region of gold. Thin films can be evaporated from a hot source onto Nafion films that are mounted above the source and rotated around the source during deposition to ensure uniform coverage. Besides, the evaporation system consists of a vacuum chamber, pump, and holding frame for the samples, crucible, and shutter. Gold to be deposited is placed in the crucible (Figure 23), and the chamber is evacuated to 10^{-6} to 10^{-7}torr. The crucible is then heated using an electron beam to evaporate gold from the crucible onto the sample. The film thickness is determined by the time that the shutter is opened and the evaporation rate of the material is a function of the vapor pressure of the material. Note that the surface mobility of the species on substrate will affect the coverage. Surface mobility is high in evaporated gold, which shows excellent step coverage. In general, evaporated films are highly disordered and have large residual stresses; thus, only thin layers of the material can be evaporated.

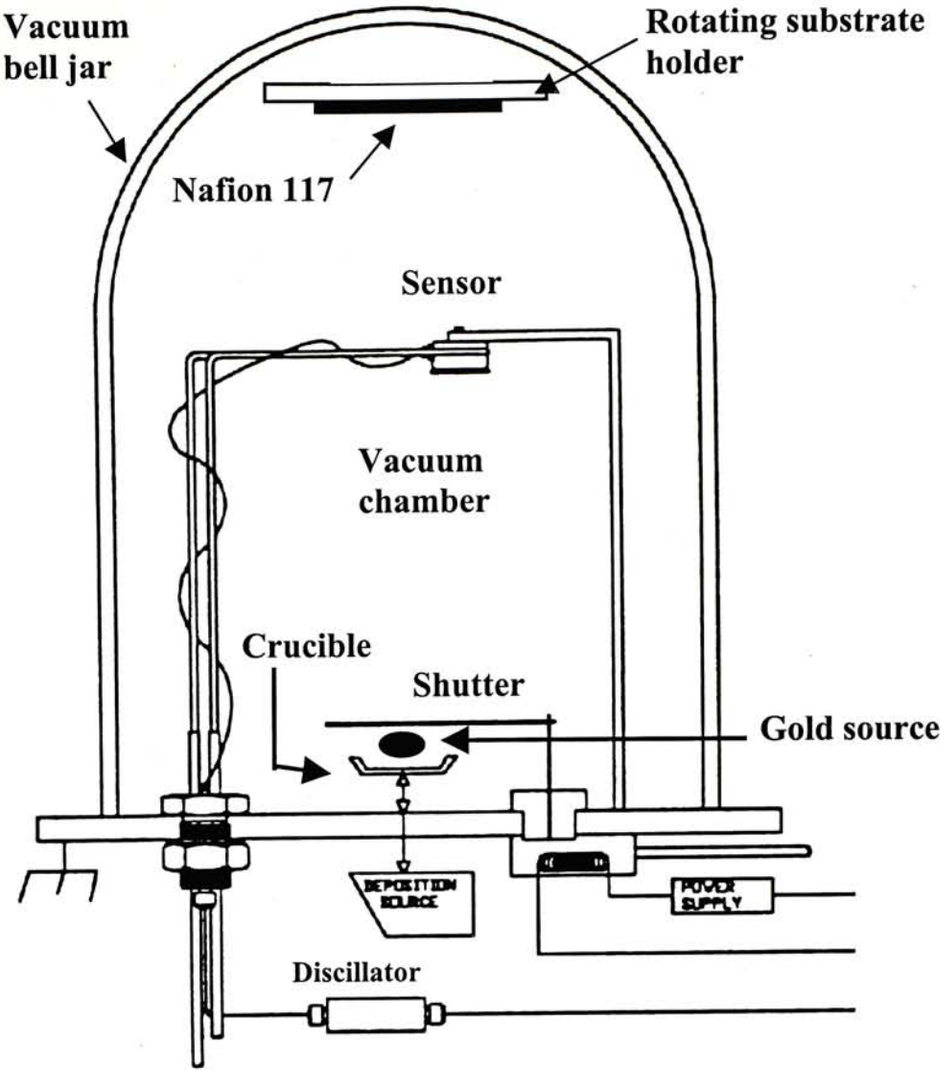

Figure 23 A typical E-beam evaporator.

4.4.3 Structural analysis of evaporation

In the previous sections, the principles of filament evaporation and E-beam evaporation have been discussed. Both working processes are similar to each other. However, the main difference is how the source metal is being vaporized so that it can be transported to the substrate surface. Since the two methods can do the thin film deposition, both evaporating progress were carried in order to short list a more convenient and reliable way of depositing the thin film (0.4μm of gold). In real practice, E-beam evaporation gives a better deposition on the polymer instead of using filament evaporation. In E-beam evaporation, only gold source is being heated up, thus a pure gold film thin can be built on Nafion surface. On the contrary, contamination level of filament evaporation is higher because the filament is heated

up to 1000°C during gold evaporation, any vaporized impurities on the filament will infect the forming the thin film. In Figure 24 and Figure 25, the performance of filament evaporated thin film and E-beam evaporated thin film are compared. Clearly, filament evaporation cannot support a pure gold thin film, tiny cracks of around 17μm appeared on the surface. The existence of these cracks lead to a poor conductive seed layer. In chemical electroplating, it is impossible to do 1.5μm of gold thin film on such a poorly-adhered gold seed layer. Besides, pumping condition of the evaporators has also been a limiting factor, as the lower the base pressure, the fewer the impurities incorporated into the growing film. By comparing the base pressure of the two evaporators, high vacuum pump in E-beam evaporator can support base pressure to 10^{-7}torr, however, high vacuum pump of filament evaporator can only give a base pressure up to 10^{-6}torr. In conclusion, in order to fabricate ICPF actuator, E-beam evaporation should be used for the 0.4μm gold deposition.

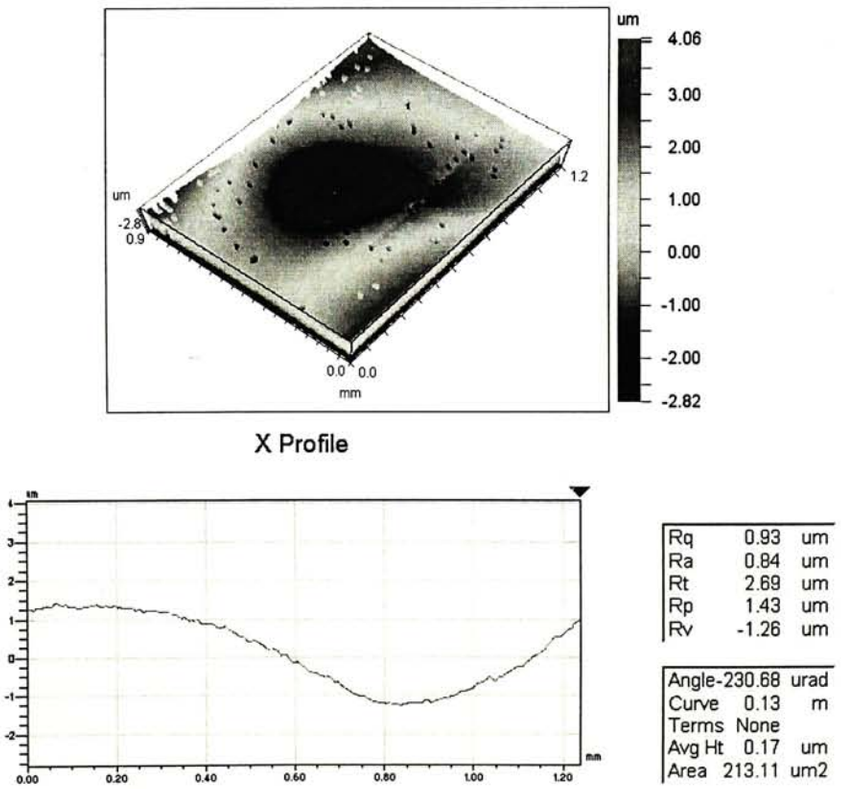

Figure 24 (Top) A 3-D Interferometric image showing the surface of gold film thin deposited by E-beam evaporator. (Bottom) Plot showing a smooth surface profile.

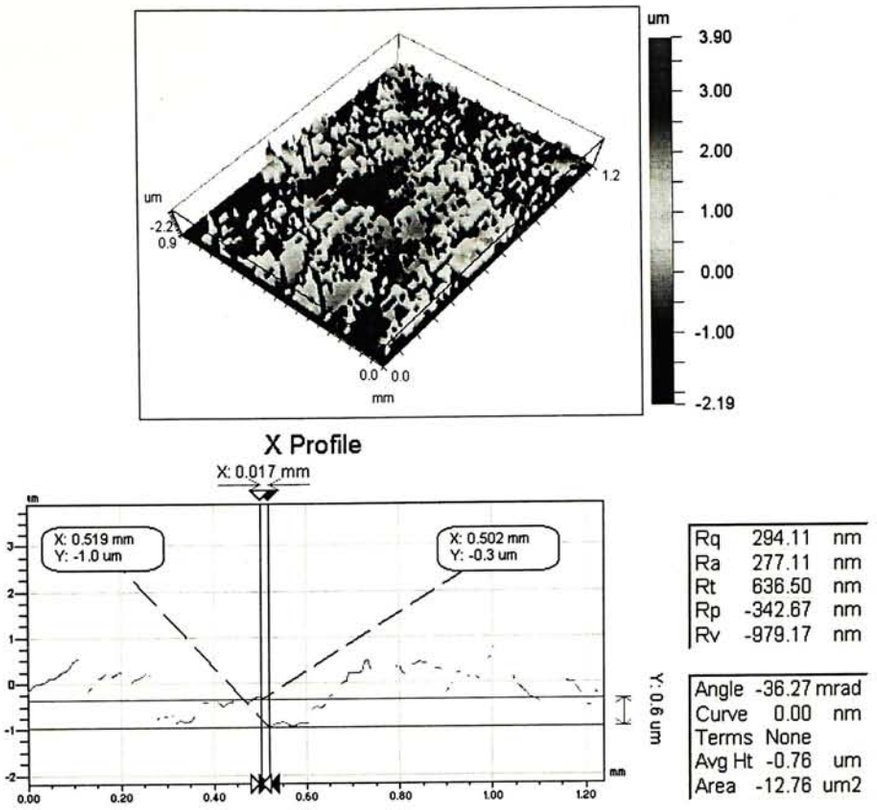

Figure 25 (Top) A 3-D Interferometric image showing the surface of gold film thin deposited by filament evaporator. (Bottom) Plot showing an unsatisfactory surface roughness.

4.5 Chemical electroplating

In ICPF fabrication, 2μm gold films are deposited on both side of Nafion 117, which added up to an ICPF. Due to the limitation that evaporation is only for thin film deposition, direct 2μm gold evaporation is not possible. As mentioned in the Section 4.4.2, deposited gold film by E-beam evaporation is highly disordered, which leaves a residual stress on the film. Therefore, in order to prevent poor adhesion and avoid cracking, 0.4μm of gold is deposited on both side of Nafion instead of 2μm. In the case of using Nafion 117 as a substrate, cracks do not appeared in 0.4μm to 0.5μm by E-beam evaporation. In addition, this thickness has already provided a good conductivity for chemical deposition. Therefore, 0.4μm of gold is first added as a seed layer for further gold electroplating. As a result, a thin film of gold is done by evaporation as a conductive medium for further thick film deposition, by chemical electroplating.

Chemical electroplating have been broadly used for metal coating in manufacturing industry, it is a commonly used technique for thick film deposition of a wide range of metals. The cell used in electroplating contains an electrolyte that is in aqueous form containing a high concentration of an ion of the metal, which is to be electroplated on to the targeted Nafion surface. Although Nafion has nonmetal surface, it can be electroplated with gold after a conductive surface, which is 0.4μm of evaporated gold placed on it beforehand. Electroplating of gold requires careful preparation of the conductive surface of Nafion, which served as a cathode in the cell. The surface of conductive layer of Nafion must be as clean and uniform as possible. Besides, the quality of gold electroplating does not only depend on surface preparation, it also depends on other factors. For instance, temperature of the ion solution, metal ion concentration, current density, time, electrolyte pH, the nature and amount of all species present in the electrolyte solution. Relatively thick film of gold (1.5μm) is electrodeposited at room temperature under 2.3V and 0.02A with platinum anode (5cm x 7cm) for more then 5 minutes. The rate of chemical electroplating will be discussed in the coming section. The setup of gold electroplating is shown in Figure 26. Gold Elconac 138 (electroplating solution from Chartermate International Ltd.) is used as electrolyte solution. A beaker containing the electrolyte is placed on a stirrer. Gold Elconac 138 is a mildly acidic cobalt-alloyed gold plating process. Different from usual type of electrolyte, Gold Elconac 138 has a higher rate of deposition without any increase for gold in solution.

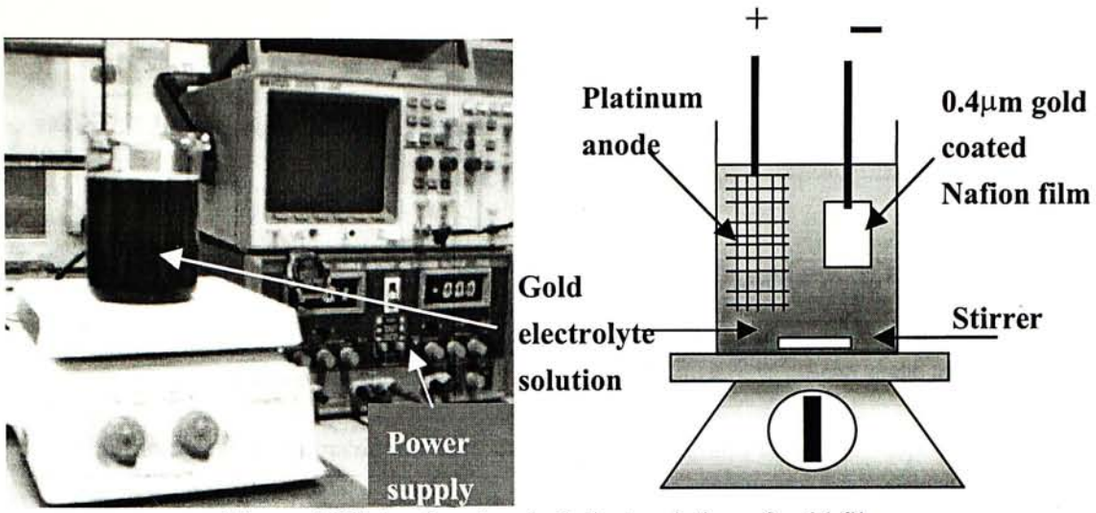

Figure 26 Setup for chemical electroplating of gold film.

4.5.1. Deposition rate calibration

Figure 27, identical metal alloy strips were used to serve as a calibrating media. First, part of the alloy strip was covered by a mask, and then the whole strip is immersed in electrolyte as cathode, while the platinum coated wire was used as anode. Under the same voltage and current supplies, different strips were chemical electroplated for different time. The masks on the strips were removed after coating. During deposition, a gold layer edge is made, by measuring the step of this edge using Alpha-Step® 500 Surface Profiler, the thickness of the chemical electroplating can be quantified (Figure 28 & Figure 29). Based on the calibration, time need to do a desired thickness of gold layer can be estimated. As illustrated in, it took 8 minutes for 1.5μm deposition.

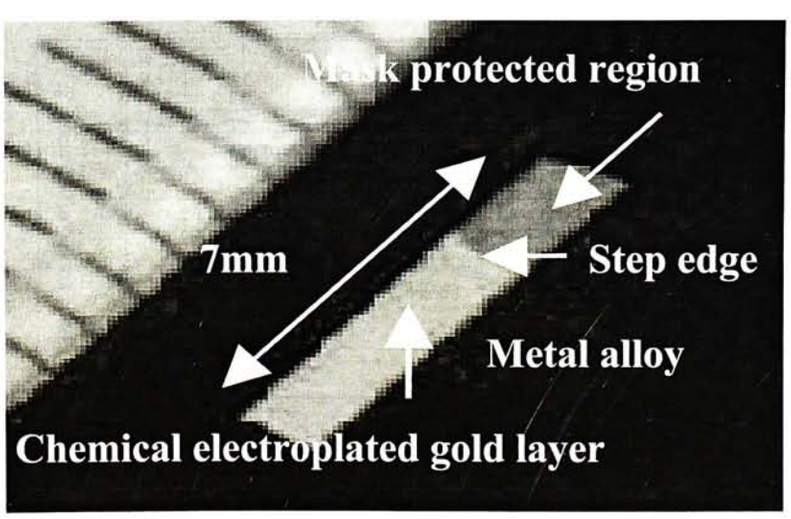

Figure 27 A typical calibrating metal alloy strip.

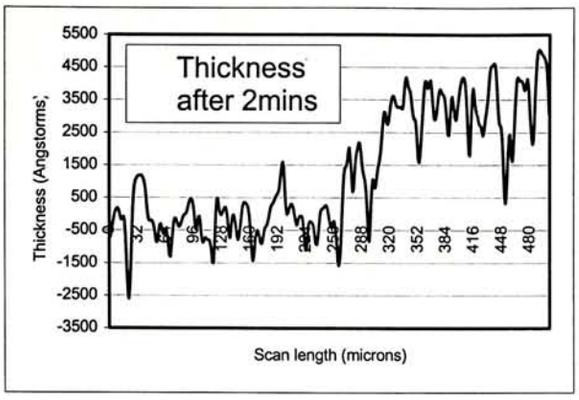

Thickness for 2mins deposition.

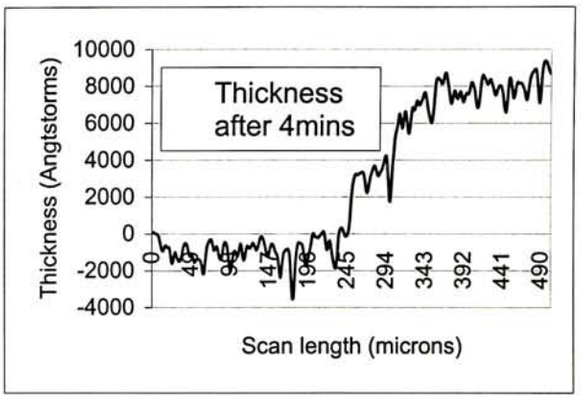

Thickness for 4mins deposition.

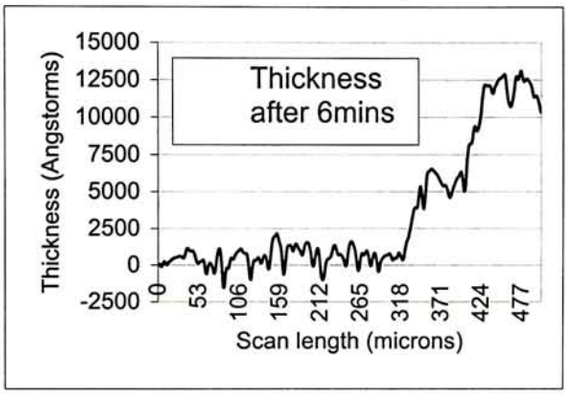

Thickness for 6mins deposition.

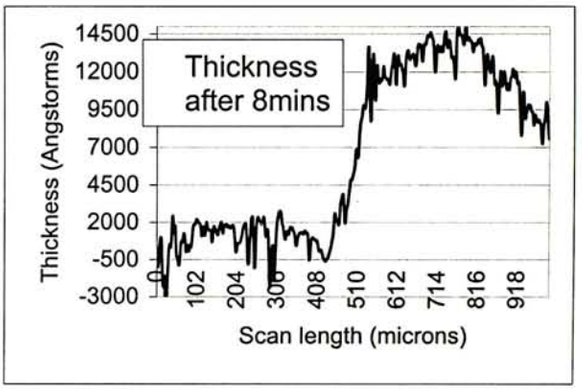

Thickness for 8mins deposition.

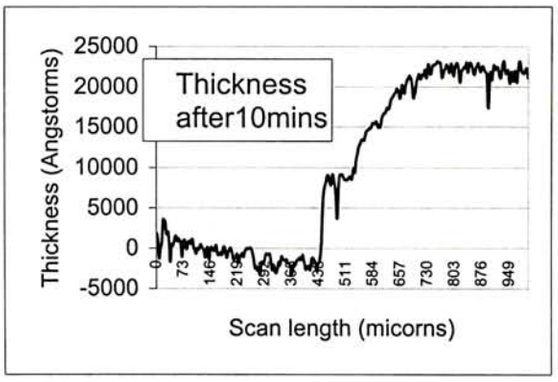

Thickness for 10mins deposition.

Figure 28 Series of plottings showing time against different thickness of deposited gold thin film.

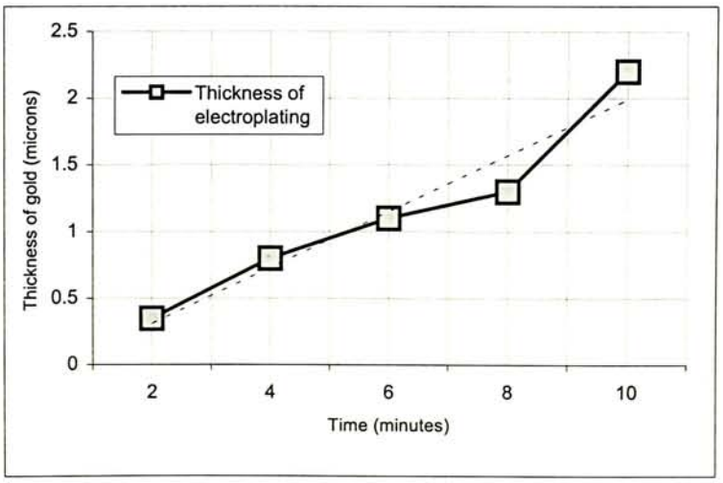

Figure 29 Shows the linear relation between the deposition thickness and time.

5 DESIGN AND PACKAGE

The goal of this project is to apply ionic polymer material for MEMS applications. Most of the existing ICPF actuator developed by other research experts is in meso scale, which a brief introduction has been given in Chapter 2. Hence, the mission of designing and fabricating ICPF micro cell-gripper has become one of the pioneer research in the world. After developing a novel and simple fabrication process, ICPF sample pieces have been successfully fabricated. Our next task is to make the sample pieces into workable actuators, just like making surface micromachines and silicon substrates into micro devices. Before laser micromachining ICPF, we had to give a design to our actuators, the micro cell-grippers. In our daily life, if we want to pick up or grasp something, the most convenient way of doing it is to use our hand and take hold of the object. We can grip things easily because we have fingers; hence, we have concocted the design of the actuator from the above idea. It is believed that if we are able to fabricate meso ICPF strips that can give large bending angle and deflection, it is possible and workable to fabricate ICPF grippers with the same degree of movement shown in Figure 30. On the other hand, if we can actuate micro strips and make them give large bending motion, we are confident to develop ICPF micro cell-gripper. The concept of micro cell-gripper is like that shown in Figure 30. Cells are free to move in a fluid, once the cells have fallen in the gripping zone of the micro cell-gripper, which is the region that the gripper's leg can reach and close as a ball. A voltage is then applied on both sides of the grippers. Finally, the legs bended toward the center and as a result grasp the cell.

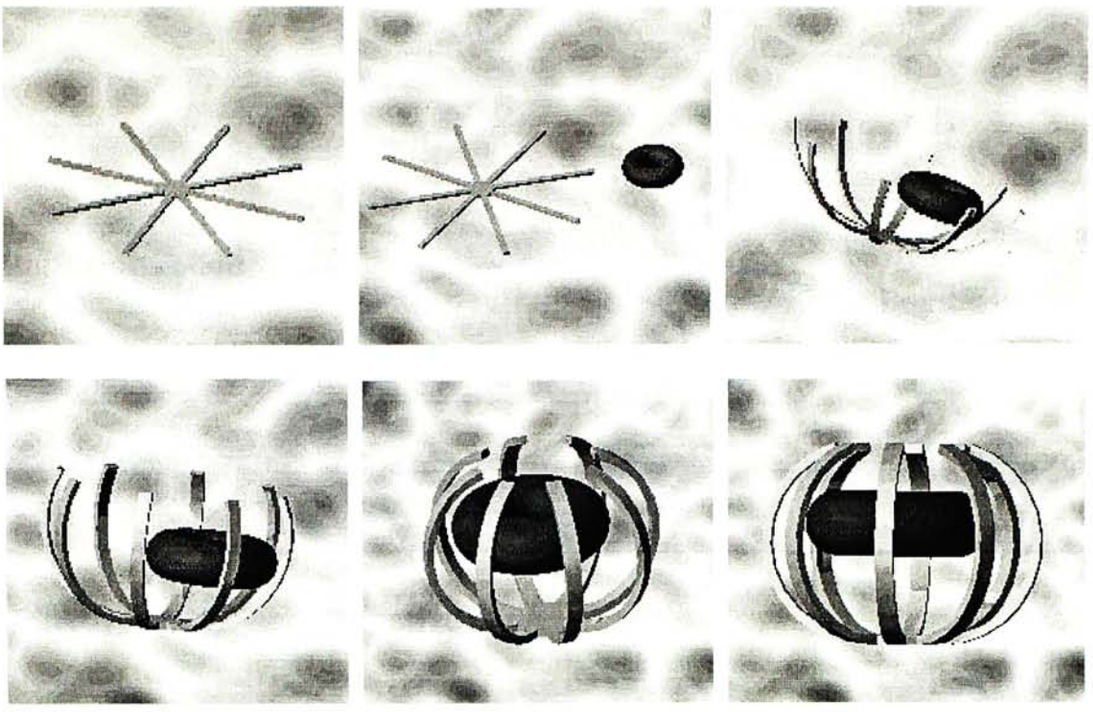

Figure 30 Series of animations showing the concept of eight legs micro cell-gripper and the moment.

There is no doubt that it is not efficient for having only one gripper to grasp one cell, that is the reason why a novel fabrication process to fabricate batch of micro cell-grippers is very important. The big picture is that an array of actuators will be fabricated and bonded on a tiny chip. As we know that ICPF actuator have the characteristic to bend towards the anode side during actuation, so adhesive bonding technique is used to make the bottom side of the actuators contact the pad on chip which serves as the cathode during actuation. Two kinds of conductive epoxy were tried: one is CircuitWork® Conductive Epoxy CW2400, another one is Epoxy resin by epo-tek®. For the anode, wire bonding technique is applied, a wire is bonded on the surface of the actuator and a positive pad. When a voltage is applied to the chips, array of actuators will start the gripping motion at the same time. In advance, controller will be built to control individual legs of individual micro cell-gripper. As shown in Figure 31, a cross sectional drawing is given to illustrate the cathode and anode bonding concept. An idea of actuator on chip is given in Figure 32.

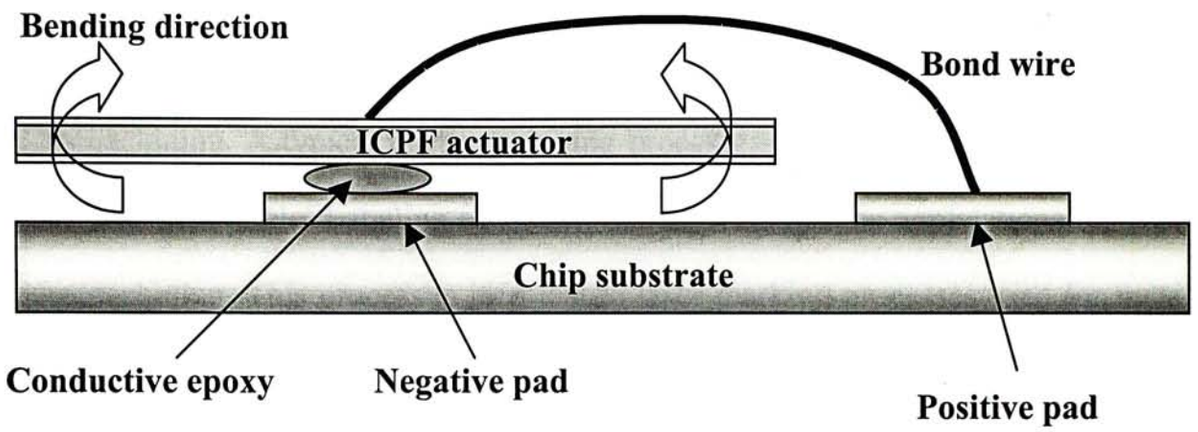

Figure 31 Cross section drawing showing the actuators bond on chip idea.

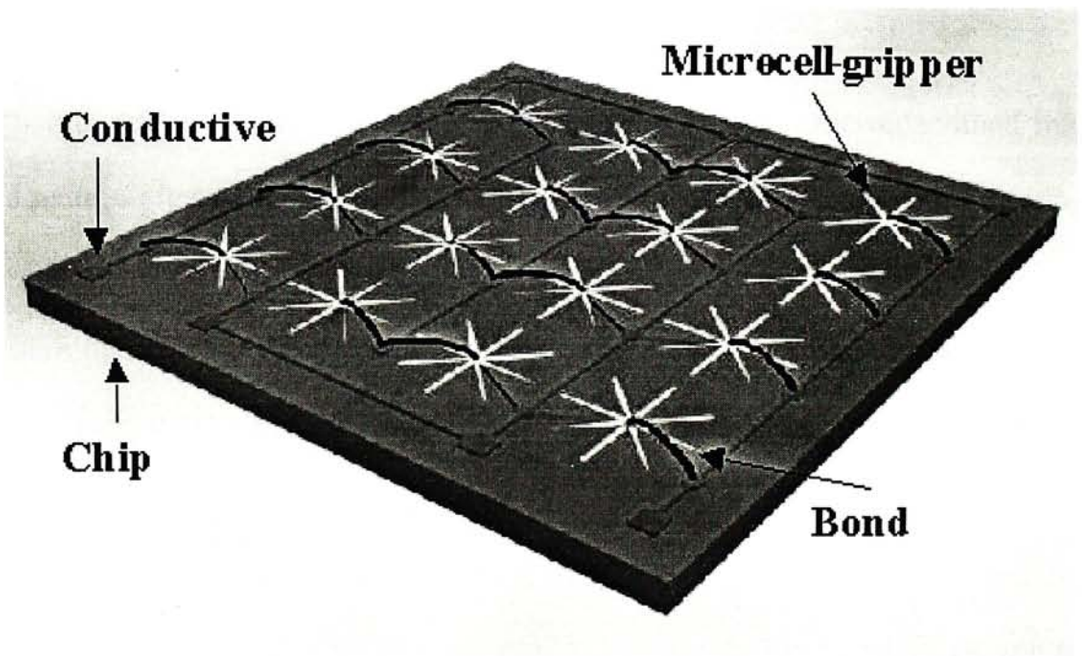

Figure 32 Array of micro cell-grippers on a chip.

6 LASER MICROMACHINING

6.1 Introduction to Laser micromachining

With the development of miniaturization of electronic components and MEMS in recent years, laser micromachining has become a demanding application for micro technologies. CO_2 and Nd:YAG lasers have been commonly used in micromachining. A typical micromachining processes produce kerfs with depth and width in micron scale. Labeling of silicon wafers is one of the applications for laser micromachining. This process is identical to laser marking processes used for metal or ceramic parts. A laser beam can also be used to repair metallic masks by vaporizing portions to alter the pattern. In addition, a laser beam can be used to repair a circuit by vaporizing defective components and redirecting channels to circumvent the defective component. Apart from electrical and integrated circuit technologies, developing micro devices is also one of the potential applications for Biomedical applications.

In this project, ionic conducting polymer film is laser micromachined into designed pattern after the gold-polymer fabrication process. In laser micromachining ICPF, a suitable laser must be selected. Due to the special composite mechanism, a laser system that can cut through the gold layer and Nafion 117 without burning the polymer or over vaporize the gold surface is desired. Both CO_2 and Nd:YAG laser were used to laser micromachine ICPF. In this Chapter, a brief description of the laser systems is given, since the two laser systems have different specifications for particular laser applications. Finally, only one of the two systems will be chosen to laser micromachine ICPF actuators.

6.2 CO_2 laser

The carbon dioxide laser is one of the most powerful and efficient lasers available. It operates in the middle infrared on rotational-vibration transitions in the 10.6μm and 9.4μm wavelength regions. CO_2 laser output occurs in several different types of gas discharge configurations in a mixture of carbon dioxide, nitrogen, and helium gases, typically with a CO_2 : N_2 ratio of about 0.8 : 1. These lasers have produced CW powers of greater than 100 kW and pulsed energies of as much as 10kJ. One of the most useful CO_2 lasers for materials application is a CW version with a cavity length of 1-2 m producing one or more kW of power. Another laser of this class is the CO laser, which emits at approximately half the wavelength of the CO_2 laser in the 5-6 μm wavelength region.

Probably the most significant area in which the CO_2 laser is used is in the general field of material processing. This includes cutting, drilling , material removal, etching, melting, welding, submelting, annealing and hardening. The other principal area is in medical applications, where it is used for cutting and cauterizing. The advantage of using a laser for these applications is that a very intense heating source can be applied to a very small area. The material ablation applications can be described in terms of CW or pulsed operations. For CW applications, the process is a thermal one in which the laser source serves as a cutting or heating tool. For pulsed operations, such as the ablation of thin films of material or drilling of small holes, the laser must reach an intensity on the target of 10^{12} to 10^{13} W/m^2 [15].

6.3 Nd:YAG Laser

The Nd:YAG laser (Figure 33) produces a high-powered beam of light at the wave length of 1064nm, which is not visible. The light, when focused through a lens system, has enough power to vaporize material and to change the thermal characteristics of a material, thereby producing a visible mark on it. The beam of light is "steered" by means of two moving mirrors controlled by a computer to produce the required mark. In this research, we focused on using Diode-pumped Nd:YAG laser to laser micromachinine ICPF actuator, a more specified explanation will be given later in this chapter. The laser beam is produced in the laser enclosure. The part of the optical system that produces the laser beam is called the resonator. The laser resonator (Figure 34) consists of a fully reflective rear mirror: a pumping chamber containing a Nd:YAG laser rod and a number of high power diode lasers, and a partially reflective output mirror through which the laser beam emerges.

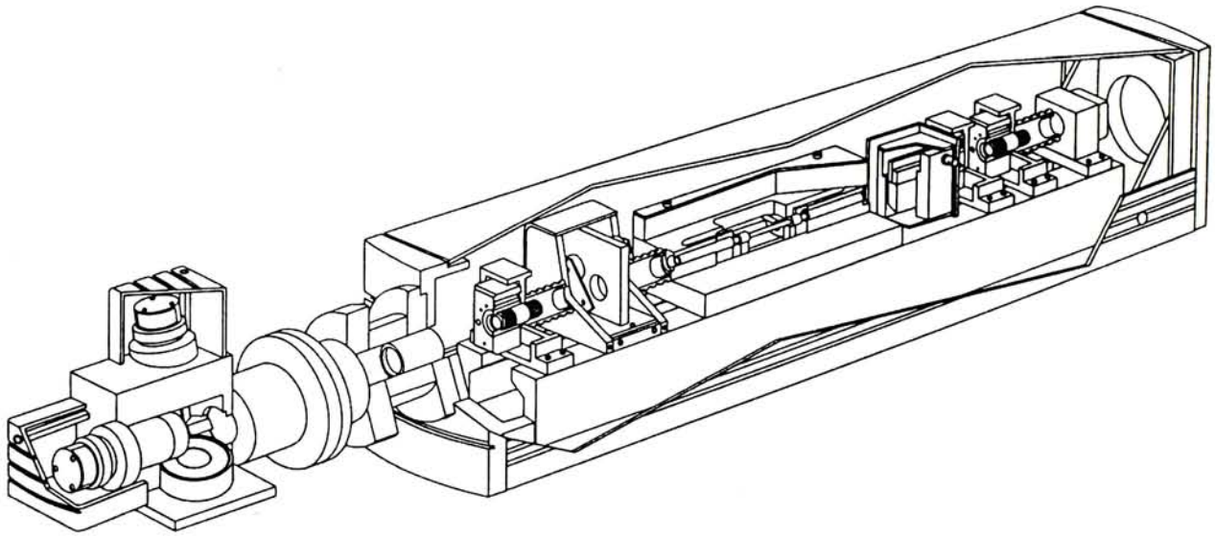

Figure 33 A typical Q-switched Nd:YAG laser [15].

The diode lasers illuminate the Nd:YAG rod which makes the rod into a light amplifier. When light of a specific color passes through the rod it increases in power. The rear and output mirrors are aligned to be parallel to each other and so light bounces backwards and forwards between them. If this light passes through the rod it

will be amplified so a large amount of parallel light is produced bouncing between the mirrors. The output mirror is only partially reflective however so some of the light is transmitted out of the laser resonator. The light emerging from the output mirror is the laser beam.

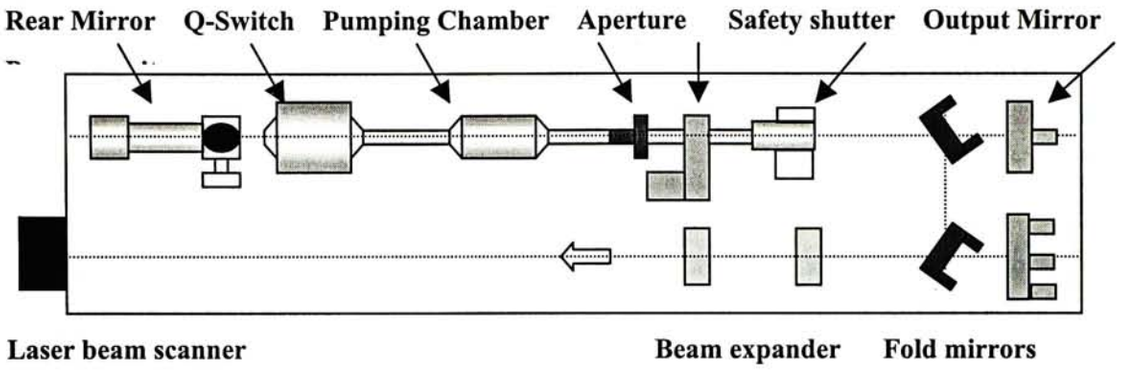

Figure 34 Laser Enclosure.

6.4 Laser micromachining of ICPF actuator

There are few components of the Nd:YAG laser system, which can improve the performance of micromachining process. When using Nd:YAG laser to micromachine ICPF actuators, devices include Q-switch, aperture, and beam expander are inevitable considerations.

Q-switch is kind of light switch. When a high frequency (27MHz) electrical signal is applied to the Q-switch, it deflects light passing through it. Light can no longer bounce backwards and forwards between the rear and output mirrors if it is deflected, so no laser beam is produced. The Q-switch can therefore be used to very rapidly turn the laser beam on and off by turning the electrical signal to the Q-switch off and on. The Q-switch also has a second function. When the Q-switch is preventing the production of the laser beam, the Nd:YAG rod can store some of the power from the diode lasers illuminating it. Therefore, when the electrical signal to the Q-switch is turned off, allowing the light to bounce between the mirrors, this stored power is released very rapidly and a very high power pulse of laser light is

produced. The power during this pulse (know as the laser peak power) can be 1000 times higher than the power produced without using a Q-switch but lasts only for a very short time (about 200ns). In this way, the Q-switch is used to produce a high power. This high power ensures a high power laser micromachining even if the laser beam is very small by creating a tiny beam focused laser spot. Aperture (Figure 35) is a small brass tube. The hole in the tube limits the size of the laser beam. When an aperture is fitted, the quality of the laser beam produced is improved, allowing the production of smaller marks on the work piece. Normally the smaller the diameter of the aperture the better the focused laser spots on the work piece. In addition, fitting smaller aperture will reduce the laser power, therefore the choice of the correct diameter of aperture is a compromise between laser power and mark size, and has to be determined for the specific application. ϕ1.5 mm aperture is used during ICPF micromachining because we would like to minimize

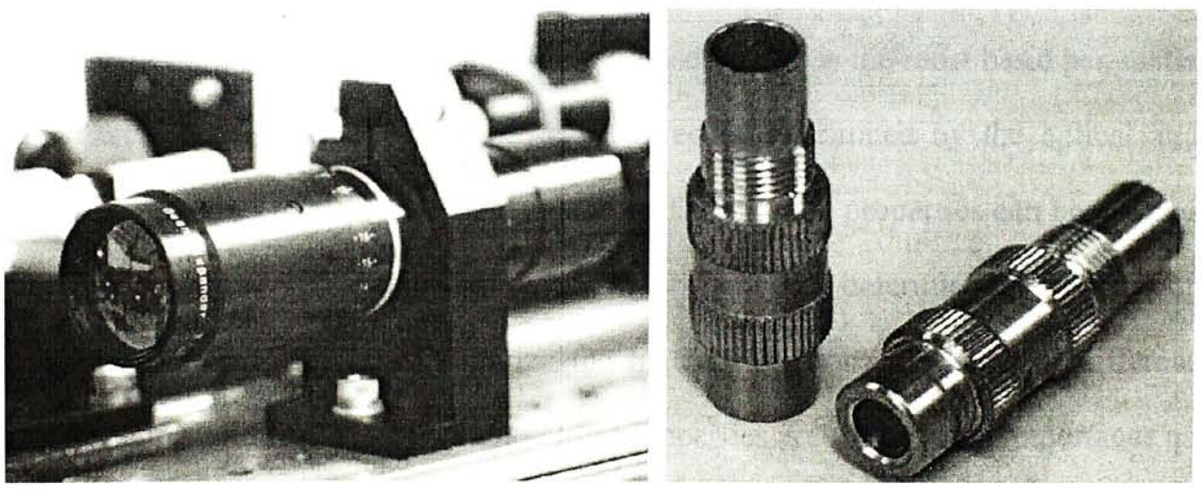

Figure 35 (Left) Zoom beam expander (Right) Apertures.

The function of the beam expander is to increase the diameter of the laser beam. Increasing the diameter of the laser beam reduces a property of the laser beam which is called divergence. By decreasing the laser beam divergence, the size of the mark on the work piece is reduced. A standard beam expander consists of two lens in

two separate mounts and increases the laser beam diameter by any amount from two times to eight times.

After tuning all the hardware devices, we started to mirocmachining ICPF actuator. The laser micromachining process is actually a thermal process. First, a concentrated laser beam incidents on the material surface and part of its energy is absorbed in the material. After the laser energy is absorbed by material, it transfers to heat energy within a limited region, which depends on the material property. When the energy intensity of laser is high enough to heat the material to the temperature of melting point, the material will melt, boil and then vapor. Melting of material and pushing out of liquid phase by reactive pressure of vapor result in disintegration of the material, giving rise to through holes in thin plates for each laser pulse. The effectiveness of laser micromachining depends upon the thermal properties and the optical properties the material.

Since ICPF is not a pure metal or polymer, laser parameters become significant for a successful laser machining. Laser power is the most basic parameter of a laser. The amount of laser power required is determined by the optical and thermal properties of the work piece material. The thermal properties can be divided into two basic categories: fixed and loss. The first category determines the amount of energy required to melt and vaporize the material. Every material is of different damage threshold for the laser energy. Loss properties are as the same importance as the first category because they determine the energy transmitted to the surrounding material during processing. Of the optical properties of material, the absorptivity of material has the largest influence on laser power requirements. The material absorptivity determines the fraction of the impinging radiation energy that is actually absorbed by the material. In short, the total amount of laser power required includes two parts: absorbed energy and unabsorbed energy. Wavelength of the light source is

very important in laser machining. The absorptivity of material is highly dependent on the wavelength of incident light, and thus certain laser will be more suitable for the processing of different classes of materials. The beam profile can be characterized by its Transverse Electromagnetic Mode (TEM). It appears that the intensity distribution of a laser cannot take just any shape. For a cylindrical symmetrical laser resonator the intensity distribution in a cross-section of the laser beam may be described by a Gaussian function times a Laguerre polynomial that is described by two numerals n and m. The laser output is said to have a mode structure, i.e., a transverse electrical mode structure, which is abbreviated to TEM_{nm} [16].

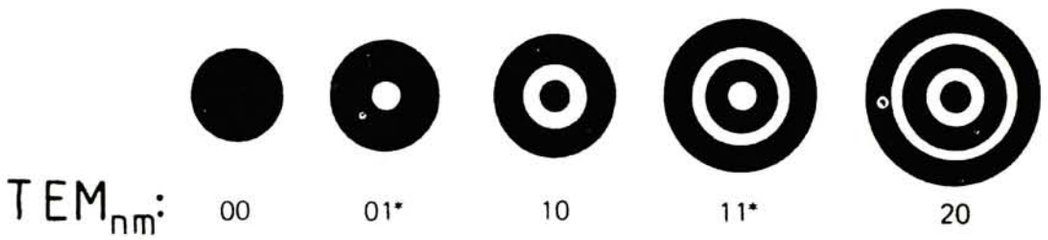

Figure 36 Examples of cylindrical transverse electrical mode patterns. The first subscript indicates the number of dark rings (white in the figure), whereas the second subscript indicates the number of dark bars across the pattern [16].

In laser micromaching ICPF actuators, TEM_{00} mode is used because it can increases beam quality of the laser. A smaller spot in focus is obtained with a larger depth of focus than with any other mode. In addition, a laser operating at a single mode gives a more stable output than a multimode laser. Practically speaking, since the only single mode that can be selected from a multimode laser is the TEM_{00} mode, this is the one chosen.. TEM_{00} has a Gaussian spatial distribution and is usually considered the best mode for laser machining because the phase front is uniform and there is a smooth drop off of irradiance from the beam center. This minimizes diffraction effects during focusing and allows the generation of small spot sizes. In laser micromachining ICPF, focal spot size is a very important parameter. It affects

the intensity (power per unit area) of laser beam at the material surface and resolution of machining. Several factors influence focal spot size such as the divergence of the beam, diffraction or the focal length, and the diameter of incoming laser beam. The size of focal spot size can be calculated as:

$$D = \frac{8}{\pi} \cdot \frac{\lambda f}{D_b} \qquad \text{Eq 1}$$

where, D_b is the diameter of incoming laser beam before focusing, λ is the wavelength of laser, and f is the focal length of lens. Laser can operate in either a continuous wave mode or a pulsed beam mode. In pulsed beam mode, short duration pulses with high energy density can be generated from low levers of continuous electrical power. For certain laser, high frequency of laser pulse means low power density per pulse. CW operation offers the advantage of smooth surface after machining. Cutting speed mainly affects the thermal diffusion in the surrounding material during machining. In pulsed mode, both frequency of laser pulse and cutting speed will influence the roughness of the machined surface. Increasing frequency of laser pulse and decreasing speed will improve the roughness.

The melting point of Nafion is lower than that of copper so its damage threshold is lower than that of copper. That means lower laser energy intensity used for cutting is required. Nafion is a transparent material for Nd:YAG laser beam (1064nm wavelength). That means Nafion is of very low absorptivity to Nd:YAG laser beam. It can only absorbs less than 5~7% energy of Nd:YAG laser. Therefore, it requires higher laser power compared to the materials with higher absorptivity for Nd:YAG laser such as copper. On the other hand, Nafion is of low thermal conductivity and low heat capacity comparing with copper. Thermal diffusion in the surrounding material during Nafion cutting is not well, giving rise to burning of the surrounding material easily. Therefore, the laser power cannot be set too high. In

order get TEM_{00} mode laser beam, an aperture with diameter of 1.5mm is used to cut Nafion. The maximum expander for beam is 8×. Then the diameter of incoming laser beam before focusing is 12mm. The maximum diameter of incoming beam before focusing of our laser is 15mm. The focal length of lens is about 100mm. The focal spot size is

$$D = \frac{8}{\pi} \bullet \frac{\lambda f}{D_b} = \frac{8 \times 1064 \times 10^{-6} \times 100}{3.14 \times 1.5 \times 8} = 22.6 \times 10^{-3} (mm)$$

The actual Nafion cutting parameters are below:

Aperture: ϕ1.5 mm

Laser power: 70% - 75% (~5W)

Pulse frequency: 2 – 4

Cutting speed (rate): ~200 mm/s

Repeat: 1

As stated early in this Chapter, we have been using CO_2 laser and Nd:YAG laser to micromachine ICPF actuator. Although both laser types can do the cuts, there exist some considerations that leads us make use of Nd:YAG laser instead of CO_2 laser. Basically, although CO_2 laser is designed for cutting and masking organic materials due to the range of wavelength (10.6μm), most rubber materials have high absorptivity at the CO_2 laser wavelength, so energy efficiency is high. The working principle of CO_2 laser is like a dot matrix printer, the cutting scanner when is a series of reflecting micro mirrors that drive a cutting path, and that is why the performance of the cutting is greatly related with the resolution (Like pixels in dot matrix printer). In terms of resolution, Nd:YAG laser definitely has better resolution, normally 10 times better then CO_2 laser, because of the limitation of wavelength. Figure 37 shows SEM photos of laser micromachined ICPF micro cell-gripper by both laser systems,

and also we can compare the micromachining performance by looking at some close up SEM images as shown in Figure 38. A clear cutting edge can be achieved using Nd:YAG laser. Conversely, there exist net residuals on the cutting edge from CO_2 Laser cut.

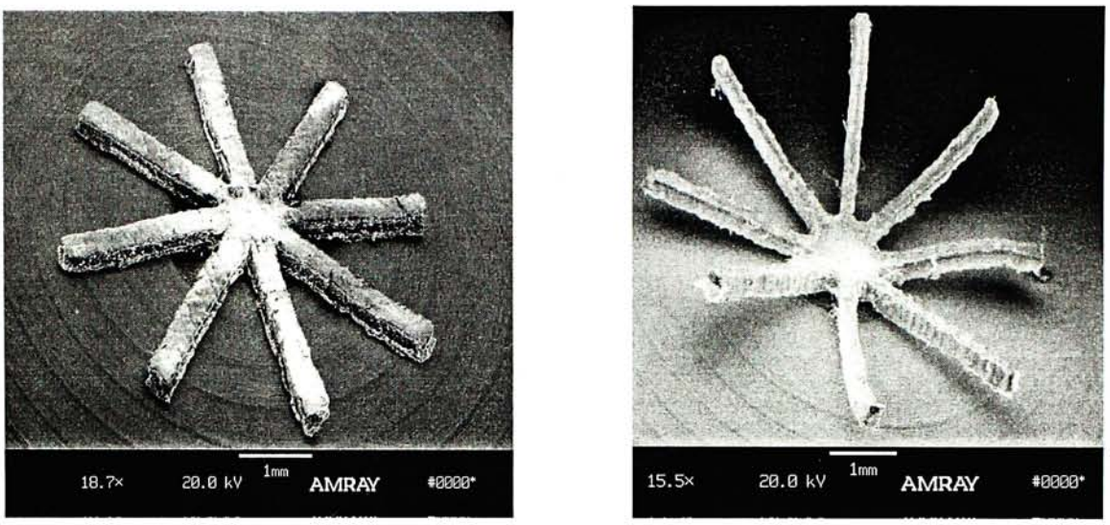

Figure 37 Star patterned ICPF micro cell-gripper using (Left) Nd:YAG laser (Right) CO_2 laser.

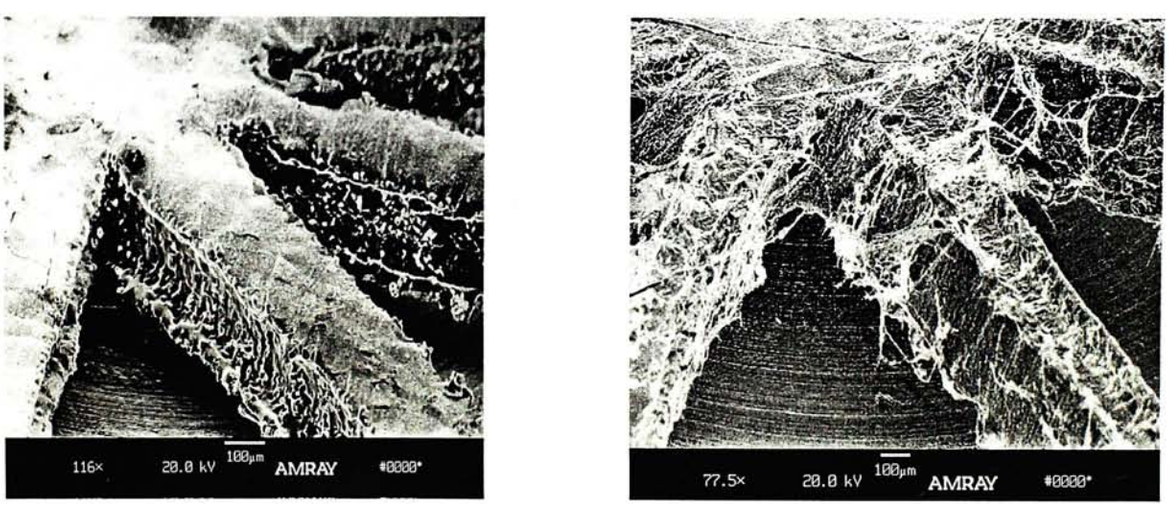

Figure 38 SEM images showing close up of ICPF micro cell-grippers cut by (Left) Nd:YAG laser (Right) CO_2 laser. Clearly, residuals exist after CO_2 laser micromachining.

We have decided to use Nd:YAG laser to laser micromachine ICPF after comparing the performance of cuts between the two types of laser system. Using Nd:YAG laser, we are able to laser micromachine micro gripper without fiber like residues. In Figure 39, an SEM image of the 200µm leg width micro gripper and its residue are shown. We have proven the successful operation of laser micromachining micro gripper with leg width of 200µm. Also, on the right of

Figure 40 shows the width of the cut residue, which is slightly wider than 200µm. In Figure 41, a spring patterned ICPF has been shown. The spring width has also been proven to be 200µm.

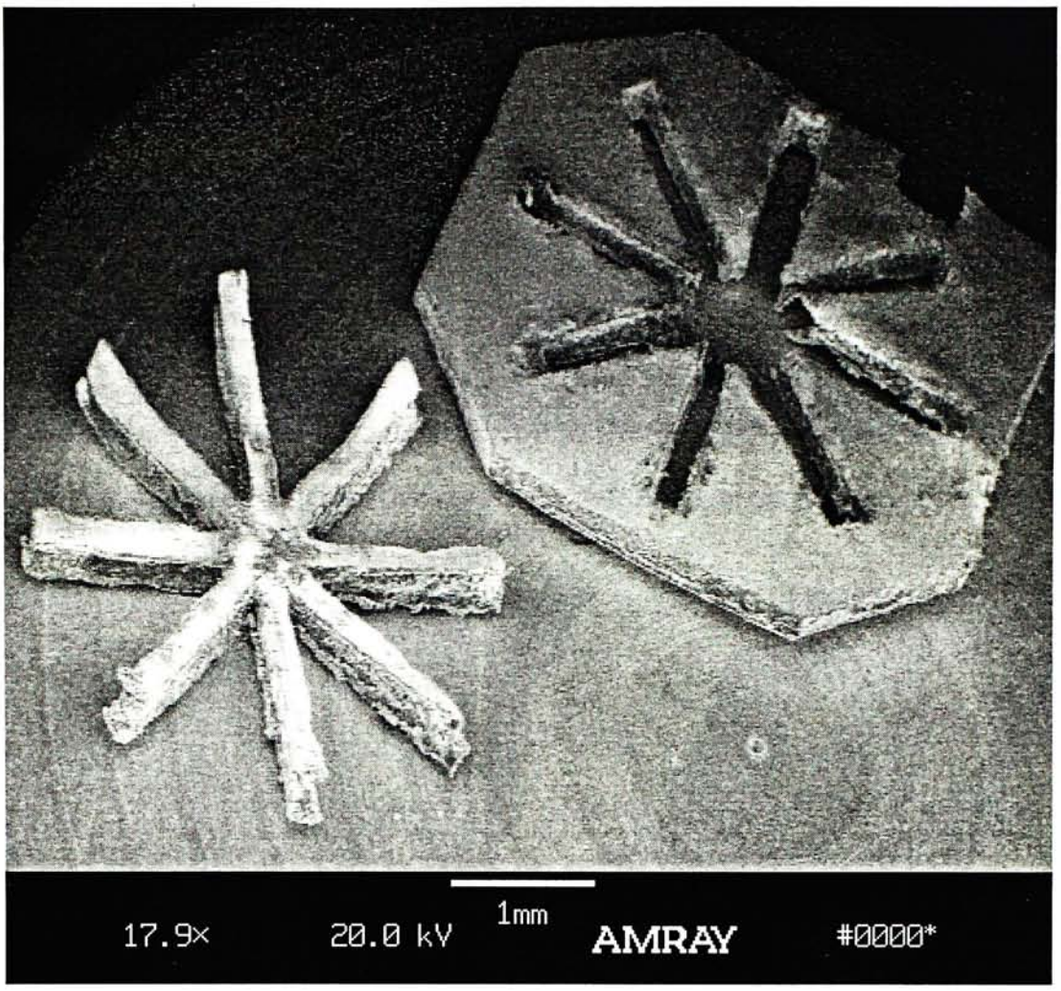

Figure 39 SEM image showing the Nd:YAG laser micromachined 200μm width, individual 2mm length micro cell-gripper and the residue.

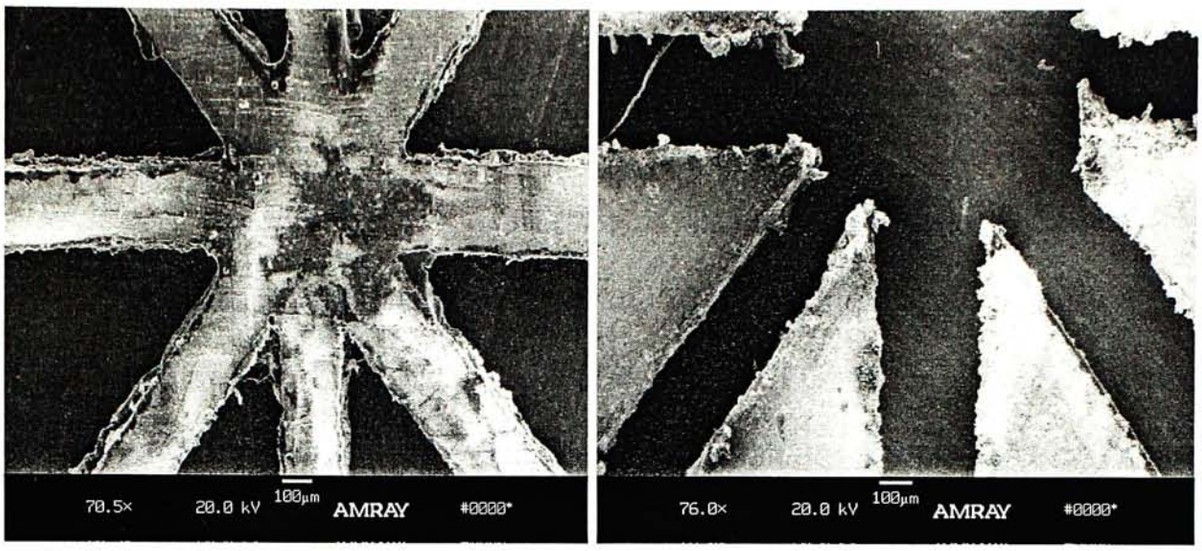

Figure 40 (Left) Nd:YAG laser micromachined actuator testified a successful 200µm cut. (Right) Showing the residual of the cut with slightly wider width ~200µm.

Figure 41 (Left) Nd:YAG laser micromachined spring pattern. (Right) Showing laser micromachined spring with spring width of ~200µm.

7 EXPERIMENTAL RESULTS AND ANALYSIS

7.1 Introduction

In Chapter 4, 5 and 6, details on how to use gold and polymer to fabricate ICPF have been discussed. After deposited 2μm of gold on both side of Nafion 117, which is 180μm thick, ICPF sample pieces with 184μm have successfully been realized. Then, Nd:YAG laser was used to laser micromachine ICPF actuator into designed multi-legs micro cell-gripper. Micro cell-grippers with leg-width of 200μm have been micromachined. However, the reliability of the composite is a major consideration before cutting the designed patterns. As mentioned before, adhesion between gold thin film and the polymer is very important in making ICPF actuator. We have to make sure every single ICPF sample pieces can give a desired bending performance without cracking the thin film or burning the polymer under a voltage supply. Based on this deliberation, a test on modulus of elasticity and a series of bending tests were carried out to estimate the performance of the ICPF sample pieces. In the early part of this chapter, a deflection calibrating method of ICPF is presented. Then, a modulus of elasticity test is given to analyze the mechanical property. In addition, relation between the ICPF actuator bending performance and the dimensions (including the width and length) will be shown. Last but not least, voltage test and frequency response test is given in order to understand how the voltage affects the actuation and maximum deflection frequency range.

7.2 Measurement setup

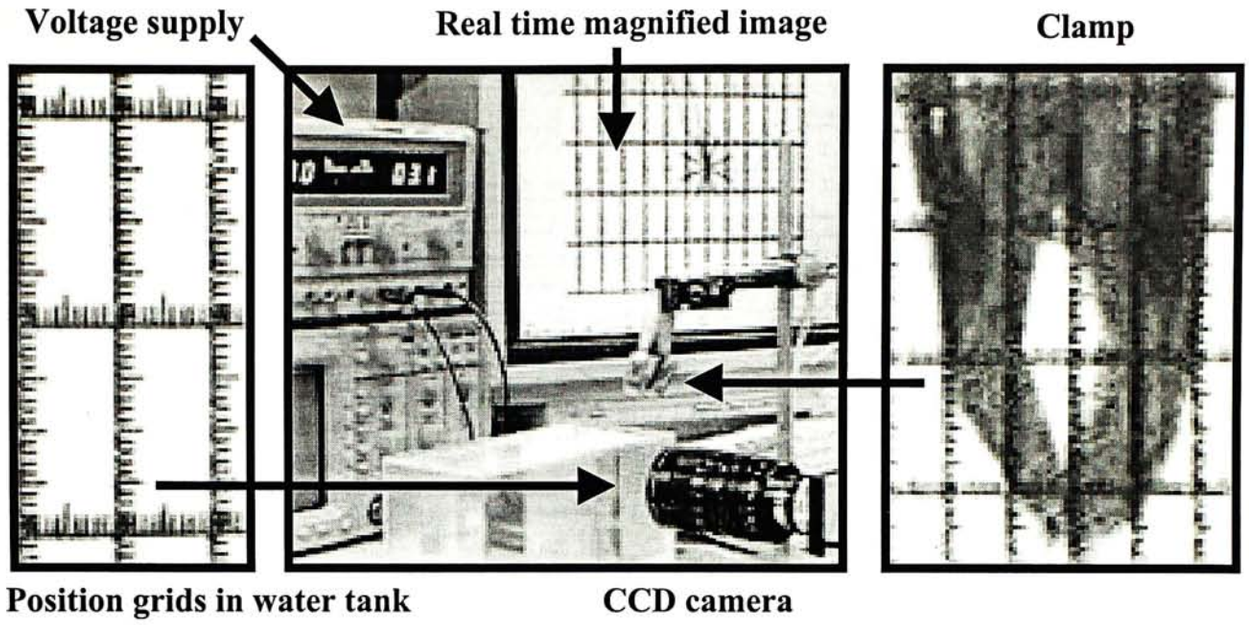

Figure 42 Experimental setup which gives real time imaging.

Figure 42 shows the setup of a deflection calibration system, which is novel way of making precise measurement with resolution of 200μm step size. All experimental processes were recorded through this system. First, ICPF strip or actuator is positioned by a clamp and attached to cathode and anode respectively (details of the clamp's mechanism will be given in Chapter 7.4). Then the clamped test sample is put into a water tank with position grids on the surface of the tank. A CCD camera is located in front of the tank and real time image is captured and recorded through a video input device (Dazzle Multimedia). By adjusting the input voltage of the DC supply, the test sample start to bend and the whole process is recorded. The recorded signal is then transferred to a computer and saved in .mpg formatted file. Individual file are opened for analysis and data processing. Compare to laser measuring system as shown in Figure 43 [10], our measuring system is relatively simpler and more economical. For the laser system, electric voltage applied on ICPF actuator can be controlled by a computer and current is measured by an

electrometer. The bending displacement is measured by laser displacement sensors, a precise measurement can be achieved.

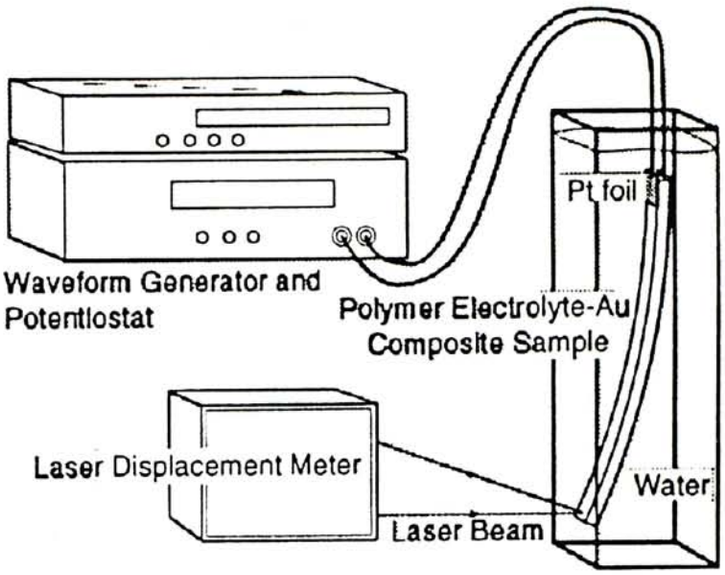

Figure 43 A displacement calibrating system with laser measuring sensor[10].

As mentioned previously, position grids are printed on the water tank as a scaled ruler for deflection measurement. Image captured by the CCD camera is magnified, thus becomes clear and easy to do calibrations. We can calculate the displacement of the strip during actuation. First, we define the radius of curvature R of a virtual circle; the limit of this radius of curvature depends on the length of the strip. Then, we set a zero angle line to indicate the original position of the strip. As we apply a voltage on it, it will bend towards the anode side. We measure the defected angle with reference to the zero angle line, which means the angle of deflection θ is known. By the relation of $S = R\theta$, where θ is the angle of deflection in radian from the zero angle line, R is the radius of curvature and S is the distance traveled by the tip of the testing ICPF strip (Figure 44). In Figure 44 (Right), the positions of the bending strip are recorded; the locus of the tip deflection path is proved a circle. With this relation, it is possible to calculate the displacement of the strip with respect to time under a constant DC voltage supply by calibrating the

distance it has deflected from the centerline. Hence, we are able to measure and calculate magnitude of bending for different test. In the coming section, magnitude of bending under different voltage, frequency will be discussed. Furthermore, relations between performance of bending with varied length and width were observed and analyzed.

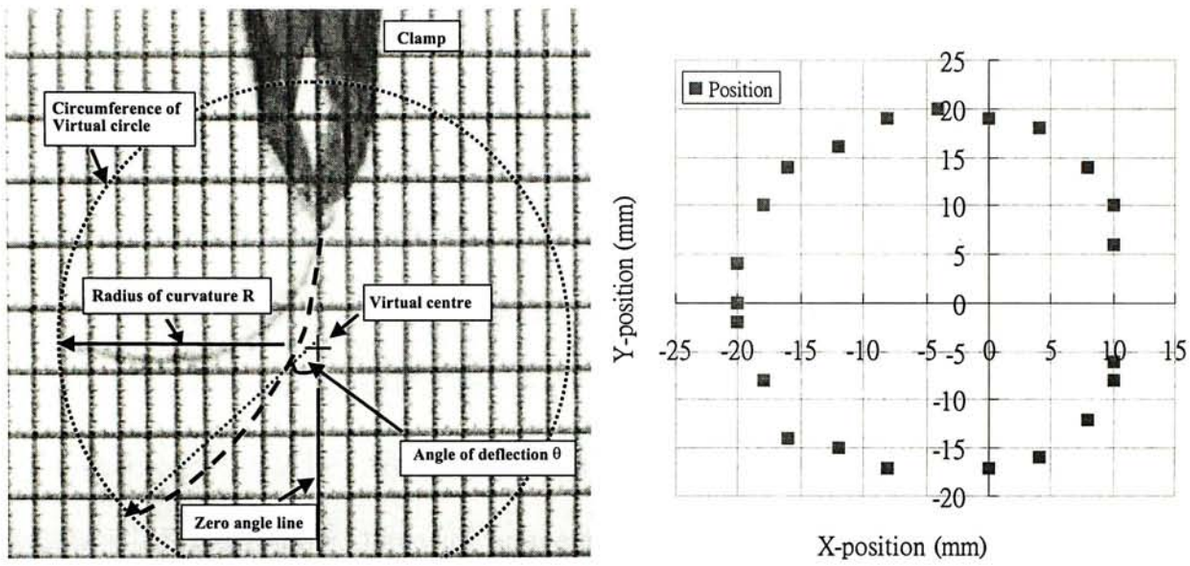

Figure 44 (Left) Method of measuring the deflection of an ICPF testing strip (Right) Tip position of ICPF strip during actuation.

In order to design and actuate micro under-water actuators using Nafion 117, some fundamental studies on mechanical behavior were performed. Since these actuators are electroactivated devices made of composite materials that can undergo large deflections, modeling ICPF involve complicate relations of dynamics, fluid mechanics and chemical sciences. Shahinpoor et al. [17] and Kanno et al. [18] are striving to produce a general workable model for ICPF actuators currently.

To find the Modulus of elasticity of Nafion 117 actuators, we introduced the following method. First, force is applied on ICPF strip using magnets ($1mm^3$) with mass of $2.4x\ 10^{-2}$g/magnet. By counting the number of magnets added, we know how much force is applied at the tip of the cantilevers. Using the predefined grid scale, the motion of the polymer actuators can be quantified (Figure 47). A CCD camera was linked to Snapper, which then connects to the computer graphics interface card of a PC.

Recorded measuring process is reviewed for obtaining the deflection δ of the suspended end. Based on a typical cantilever beam equation, we can obtain the simplified relation for beam deflection, force applied and the beam dimensions:

$$E = \frac{Fl^3}{3\delta I} \qquad \text{Eq 2}$$

where l is the beam length and I is the moment of inertia about the neutral axis, which is equal to $wt^3/12$ for a rectangular cross-sectional beam (w is the width, and t is the thickness of the beam). The experimentally determined E of Nafion actuators (1mmx10mmx180μm) with 2μm Au layers on each side is $3.3945 \times 10^8 N/m^2$, which is close to the value of $2.2 \times 10^8 N/m^2$ given by Kanno et al. [18] using laser deflection measurements for ICPF with dimensions of 10mmx2mmx184μm. In calculating the modulus of elasticity E, linearity between the loading and deflection of the beam is found to obey Hooke's law and is shown in Figure 45. As we can see, the deflection of the beam increased by 0.5mm for every additional force by adding one magnet. From equation 2, we can calculate the modulus of elasticity of ICPF with different dimensions and different applied force. Noted that the Modulus of elasticity of a particular material is a constant, after calculations, the magnitude of Modulus of elasticity in different conditions are plotted in Figure 46. Due to experimental variations, the measured modulus of elasticity are not the same, however, are within a range of $2.989 \times 10^8 N/m^2$ and $4.021 \times 10^8 N/m^2$. For all the measurements, the mean value of modulus of elasticity of ICPF is $3.3945 \times 10^8 N/m^2$.

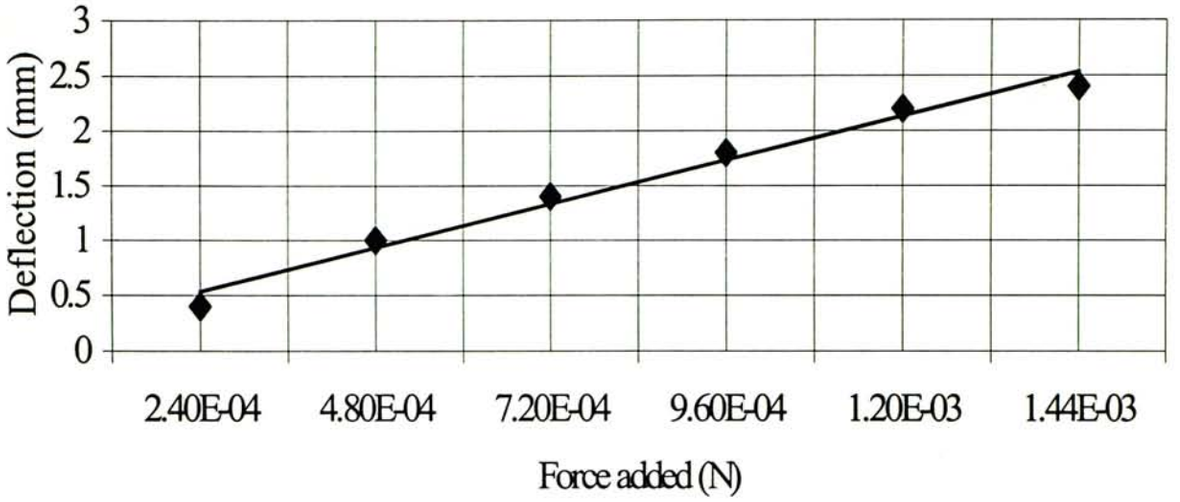

Figure 45 Experimental results of the deflection due to loading for a 1mmx10mmx0.184 mm beam.

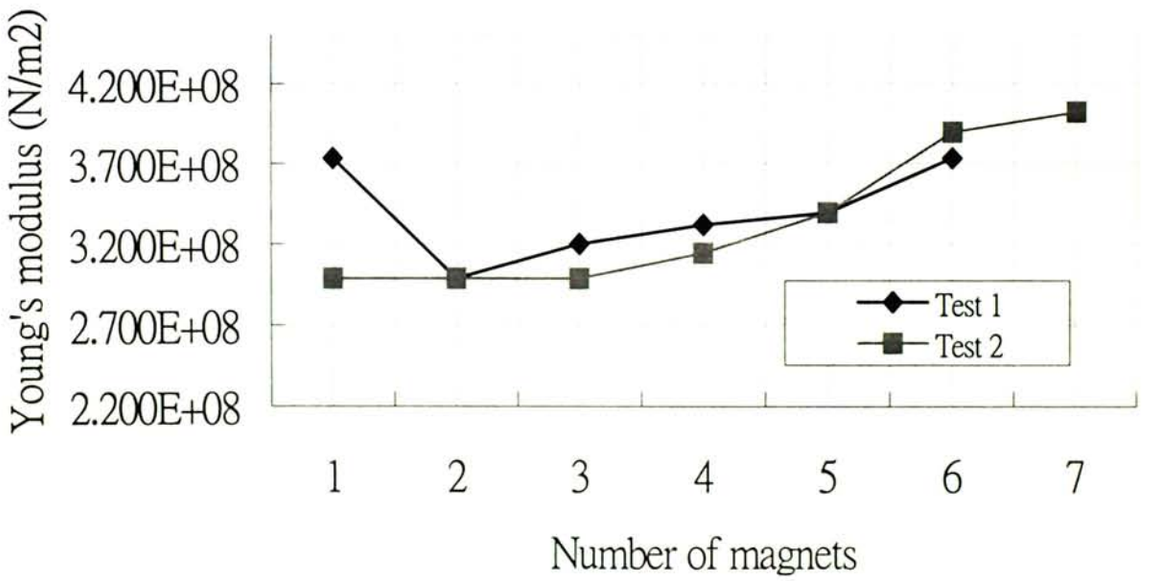

Figure 46 Calculated modulus of elasticity of ICPF from experimental data.

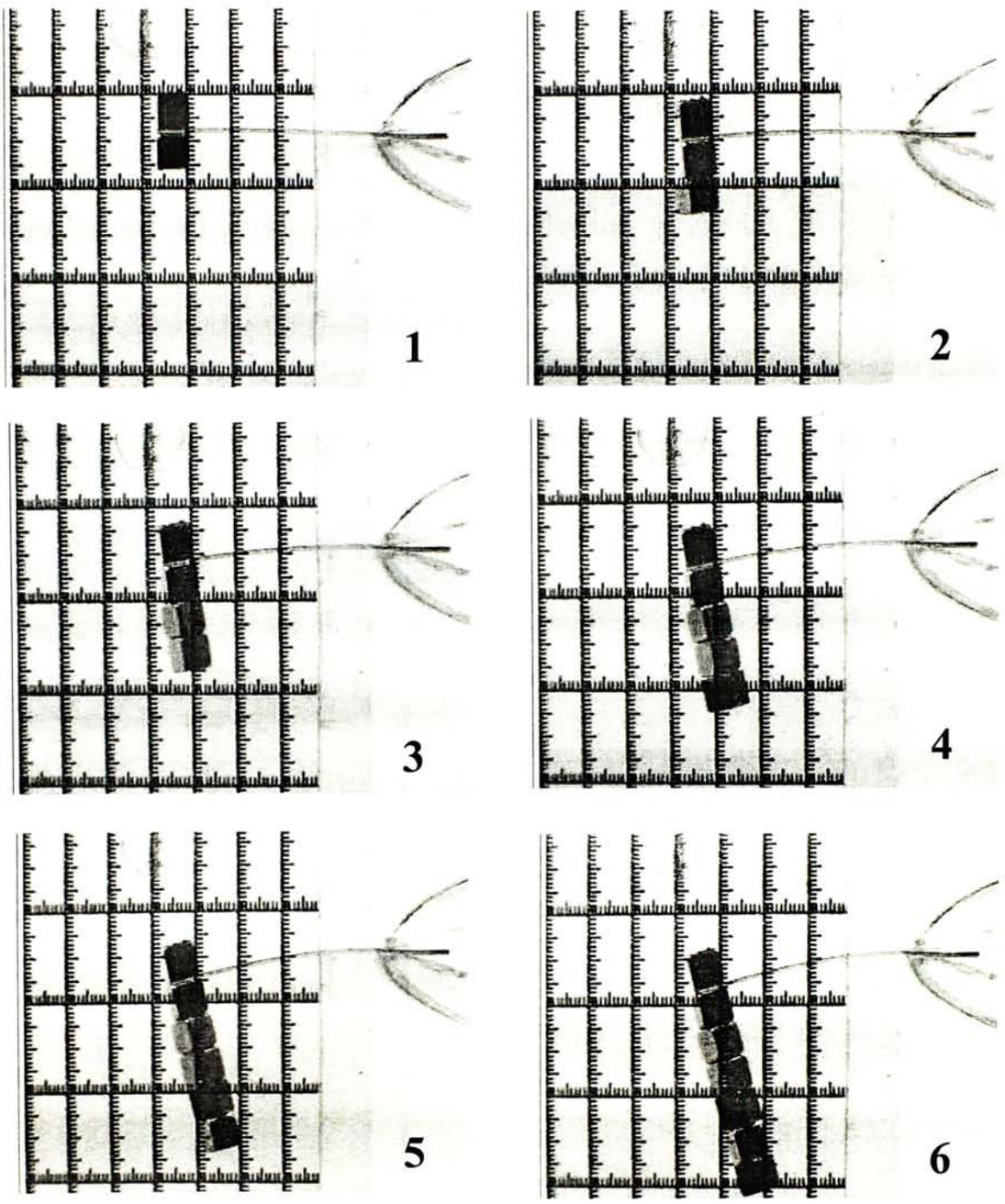

Figure 47 Series of images showing how the cubic masses is used to calibrate the modulus of elasticity of an ICPF strip.

7.3 Width test

The aim of this experiment is to study how the width of individual ICPF actuator's leg affects the bending performance. ICPF sample strips with constant length (24mm) and thickness (184μm), but with different widths were tested. Three sets of ICPF strips were use and they were classified as 0.5mm, 1mm and 1.5mm width strips. In these experiments, a constant 4.5DC voltage is applied on the actuator during actuation. By using the deflection measuring technique that was presented in Chapter 7.2, deflection of particular strip was recorded for calculation and analysis. During experiments, ICPF test strip is positioned in a clamp as shown in Figure 48. The clamp was specially made to have conductive contact surface on both sides to serve as cathode and anode, respectively. Voltage is applied through the two electrodes to the conductive surface of ICPF strip, and consequently, the ICPF strip is actuated and bended.

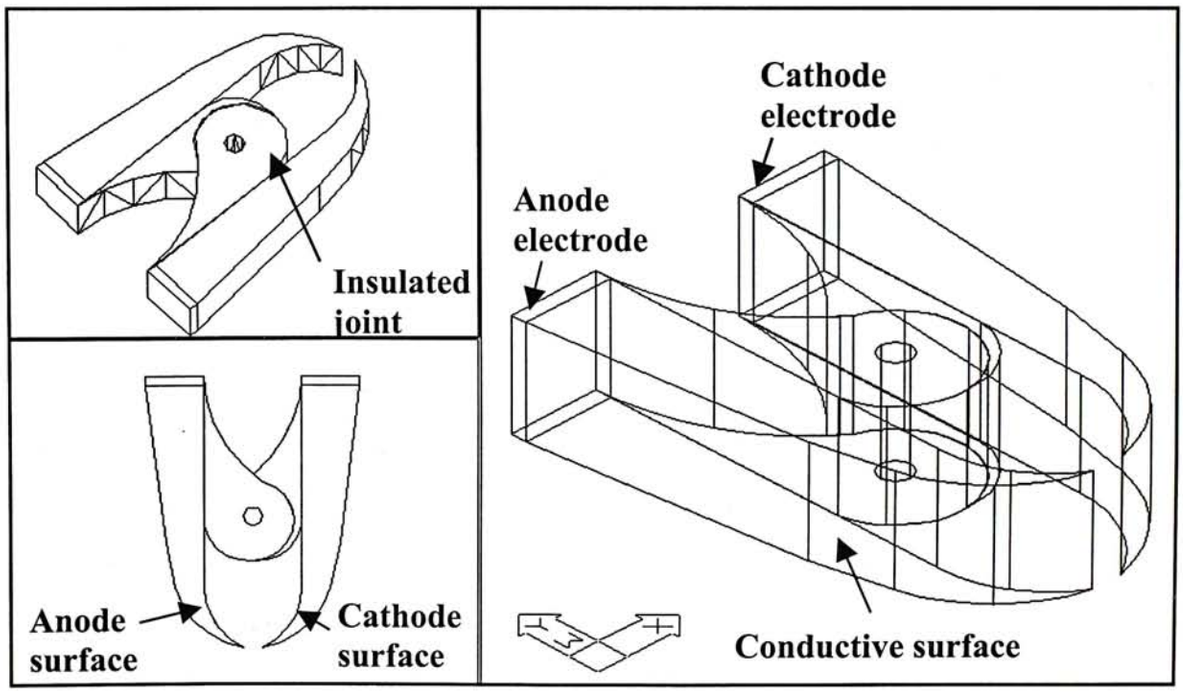

Figure 48 3-D view and plane view showing the mechanism of an ICPF testing clamp.

In the first part of width test, time needed for every single test strip to complete a bending cycle is recorded. A complete bending cycle means that a test strip, start from an original strip position, is actuated to give a maximum left

deflection and then a maximum right deflection (Figure 49). Base on the fact that different cycle time is needed for different width of the actuator, we would like to optimize the width of actuators in order to obtain the fastest bending response legs. Before actuation, the strip was located in an original strip position, then a 4.5DCV is applied on the strip surface, and eventually it will bend to the anode side (left hand side in this case). After a certain time, a maximum left deflection is reached. Then by reversing the polarity of the electrodes, thus, previous positive anode now became the negative cathode. A maximum right deflection is obtained. Finally, the strip is made to bend back to the original strip position and completed one bending cycle. Time consumed for this cycle is recorded and the complete experimental flow is monitored under a computer-linked visual system as mentioned in Chapter 7.1. The results are plotted in Figure 51. Keeping the length of the actuator to 24mm under constant voltage supply, we can see that the cycle time needed reduce with the width. Strip with greater width consume more time to complete actuation. A strip with 1.5mm width took 113 seconds to complete a cycle, however, it took only 80 seconds for 1mm width strip and 73 seconds for 0.5mm width strip. Therefore, without considering other factors, we should reduce the width of the actuator as we could in order to achieve the fastest motion. However, in real situation, it is impossible to do that because of several limitations. The first one is the actuator thickness, as Nafion 117 itself has a thickness of 180μm, if we reduce the width of the actuator strip to this scale, ICPF actuator leg becomes similar to a square beam that is hard to give large deflection. Thus, it is inappropriate to scale down the width of ICPF actuator legs to less then or equal to the thickness of ICPF. Besides, during laser micromachining, the laser spot energy is high enough to burn the cutting edge and if the target cutting width of ICPF exceeds the minimum resolution of the laser system, the gold on Nafion will be burned. Recently, we can minimize the cutting resolution

to ~200μm. Furthermore, smaller ICPF width means less contact area for anode and cathode, this will affect the conductivity of the actuator. In short, due to other limiting factors, the width of the ICPF actuator should not be less then 200μm without improving these limits by after advanced technologies.

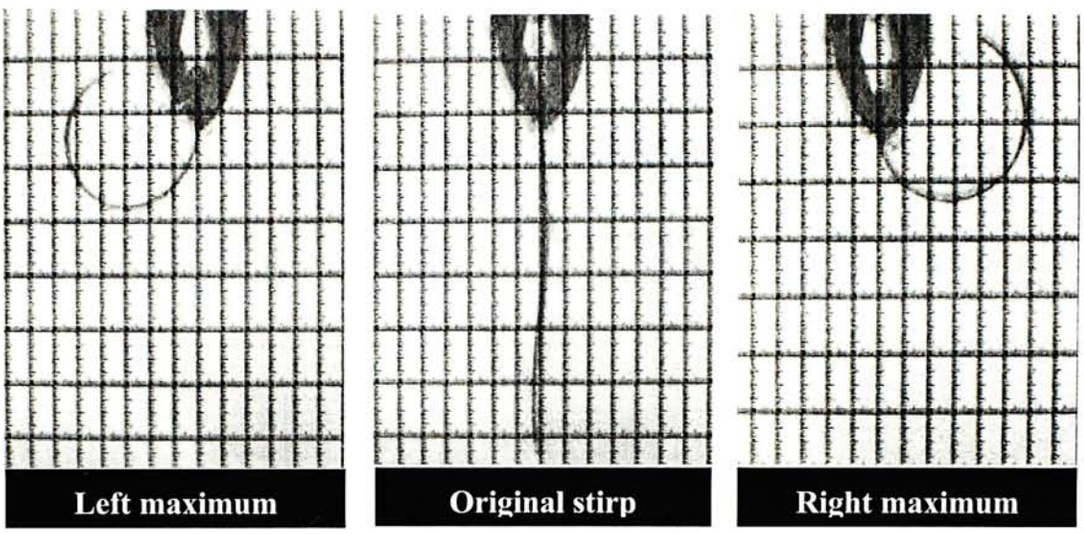

Figure 49 Series of captured images showing the maximum deflection under ±4.5V with strip dimensions of 1.5mmx24mmx0.184mm.

The second part of the width test is to find out the relation between rate of actuation and the width of actuator. In a particular period, comparisons are made in terms of different bending rate of ICPF. For a 24mm length strip, the radius of curvature of deflection is 16mm. Figure 50 shows that the rate of bending is faster in smaller-width strip than that of larger-width strip. After 20 seconds of actuation, the deflecting angle of strips were 100°(0.5mm wide strip), 90°(1mm wide strip) and 30°(1.5mm wide strip), respectively, and after further 10 seconds actuation (totally 30 seconds actuation), the 0.5mm wide strip already reach a bending angle of 145°. However, only 50° for the 1.5mm width strip. Thus, this experimental result has testified that the less the width of ICPF, the faster actuation rate achieved. Figure 52 and Figure 53 show the rate of left and right actuation, respectively. Clearly, in every actuating period, the deflection is greater for ICPF strip with less width.

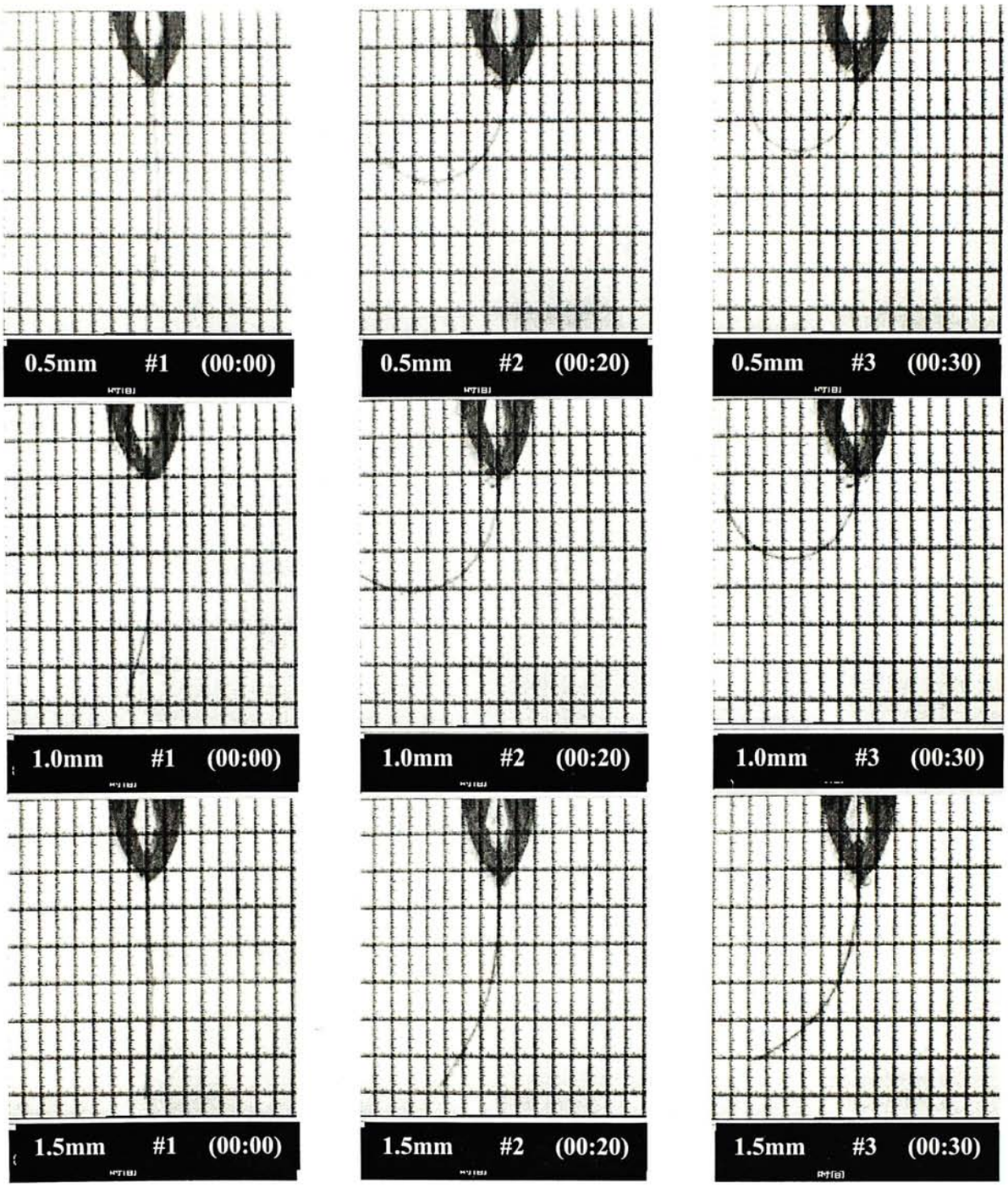

Figure 50 Different width strips with different bending rate are shown.

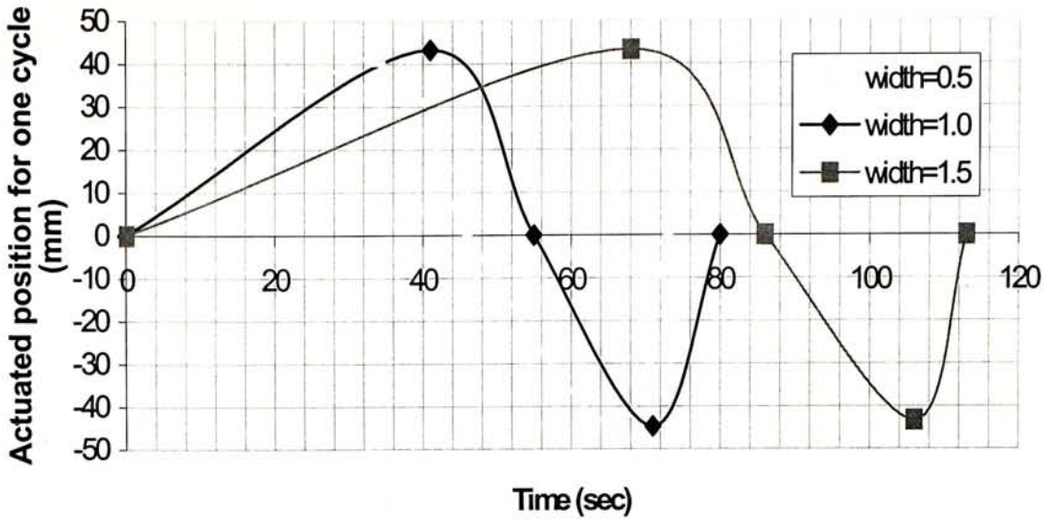

Figure 51 Cycle time of ICPF strip with different width.

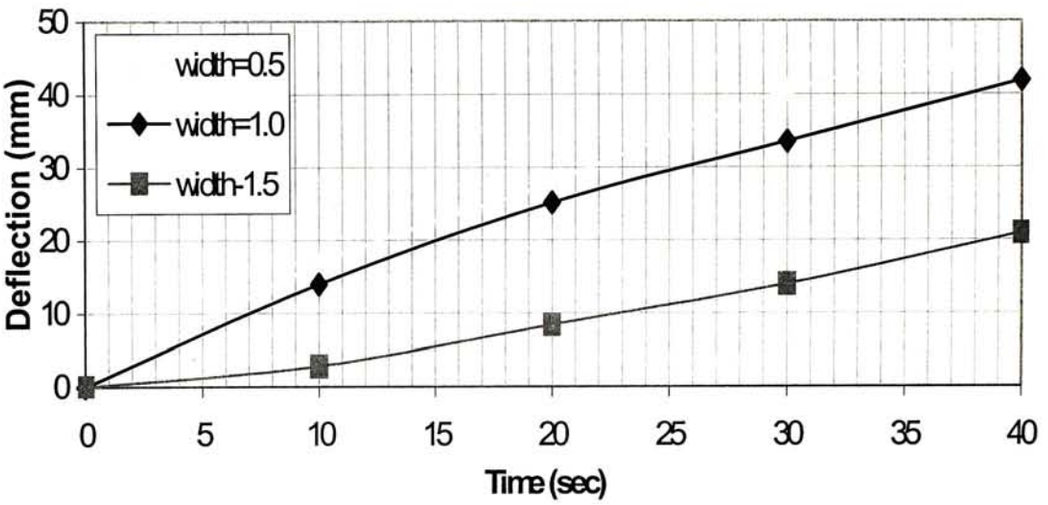

Figure 52 Rate of left actuation for different width strips.

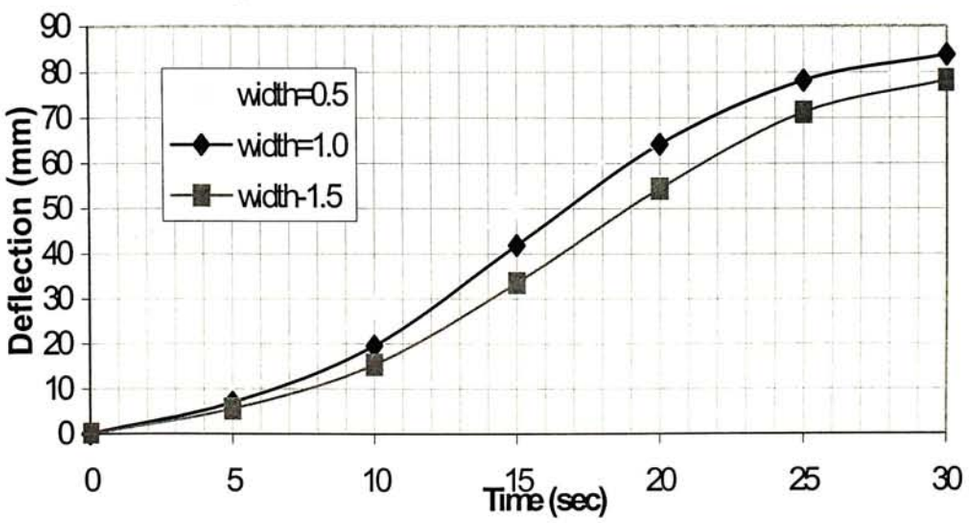

Figure 53 Rate of right actuation for different width strips.

7.4 Length test

Similar to width test, length test was carried out in order to study the bending performance of ICPF actuators with different length. In this experiment, as shown in Figure 54, strips of ICPF with 8mm, 16mm and 24mm were tested. With a specified deflection measuring technique that have been mentioned previously, the radius of curvature of the 8mm strip is 6mm, 16mm strip is 12mm, and 24mm strip is 18mm. Obviously, a linear relation between the length of ICPF strips and radius of curvature of a virtual circle is achieved. Since the width and the thickness of the test strips in this experiment are fixed to 1mm and 184μm correspondingly, it turns out that the rate of bending motion among the strips do not have significant variation. However, the length of strip was shown to affect the closure of ICPF actuator. In Figure 54, series of image showing the maximum left and right deflection and deflecting angle of individual ICPF strips with different length. For 8mm long strip, the maximum deflecting angle is 110°(Left), 70° (Right), for 16mm long strip, the maximum deflecting angle is 140°(Left), 110° (Right), and finally for 24mm long strip, the maximum deflecting angle is 155°(Left), 160° (Right). The more the deflecting angle of the strip means a better closure of the actuator. Therefore, in designing ICPF actuator, we have to find out the minimum length of the actuator leg that can be used to do the grasping motion. Note that apart from the length, actuating voltage can also vary the maximum deflecting angle as well as the rate of actuation, hence, voltage tests were carried out in this chapter following this section. Figure 55, shows the cycle time of ICPF strip with different length. It is interesting to point out that the rate of the first actuation of ICPF is always less then that of the second actuation. For example, time needed for all strip with different length to deflect from original position to the left maximum deflection and then back to the original position (left cycle) is around 55seconds, however, it just took 25 seconds for the right cycle. We are still investigating this phenomenon. One possible explanation is due to excessive

cumulated stress in Nafion layer during the left cycle, therefore, in the right cycle, more energy is release to the water molecules thus speed up their motion. The rate of left and right actuation for different length strips is shown in Figure 56 and Figure 57. We can see that the maximum left deflection of a 24mm long strip is 48mm, which is about twice that of 16mm long strip (28mm) and three times that of 8mm long strip (13mm). Similar results were recorded for right actuation.

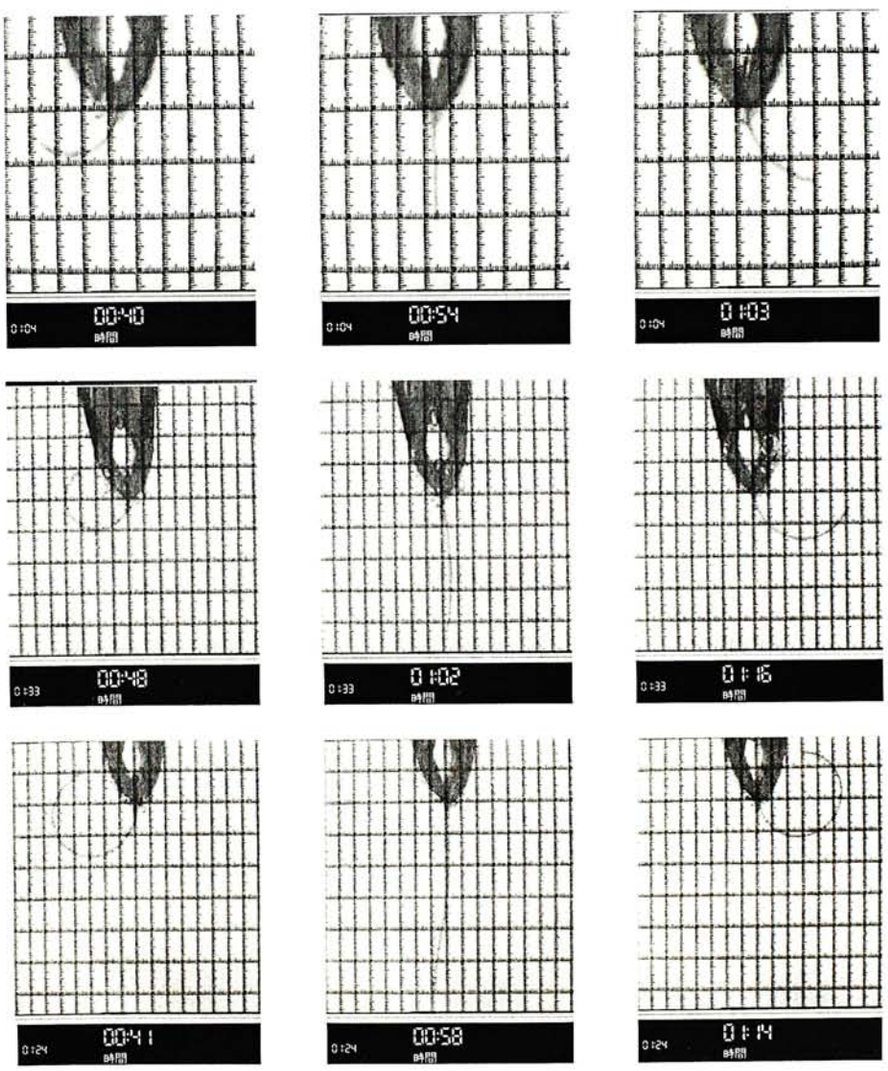

Figure 54 Series of image showing the maximum left and right deflection for (Top) 8mm strip, (Middle) 16mm strip and (Bottom) 24mm strip.

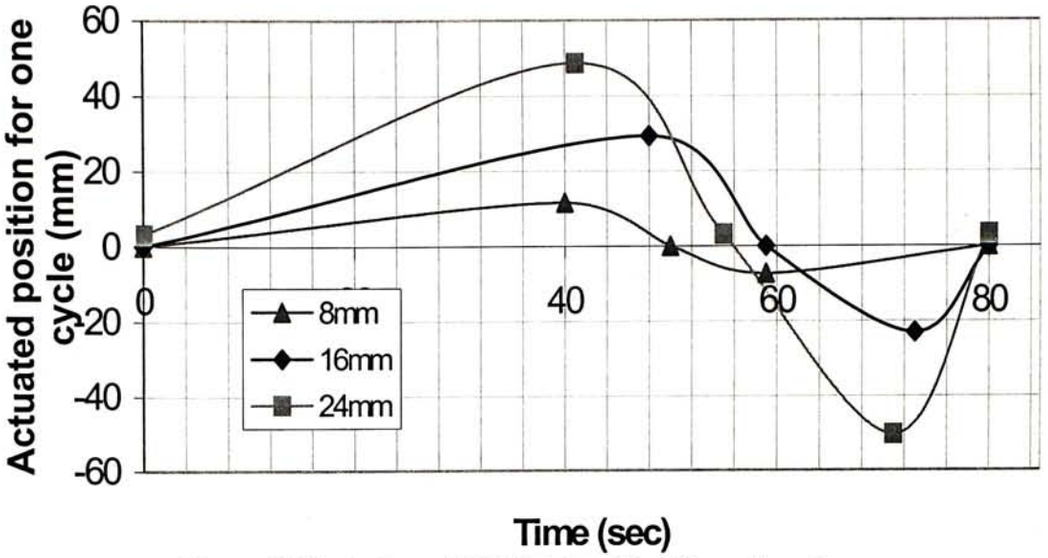

Figure 55 Cycle time of ICPF strip with different length.

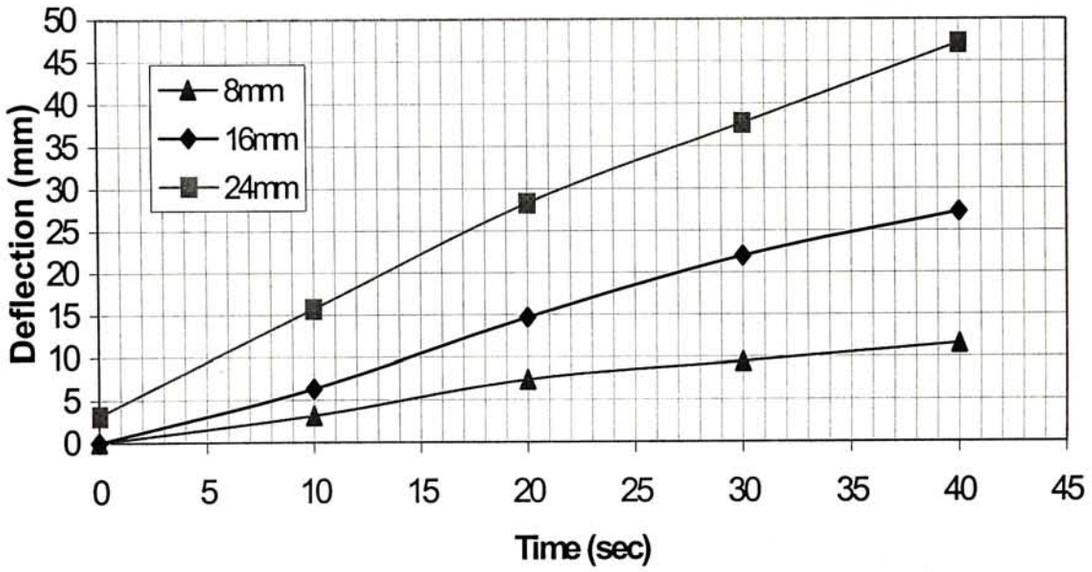

Figure 56 Rate of left actuation for different length strips.

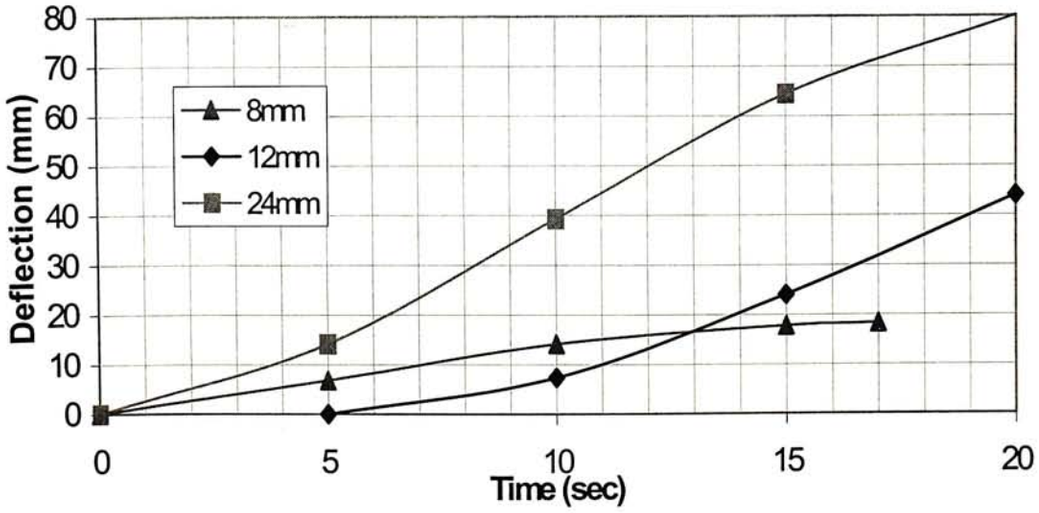

Figure 57 Rate of right actuation for different length strips.

7.5 Voltage test

One of the advantages of using ICPF to build actuator is that it can give a large deflection with a low voltage supply: usually around 2 to 5V, which depends on the dimension and mechanism of the device. For our ICPF strips or ICPF actuators, the range of voltage input is from 3.5V to 4.5V. However, it has been discovered that excessive large voltage (larger than 7V) will burn the ICPF and will lead to a peeling off problem, thus stop the bending motion. On the other hand, an insufficient voltage, which is lower than 3.5V cannot not even actuate the strip to give any bending moment. Therefore, magnitude of voltage applied on the ICPF surface is an important parameter apart from the dimension during actuation. In voltage test, strip with same dimension (1mm x 24mm x 0.184mm) were actuated with 3.5V, 4.5V and 5V, respectively. Among the three range of voltage supply, the higher the voltage provided, the higher the strip bending rate achieved and the greater deflection it gave (Figure 58). As in Figure 59, under 3.5V, it took 230 seconds to complete a bending cycle, however, it reduced to 62 seconds, nearly 4 times shorter, for a strip with 5V to finish a cycle. Besides the rate of actuation, the maximum deflecting angle increases with voltage. For 3.5V input, the maximum left deflecting angle is 140° and right deflecting angle is 110°. For 5V input, the maximum left deflecting angle is increased to 160° and right deflecting angle is increased to 150°. Therefore, it is supposed to get a faster response and larger deflection when ICPF actuator is actuated by a higher voltage (Figure 61). However, the actuating voltage should not be larger then 7V due to two reasons. The first reason is that too large voltage will burn the contact point between the clamping system and the actuator, thus stop actuation. The other reason is that an excessive voltage will trigger peeling off problem that also prohibit actuation.

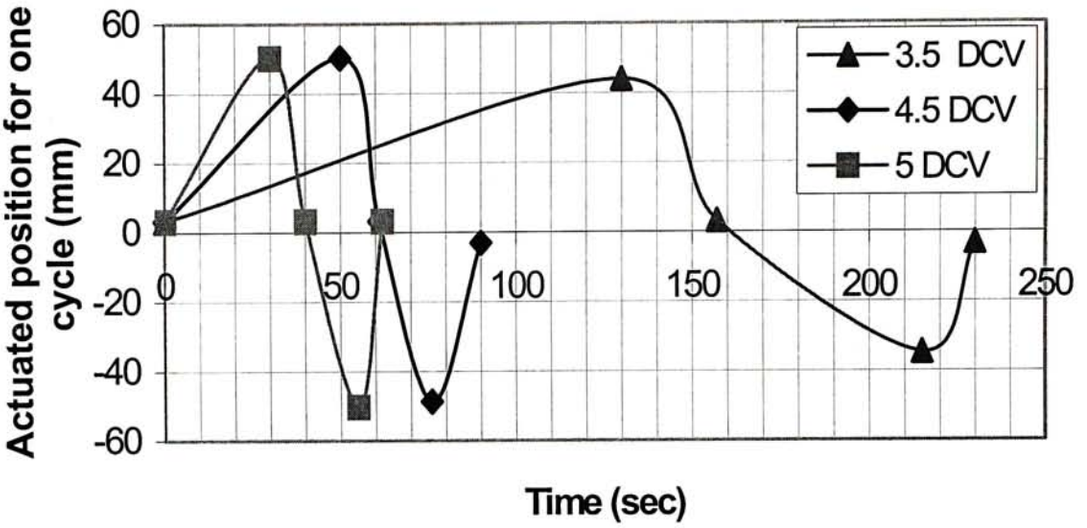

Figure 58 Time needed for ICPF strip, with same dimensions but different voltage, to run through a bending cycle.

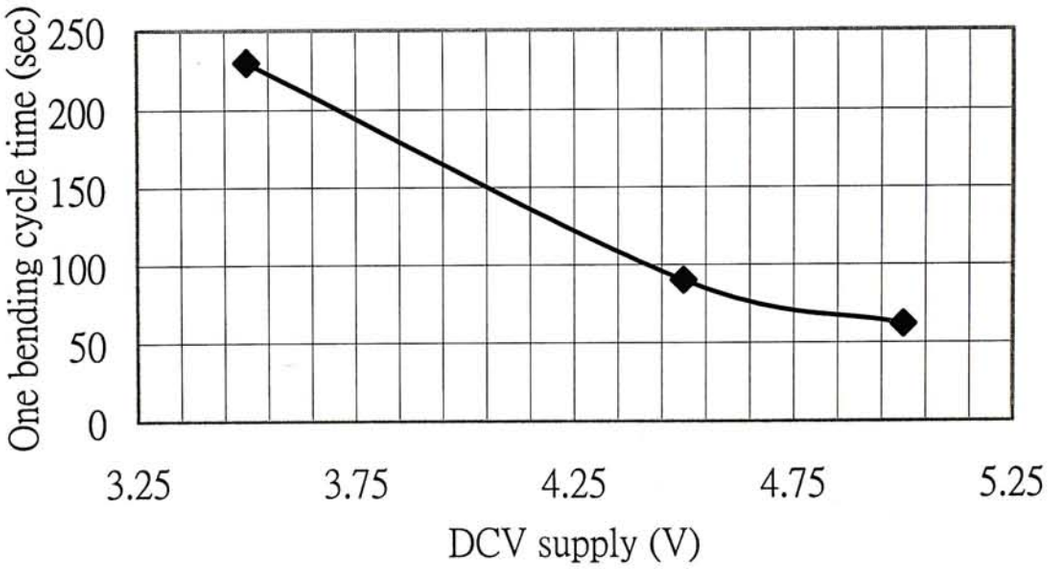

Figure 59 Cycle time needed against the DCV supply.

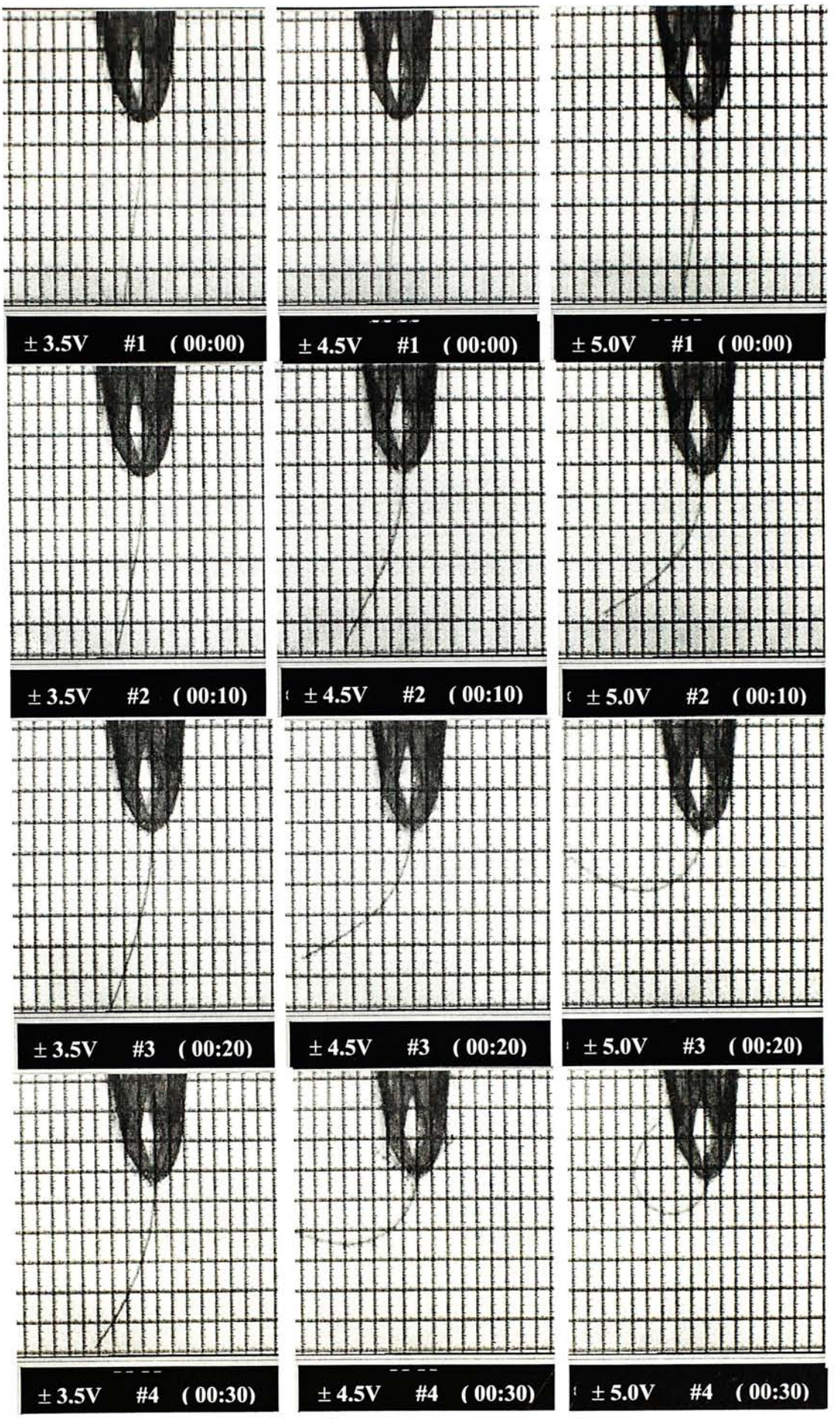

Figure 60 The bending performance of ICPF strip under different voltage supply.

8 MICRO GRIPPER ACTUATION

8.1 Development of micro gripper

As shown in Chapter 4, a novel ICPF fabrication process was developed: 2 μm of gold thin film is successfully deposited on Nafion 117. As mentioned before, it is extremely important to have reliable and repeatable fabrication process in order to laser micromachine and actuate ICPF micro actuators. As shown in Figure 61, we can see the difference on whether having a good fabrication process or not affects the actuator performance. Consider the two images on the left, which show first batch of ICPF strips fabricated by filament evaporation that has around 1.5μm of gold deposited on Nafion 117. However, we did not have appropriate surface pretreatment of Nafion 117 and the gold deposition condition at that time, therefore the first batch of ICPF strip gave only little deflection even under 7V. Also, the surface of the contact point burned out after exposure to high voltage for minutes. However, as we keep on improving our fabrication technique as mentioned in Chapter 4, we have overcame the peeling off problem, alleviated the residual stress between ICPF and electrode layers, and fabricated ICPF strips that gave good bending performance.

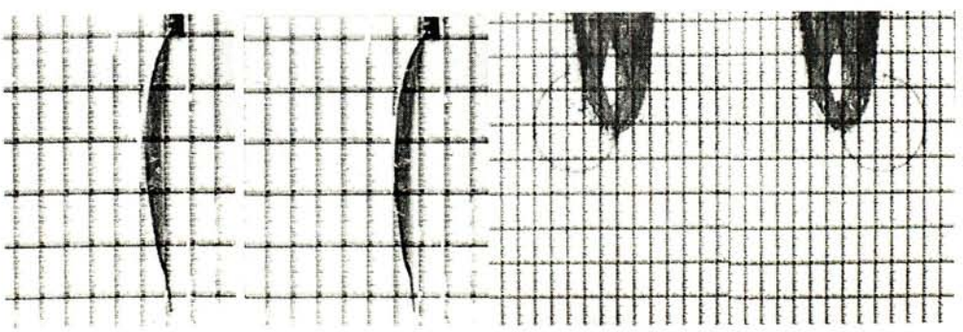

Figure 61 Bending limit of ICPF strip (Left) First generation (Right) Latest generation.

8.2 Micro gripper

As there has been a great improvement in getting large bending performance ICPF under a low voltage supply (4.5V), the reliability and repeatability of ICPF ensure a further development of micro gripper. After carried out series of experimental studies on the electrical and mechanical properties of ICPF, we can estimate effects that may occur during miniaturization of actuators in terms of the width and length of the actuator as well as the voltage input. First, we used laser to cut out star patterned actuator with individual legs of 300μm and actuated it under 15V, with the actuator mounted on a base (cathode) and a wire is bonded on the top surface as the anode (Figure 62). We also fabricated actuators with leg width of 500μm (Figure 63). A clamp is used to hold the actuator and the two contact points are used to serve as electrodes in this case. Recently, by improving the quality of fabricate ICPF, which made it possible to obtain a 2 legs actuator with 1mm in leg width as shown in Figure 64, which can give large deflection and implement a grasping motion under 4.5V supply. The latest result is that we are able to laser micromachine 2 legs gripper with legs of 300μm. Applying 4.5V on it can give a large grasping motion (Figure 65).

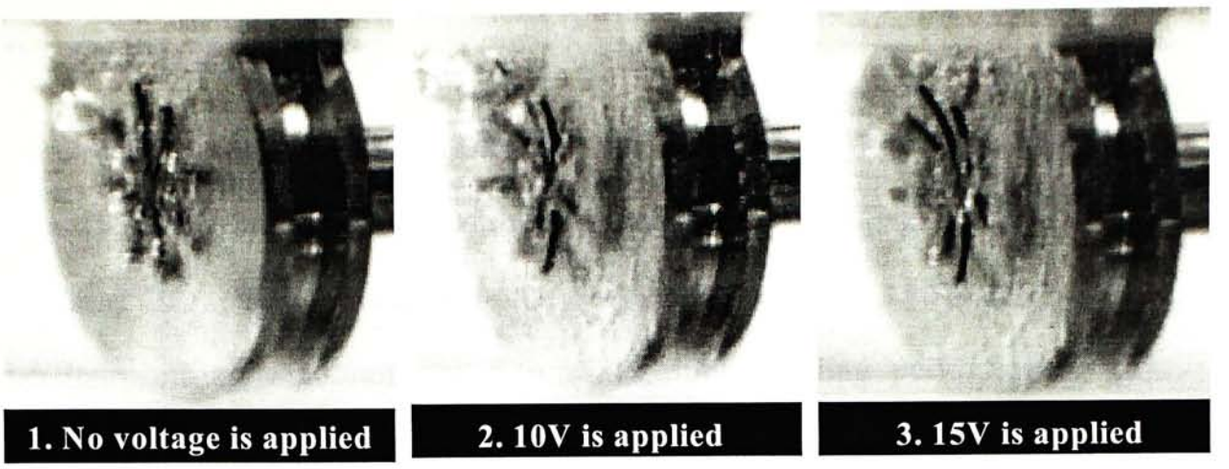

Figure 62 Star patterned 8 legs micro gripper with Voltage applied: 15V, Current applied: ~0.05A Dimensions: Width 0.3mm/leg Length 3mm/leg Thickness 0.2mm.

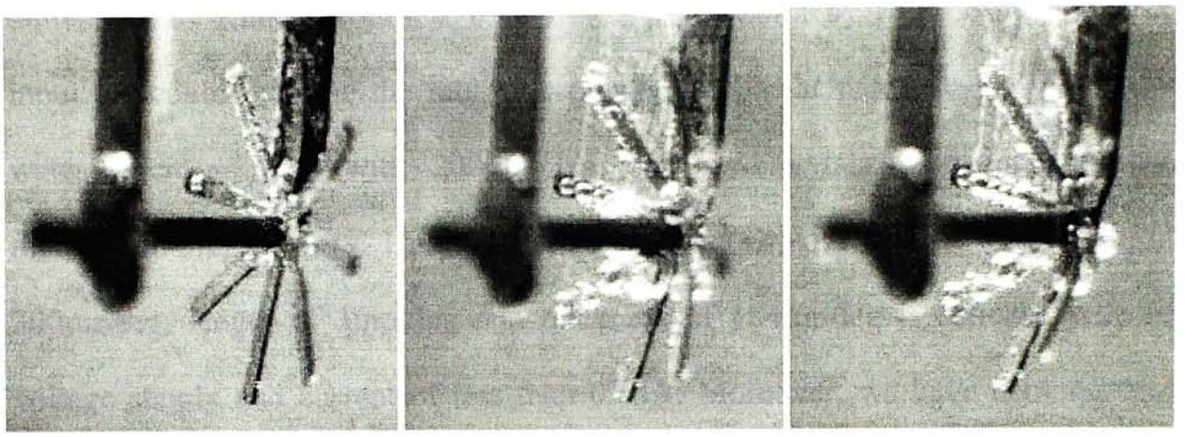

Figure 63 Star patterned 8 legs micro gripper with Voltage applied: 15V, Current applied: ~0.05A Dimensions: Width 0.5mm/leg Length 4mm/leg Thickness 0.2mm.

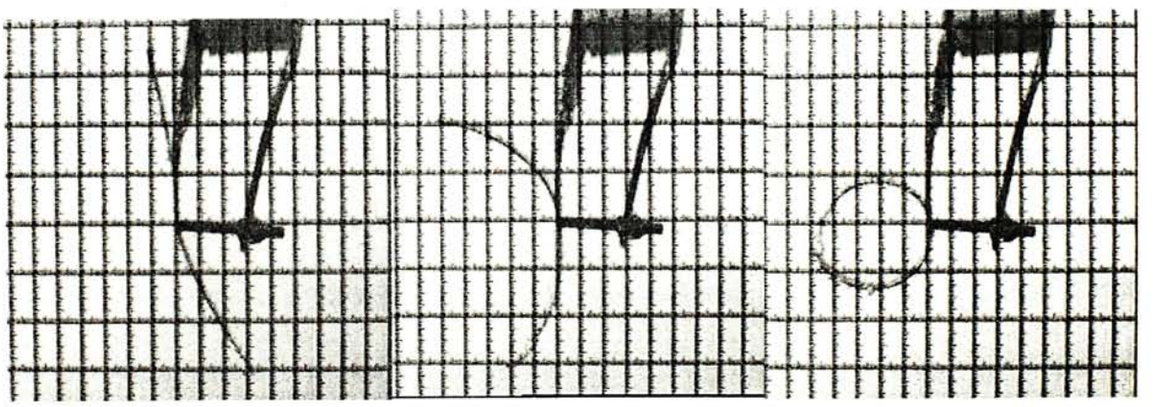

Figure 64 Shows a 2 legs ICPF actuator that have a grasping motion under 4.5V.

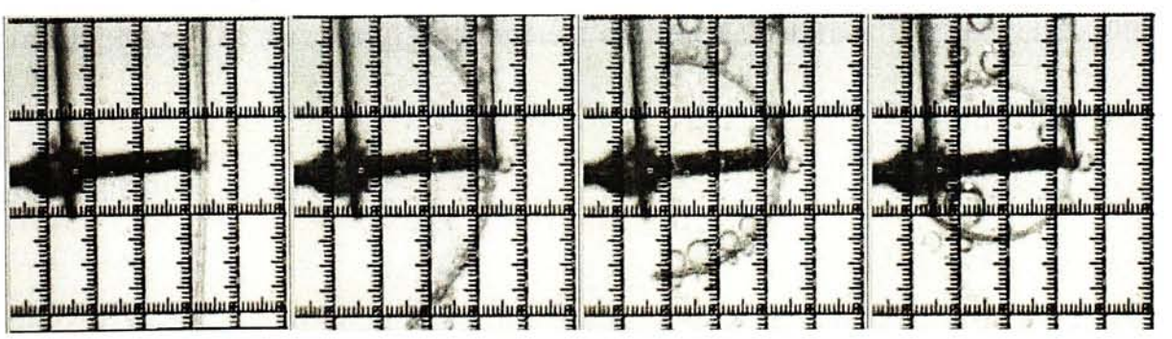

Figure 65 Laser micromachined 2 legs ICPF actuator with 300μm leg width and 15mm in total length.

9 CONCLUSION

We have successfully created an ICPF composite using Nafion 117 sandwiched by 2μm of gold electrodes. Introducing a novel and reliable fabrication process, we have overcome the adhesion problem between gold and perfluorosulfonic acid polymer film. Thus, high bending performance ICPF is fabricated and is successfully actuated under ±4.5V without any gold thin film peeling off. A more than 180° deflection is achieved for an ICPF strip with dimension of 1mm x 16mm x 0.184mm. Furthermore, by controlling the voltage input we could increase the rate of bending of ICPF actuator. In addition, under-water micro-grippers with 200μm leg width were fabricated using a laser-mciromachining process. Under-water micro gripper with dimensions of width of 300μm/leg, length of 3mm/leg and thickness of 184μm/leg is actuated with 15V voltage supply and current of less than 0.05A. Moreover, we have demonstrated a two-leg gripper that can close the legs to implement a grasping motion. This research is significant in that we have developed a technique to micro-fabricate and batch produce under water micro-robotic manipulators suitable for applications in transporting micro objects in bio-medical areas.

Our future work includes refining our laser system to further reduce the feature size of the micro Nafion polymer structures, and to design other innovative micro actuators using Nafion. In parallel, we are also developing the capability of using an electronic controller to control individual fingers on a micro under-water manipulator. The successful development of these actuators will enable effective and fast control of under-water micro objects and lead to new applications in cellular manipulation.

10 APPENDIX

10.1 Procedures in using E-beam evaporator

Initial Start Up

Check that all valves are closed; all switches are off. Supply compressed air and cooling water to system.

- Press the "System" on.
- Turn on Mech Pump (mechanical pump).
- Turn on thermocouple gauge and switch to TC –1 position.
- Thermocouple needle should indicate 50 millitorr very quickly. Open Regen Valve. When TC-1 reads below 50 millitorr, turn on HI-VAC (Cryopump). After thirty minutes, close Regen Valve. After 3 hours, the HI-VAC is ready to pump the chamber.

Prepare For Evaporation

- Open Vent valve to let the gas into the Chamber. Lift off Bell jar.
- Place Source materials in crucible(s) and samples(s) on the sample holder.
- Choose appropriate Shunt position according to the material melting point. The higher is the melting point, the lower is the shunt position.
- Recover the Bell jar.

Pump To High Vacuum

- Close Vent valve. Open Rough valve. Wait for pump the chamber to less than 50 milltorr. Turn Discharge gauge selector switch to "on" position.

- Close Rough valve, open HI-VAC (High Vacuum Valve). The Chamber is pumped to high vacuum.
- Turn off the Mech Pump.
- Turn the Discharge gauge (high vacuum gauge) selector switch to 10^{-4} position and push the "Meter Read" button. If the Chamber pressure is too high, the gauge needle will swing full right then drop back to zero, and the pilot light will go off. Wait a few seconds and again push "Meter Read". Wait for the pressure is lower than $5X10^{-5}$ Torr.

Evaporation

- Check that all current Adjust knobs are at zero.
- Water flow to "Minigun" and Crystal monitor on.
- Input the Source material's density data etc. into the Crystal monitor.
- Main power, Filament and Beam power (high voltage breakers) are on.
- Switch on "Filament power".
- Adjust to "10" on dial, wait 5 seconds.
- Slowly adjust up to 0.75 amps.
- Key on "High voltage" switch. Switch on "Beam power".
- Adjust to "15" on dial, wait 15 seconds.
- Slowly adjust power, watch as beam sweeps crucible.
- With beam in middle of crucible, adjust "Filament power" to 1.0 amps.
- Readjust "Beam power" to locate the beam in the middle of the crucible.
- Open Source shutter, deposit material.
- Slowly decrease "Beam power" to zero. Switch off "Beam power".
- Key off "High voltage" switch.
- Slowly decrease "Filament power" to zero. Switch off "Filament power".

- Turn off all breakers.
- Turn off with water flow to "Minigun" and the Thickness monitor.

Opening Up System

Close HI-VAC Valve, wait one minute, turn off the Discharge gauge, open Vent Valve.

Closing The System Down

- If the system is open to air, place the bell jar on the baseplate. Turn on the Mech Pump and then open the Rough Pump to pump the Chamber to basic vacuum as above if time permits.
- Turn off the HI-VAC Pump.
- Close the HI-VAC Valve. Allow ample time for the cryopump to warm.
- Turn off all switches and the main circuit breaker.
- Remember, when closed down, the bell jar should in place and under vacuum. All valves should close and switches off.

10.2 Procedures in using Thermo couple evaporator

- Power on switch, tap on H_20
- Press diffusion chamber (heater)
- Press rotatory pump, wait for 30minutes
- Turn handle to backing, press air pump for 5 minutes
- Open flask, replace vision glass, place target metal and substrate
- Close shelter, position the bell jar, press release air button
- Add liquid Nitrogen "N_2"

- Turn handle to roughing for 5 minutes
- Turn to backing again
- Pull out the handle and turn to open valve
- Wait for an hour and add liquid Nitrogen once more
- Start evaporation after 1 hour, check high vacuum before
- Power on meter reading, tap on water switch
- Press x-detector and LT button to check readings
- Increase current gradually to 60A for gold evaporation
- Open shutter for evaporation
- Close shutter after evaporation
- Check readings again and then power off reading meters
- Reduce current gradually, then power of LT
- Turn handle to backing after pushed in
- Release air into the bell jar after cool down
- Remove evaporated substrate and close the bell jar, turn to roughing again
- Position the handle back to normal and power off all the switches
- Close all water source

11 REFERENCE

1. J. Ok, M. Chu, and C. J. Kim, "Pneumatically Driven Microcage for Micro objects in Biological Liquid", Proceedings of IEEE MEMS 1999, pp. 459-463.

2. M. Shahinpoor, Y. Bar-Cohen, J. O. Harrison and J. Smith, "Review Article Ionic Polymer-metal composites (IPMCs) as Biomimetic Sensors, Actuators and Artificial Muscles - a Review", Smart Mater. Struct., 1998, R15-R30.

3. Y. Bar-Cohen, S. Leary, A. Yarvrouian, K. Oguro, S. Tadokoro, J. Harrison, J. Smith and J. Su, "Challenges to the application of IPMC as actuators of planetary mechanisms", Proceedings of SPIE Vol.3987 (2000).

4. S. Guo, T. Fukuda, T. Nakamura, F. Arai, K. Oguro and M. Negoro, "Micro Active Guide Wire Catheter System-Characteristic Evaluation, Electrical Model and Operability Evaluation of Micro Active Catheter", Proceedings of the 1996 IEEE International Conference on Robotics and Automation Minneapolis, Minnesota-April 1996.

5. Ralf Fischer, Detlef Zuhlke, Johannes Hankes, "Gripping technology for automated micro-assembly", Proceedings of SPIE, Microrobotics and Microsystem Fabrication Vol. 3202 (1997).

6. Yves Bellouard, Armin Sulzmann, Jacques Jacot and Reymond Clavel, "Design and highly accurate3D displacement characterization of monolithic SMA micro gripper using computer vision", Proceedings of SPIE, Microrobotics and Microsystem Fabrication Vol. 3202 (1997).

7. Stephanus Buttgenbach and Jurgen Hesselbach, "Shape memory alloy microactuator systems", Proceedings of SPIE, Microrobotics and Microsystem Fabrication Vol. 3202 (1997).

8. W. Nogimori, Koichi Erisa, Mitsuhiro Ando and Yoshihiro Naruse, "A Laser-Powered Micro Gripper", Micro Electro Mechanical Systems, 1997. MEMS ' 97, Proceedings, IEEE., Tenth Annual International Workshop on , 1997.

9. Y. Bar-Cohen, S. Leary, M. Shahinpoor, J. O. Harrison and J. Smith, "Electro-Active Polymer (EAP) actuators for planetary applications", Proceedings of SPIE, Newport Beach, CA, 1-2March, 1999, paper 3669-05.

10. K. Onishi, S. Sewa, K. Asaka, N Fujiwara and K. Oguro, "Biomimetic Micro Actuators Based on Polymer Electrolyte/Gold Composite Driven by Low Voltage", 0-7803-5273-4/00@2000 IEEE.

11. David R. Lide, "CRC handbook of Chemistry and Physics", 78th edition 1997-1998.

12. T. Fukuda and W. Menz, "MicroMechanical Systems, principles and technology", Handbook of sensors and actuators, Volume 6, 1998.

13. Richard C. Jaeger, "Volume V Introduction to Microelectronic Fabrication", Addison-Wesley Publishing Company 1993.

14. Gray E. McGuire, "Semiconductor Materials and Process Technology Handbook for Very Large Scale Integration (VLSI) and Ultra Large Scale Integration (ULSI)", Noyes Publications 1998.

15. William T. Sifvast, "Laser Fundamentals", Cambridge University Press 1996.

16. C. J. Nonhof, "Material Processing with Nd-Lasers", Electrochemical Publications Limited 1988.

17. M. Shahinpoor, Y. Bar-Cohen, J. O. Harrison and J. Smith, "Review Article Ionic Polymer-metal composites (IPMCs) as Biomimetic Sensors, Actuators and Artificial Muscles- a Review", Smart Mater. Struct.7 (1998) R15-R30.

18. R. Kanno, S. Tadokoro, T. Takamori, and K. Oguro, "3-Dimensional Dynamic Model of Ionic Conducting Polymer Gel Film (ICPF) Actuator", IEEE International Conference on System, Man and Cybernetics, 1996, vol. 3, pp. 2179-2184.